DEPARTMENT OF PHYSICS, UNIVERSITY OF JYVÄSKYLÄ
RESEARCH REPORT No. 10/1979

LEVEL STRUCTURE OF THE TRANSITIONAL ODD-MASS NUCLEI $^{141-149}$Pm

BY

MATTI KORTELAHTI

Academic dissertation
for the Degree of
Doctor of Philosophy

Jyväskylä Finland
August 1979

ISBN 951-678-207-8

DEPARTMENT OF PHYSICS, UNIVERSITY OF JYVÄSKYLÄ
RESEARCH REPORT No. 10/1979

LEVEL STRUCTURE OF THE TRANSITIONAL ODD-MASS NUCLEI $^{141-149}$Pm

BY

MATTI KORTELAHTI

Academic dissertation
for the Degree of
Doctor of Philosophy

To be presented, by permission of the
Faculty of Mathematics and Natural Sciences
of the University of Jyväskylä,
for public examination in Auditorium S-212 of the
University on September 1, 1979, at 12 o'clock noon.

Jyväskylä Finland
August 1979

URN:ISBN:978-951-39-9891-2
ISBN 978-951-39-9891-2 (PDF)
ISSN 0075-465X

University of Jyväskylä, 2024

Preface

This work has been carried out during the years 1976 - 1979 at the Department of Physics, University of Jyväskylä. I wish to express my thanks to this institute for the excellent working conditions provided for me.

It is a pleasure for me to express my sincere gratitude to my teacher, Professor A. Pakkanen. His continuous interest and encouragement has been of great value during the course of studies involved in the preparation of this thesis.

To my coworkers, Dr. M. Piiparinen, Mr. T. Komppa, Phil. Lic., and Mr. R. Komu, Lab. Eng., I am greatly indebted.

I would like to thank the staffs of the cyclotron, the computer, the target laboratory and the machine shop at JYFL for their assistance and co-operation. I wish to thank all my other colleagues, as well.

I am indebted to Professor P. Lipas for revising the language of the manuscript. My thanks also go to Miss P. Pitkänen, who carefully typed this thesis, and to Mr. T. Näränen, who skillfully finished the drawings.

I finally wish to thank my wife and my daughter and son for their patience and support throughout my work.

For financial support I am indebted to the Emil Aaltonen Foundation and the Oskar Öflund Foundation.

Jyväskylä, June 1979

Matti Kortelahti

LEVEL STRUCTURE OF THE TRANSITIONAL ODD-MASS NUCLEI $^{141-149}Pm$

Abstract

The level structures of the five odd-mass nuclei $^{141-149}Pm$ have been studied by methods of in-beam γ-ray and electron spectroscopy using (p,xn) and (^3He,xn) reactions. Over twenty new levels were observed in each of the nuclei investigated. The spins of the levels range between 1/2 and 21/2. The missing isomeric $h_{11/2}$ state ($T_{1/2}$ = 12 ns) was observed in ^{147}Pm. Comparisons between experimental and theoretical results have been made. Calculations for all isotopes have been performed using the quasiparticle-vibration model with an intermediate coupling. Positive-parity levels can be interpreted as members of multiplets of the last odd proton coupled to the quadrupole vibrations of the core. The cluster-vibration model has been applied to Pm isotopes, specially to ^{145}Pm, under the assumption of the Z = 64 subshell closure. Positive-parity levels are explained very well when the cluster consists of three proton holes in the $g_{7/2}$ and $d_{5/2}$ shells. The results strongly support the assumption that the Z = 64 closure persists also for the Z = 61 promethium nuclei. The probable band structures of ^{149}Pm are discussed on the basis of calculations made using an axial particle-rotor model. The results on negative-parity levels are also compared with the predictions of the triaxial particle-rotor model.

Contents

1. INTRODUCTION

The odd-mass promethium isotopes are situated in the region ($A \lesssim 150$ and around the $N = 82$ shell) where the shape of nuclei is assumed to be transitional between spherical and deformed. The odd-A Pm nuclei investigated in this work have proton number $Z = 61$ and the neutron number varies between 80 and 88. In this region the isotopes behave very different ways and, as we shall see, no theoretical model can explain the characteristics of all the Pm nuclei. The nuclei which have the closed neutron shell $N = 82$ are supposed to be nearly spherical, and the lowest excitations are characterized by almost pure single-particle states. On the other hand, the $N = 88$ nuclei come near to being deformed because a sudden increase in deformation occurs in the neighbourhood of $N = 89$ and the $N = 90$ nuclei are strongly deformed with typical rotational bands.

The even-even nuclei in the transitional region are supposed to be vibrational nuclei performing small surface oscillations about a spherical equilibrium shape. The spectra of transitional odd-A nuclei are usually interpreted so that the last odd nucleon or hole is coupled to the core vibrations. The strength of the coupling is assumed to be something between weak and strong. Such an intermediate-coupling approach in the unified nuclear model has been used by various investigators in the region of $A \lesssim 150$. This model has been applied to $^{145,147,149}Pm$ by Choudhury[1] and to $^{147,149}Pm$ by Heyde and Brussaard[2]. However, both these groups have had few experimental results to adjust the parameters needed for the model and to make comparisons between experimental and theoretical results.

Another applicable vibrational model is the cluster-vibration model[3,4] which extends the above approach to nuclei with a few particles or holes outside a single closed shell. Here we have applied this model to odd $_{61}Pm$

isotopes under the assumption of a Z = 64 subshell closure[5] which persists even for nuclei with three protons off (Z = 61). The cluster consists of three proton holes in the Z = 50 - 64 shell.

An opposite approach to nuclei in this transitional region is to couple the particle motion to the rotations of the core nucleus[6]. The coupling of the particle to the rotor gives rise to rotational bands modified by the Coriolis interaction. The rotational approach is applied to odd-A transitional nuclei especially for unique-parity states which are based on high-spin single-particle configurations such as $h_{11/2}$, $h_{9/2}$, $i_{13/2}$, etc. These groups are easily identified experimentally since they are strongly populated in (α,xn) and (heavy ion, xn) reactions. The level spectra can alternatively be interpreted by coupling an odd nucleon in a single j shell to a triaxially deformed core[7]. Since axially symmetric nuclei cannot rotate around their symmetry axis, one obtains in the axially deformed nuclei normal-ordered rotational bands with $\Delta I = 1$ based on Nilsson states. The triaxial odd-A rotors can rotate around all intrinsic axes and the spectrum is composed of $\Delta I = 1$ and $\Delta I = 2$ bands. This triaxial model seems to be very suitable for interpreting the so-called decoupled bands with $\Delta I = 2$ which are built on unique-parity states. When the particle and core angular momenta are nearly aligned, the Coriolis force becomes very small and there is no longer an appreciable coupling between the particle and the core. Thus the differences in energy of these levels are just those of the core itself and $\Delta I = 2$. The unfavoured states with $\Delta I = 1$ are shifted to higher energies.

Knowledge of the structure of the odd-A Pm isotopes has been poor both experimentally and theoretically. Thus in the present study, by means of in-beam gamma and electron spectroscopy, we have collected data on these Pm nuclei for systematic comparisons. These experimental measurements and results comprise the first part of the present work. The experimental situation before this work is explained in connection with each nucleus investigated.

The last part of this study consists of theoretical predictions for Pm nuclei. These results we have calculated by using the quasiparticle-vibration model with an intermediate coupling, the cluster-vibration model, the axial particle-rotor model and the triaxial particle-rotor model. Main attention is paid to the intermediate-coupling model where the extra proton is coupled to the quadrupole vibrations of the core. The $g_{7/2}$, $d_{5/2}$, $d_{3/2}$, $s_{1/2}$ and $h_{11/2}$ orbitals are allowed for the particle. In the calculation of the matrix elements of the interaction between the core and the last proton we have taken into account the quasiparticle character of the active nucleons by including a factor $u_j u_{j'} - v_j v_{j'}$. These particle and hole amplitudes are taken from stripping and pick-up reaction experiments. In the previously mentioned calculations[1,2] only the $g_{7/2}$ and $d_{5/2}$ orbitals were allowed for the odd proton, and also the effects of pairing were ignored. With the aid of the calculated wave functions we have determined magnetic dipole and electric quadrupole moments, transition rates and spectroscopic factors. The calculations using the cluster-vibration model are presented in chapter 4.

In addition, we have calculated for ^{149}Pm, which behaves as a nearly stable deformed nucleus, excitations and electromagnetic transition rates by using an axial particle-rotor model[8]. The lowest experimental positive-parity states have been interpreted as the lowest excitations of the $1/2^+$[411], $3/2^+$[411] + $5/2^+$[402], $5/2^+$[413] + $7/2^+$[404] and $7/2^+$[413] rotational bands. Most of the negative-parity states belong to the $h_{11/2}$ band and these are compared with predictions of the axial particle-rotor model. We have also calculated the level order for the $h_{11/2}$ band using the triaxial particle-rotor model of Meyer-ter-Vehn[7]. The results of this calculation are presented in chapter 4.

This thesis is based on the following published papers and research reports:

1. M. Kortelahti, A. Pakkanen, M. Piiparinen, T. Komppa and R. Komu:
   Structure of odd-A Pm nuclei (I). ^{147}Pm
   Nucl. Phys. A288 (1977) 365
   https://doi.org/10.1016/0375-9474(77)90337-2

2. M. Piiparinen, M. Kortelahti, A. Pakkanen, T. Komppa and R. Komu:
   Structure of odd-A Pm nuclei (II). ^{141}Pm and ^{145}Pm
   Dept. of Physics, Univ. of Jyväskylä, Res. Report No. 6/1977

3. M. Kortelahti, M. Piiparinen, A. Pakkanen, T.Komppa, R. Komu,
   S. Brant, Lj. Udovičić and V. Paar:
   In-beam study of ^{145}Pm and the cluster-vibration model for odd Pm nuclei
   Dept. of Physics, Univ. of Jyväskylä, Res. Report No. 4/1979
   https://doi.org/10.1016/0375-9474(80)90554-0

4. M. Kortelahti, A. Pakkanen, M. Piiparinen, E. Hammarén, T. Komppa
   and R. Komu:
   In-beam study and the rotational description of low-lying levels
   in the N = 88 nucleus ^{149}Pm
   Dept. of Physics, Univ. of Jyväskylä, Res. Report No.8/1979
   https://doi.org/10.1016/0375-9474(79)90011-3

2. EXPERIMENTAL PROCEDURE

2.1. Singles γ-ray spectra and excitation functions

Odd-mass Pm nuclei were produced by (p,2n), (p,3n) and (^{3}He,3n) reactions using p and ^{3}He beams from the 90 cm cyclotron of the University of Jyväskylä. Self-supporting (0.8 - 1.1 mg/cm^2) targets of Nd and ^{141}Pr and also thicker ($\approx$ 10 mg/cm^2) targets of Nd_2O_3 and Pr_2O_3, mounted on mylar foils, were used. The target materials were enriched to 98 % in ^{142}Nd, to 93 % in ^{144}Nd, to 94 % in ^{145}Nd, to 95 - 98 % in ^{146}Nd, to 95 % in ^{148}Nd and to 96 % in ^{150}Nd. Natural Pr is isotopically pure ^{141}Pr. In order to study excitation functions of in-beam γ rays the energy of the proton beam was varied from 11.8 MeV to 20.4 MeV depending on the target. The energy of the ^{3}He beam was ranged from 19.0 MeV to 26.8 MeV.

The γ-ray spectra were measured employing 40, 55 and 70 cm^3 Ge(Li) and 0.5, 1.0 and 7.5 cm^3 hyperpure Ge detectors. The resolutions of the large coaxial Ge(Li) detectors were 1.9 - 2.7 keV FWHM at 1.33 MeV and that of the small Ge detectors was 600 eV FWHM at 122 keV energy.

The energies of the γ rays arising from the reactions were determined with the aid of the ^{152}Eu and ^{133}Ba sources, the transition energies of which are accurately known[9]. The peaks in both γ-ray and electron spectra were fitted to a convoluted Gaussian-plus-exponential function using the computer program KAMPI[10].

2.2. Angular distribution experiments

Angular distributions of γ rays were measured at six angles between $\theta = 90^o$ and $\theta = 161^o$ with respect to the beam line. The spectra were recorded with a large Ge(Li) or a hyperpure Ge detector positioned at a distance of 18 cm from the target. Another Ge(Li) detector was kept at a fixed 90^0 angle to the beam axis and served as a monitor detector. Two different methods were used for the normalization of the γ-ray spectra collected at various angles by the movable detectors: (i) normalization to the peak of an isomeric, isotropic γ-ray transition recorded by the movable detectors; and (ii) normalization to selected γ peaks in the monitor spectra measured simultaneously.

Many of these γ-ray angular distributions show large anisotropics (cf. fig. 3) that may be interpreted and well understood in terms of nuclear alignments. The incoming projectile together with the target forms an excited compound nucleus with a large component of angular momentum in the plane perpendicular to the beam direction. The decay of the compound system, initially by evaporation of neutrons and subsequently through the emission of γ rays, has little influence on this alignment so that the lower-lying states of the final nucleus still possess a large alignment. This gives a possibility to measure angular distributions of the γ transitions from these states.

The angular distribution of γ rays emitted from the aligned nuclear state can be expressed in terms of Legendre polynomials[11),

$$W(\theta) = A_0 + Q_2A_2P_2(\cos\theta) + Q_4A_4P_4(\cos\theta),$$

where θ is the angle of the detector with respect to the beam axis. The quantities Q_2 and Q_4 are geometrical coefficients due to the finite size of the detectors. The function $W(\theta)$ was fitted by the least-squares procedure to the experimental data using the program ANDIST[12). The magnitude and sign of the measured angular distribution coefficients A_2/A_0 and A_4/A_0 are sensitive to the spins involved in the transition. For example, pure dipole $\Delta I = 0$ transitions are characterized by a large positive A_2/A_0 and zero A_4/A_0, but $\Delta I = \pm 1$ by a negative A_2/A_0 and zero A_4/A_0, and the pure quadrupole $\Delta I = 2$ transitions by a positive A_2/A_0 and a smaller negative A_4/A_0. However, if the transition is not pure, the angular distribution coefficients are very sensitive to the multipole mixing ratio δ.

Attenuation of nuclear alignment is described by a parameter σ which characterizes the width of an assumed Gaussian distribution for the magnetic substates of each partially aligned nuclear state formed in (p,2n) and (^{3}He,3n) reactions. The attenuation coefficients α_2 and α_4 are determined[11)] by the relative width (σ/I_i) of the Gaussian distribution.

2.3. In-beam electron measurements

The electron spectra were measured using an intermediate-image magnetic plus Si(Li) electron spectrometer[13)]. The resolution for 300 - 700 keV electrons was better than 3.5 keV. Energy and efficiency calibrations were performed using thin radioactive sources of ^{152}Eu and ^{133}Ba. In addition to the prompt in-beam spectra, delayed components were also measured using the rf timing method described in sect. 2.5. The electron and γ-ray intensities were normalized to each other with the aid of some transition of known multipolarity. Since the mean acceptance angle of the electron spectrometer is $\theta \approx 50^0$, the effects caused by angular distributions of electrons can be ignored when the corresponding γ-ray spectra are measured at 125^0 to the beam line.

2.4. Gamma-gamma coincidence experiments

In order to establish the level schemes,three-parameter $\gamma\gamma$-time coincidence spectra were measured using two large-volume Ge(Li) detectors. In these experiments the two Ge(Li) detectors were placed at $\pm 125^{0}$ to the beam direction. The detectors were shielded with lead in order to reduce the scattering of γ rays from one detector into the other. The parameters were the two γ-ray energies and the time between the γ rays. The data were recorded event by event on magnetic tape during the experiment using[14] the computer PDP-11/45. The $\gamma\gamma$ coincidence spectra are obtained from subsequent off-line sorting of the tapes by setting gates on photopeaks. The events caused by the Compton continuum and chance coincidences were subtracted.

2.5. Lifetime measurements

Lifetime measurements of the excited states in the Pm nuclei were performed in the nanosecond region. Two different methods were applied for determining half-lives. The first method makes use of the natural beam structure of the cyclotron beam. A time-to-amplitude converter was started by the γ ray and stopped by the cyclotron radio-frequency (rf) signal, and the delay of γ rays between cyclotron beam pulses was measured. The data were stored in a two-parameter mode event by event on magnetic tape. The parameters are the γ-ray energy and the time between the γ ray and the beam burst. Both the small Ge and the large Ge(Li) detectors were used. With the 1 cm^3 Ge detector a slope of ≈ 0.7 ns in the time spectrum was obtained. The second method corresponds to the conventional delayed $\gamma\gamma$ coincidence technique. The signal of a NaI scintillation counter was used instead of the rf signal. In addition to the time spectra of certain γ rays we measured also delayed γ-ray spectra by setting several gates on the time spectrum.

3. MEASUREMENTS AND CONSTRUCTION OF LEVEL SCHEMES

3.1. The nucleus ^{141}Pm

The level structure of the ^{141}Pm nucleus has been previously studied only by the β decay[15] of ^{141m}Sm and ^{141g}Sm. No reaction data on ^{141}Pm have been published. The ground-state spin of ^{141}Pm has been measured to be 5/2 with an atomic beam method[16], and positive parity is strongly favoured by the shell model. Spins and parities for some low energy levels are proposed in ref. 15.

Singles γ-ray spectra were measured from the ^{142}Nd(p,2nγ)^{141}Pm reaction at bombarding energies E_p= 14.9, 15.8, 16.8, 17.8, 19.0 and 20.2 MeV and from the ^{141}Pr(^{3}He,3nγ)^{141}Pr reaction at $E_{^3He}$ = 19.0, 21.6, 23.9, 26.0 and 26.8 MeV. Fig. 1 shows a portion of one typical γ-ray spectrum measured at 125^o with respect to the beam direction.

Three-parameter ($\gamma\gamma$t) coincidence experiments were performed using two large Ge(Li) detectors. Coincidence measurements were made at 20.2 MeV in the (p,2nγ) reaction and at 26.8 MeV in the (^{3}He,3nγ) reaction. Four typical coincidence spectra are shown in fig. 2.

Measurements of short lifetimes were performed between natural cyclotron beam bursts using 1.0 and 7.5 cm^3 Ge detectors. We did not find any lifetimes measurable with this system (approximately 1-50 ns); the only delay we could find in ^{141}Pm was caused by the $h_{11/2}$ level at 628.8 keV. The half-life of this level[15] is known to be 0.59 ± 0.02 μs. Our lifetime result for the 777.4 keV transition from

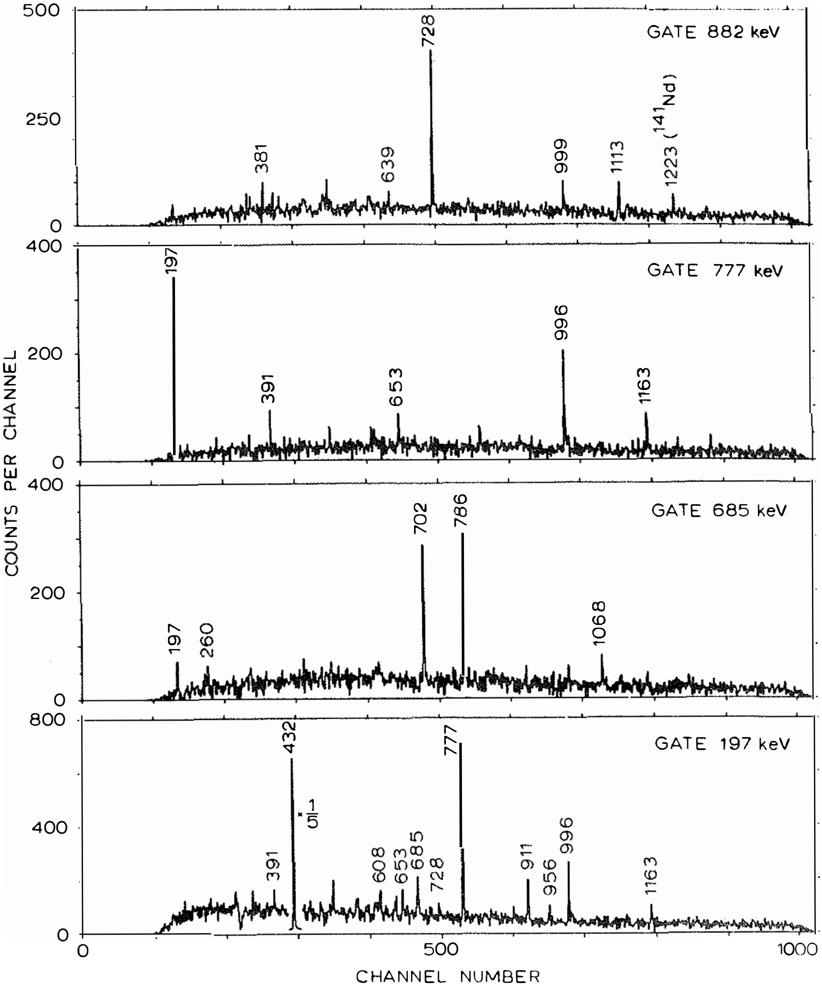

Fig. 2. Typical $\gamma\gamma$ coincidence spectra from the $^{141}Pr(^{3}He,3n\gamma)^{141}Pm$ reaction. The 1223 keV γ ray in the 882 keV gate arises from the contribution of the 886.3 keV ^{141}Nd transition in the gate.

the 974.3 keV level, $T_{1/2} < 1.0$ ns, strongly disagrees with the earlier result of 56 ± 11 ns measured using the delayed coincidence technique[17].

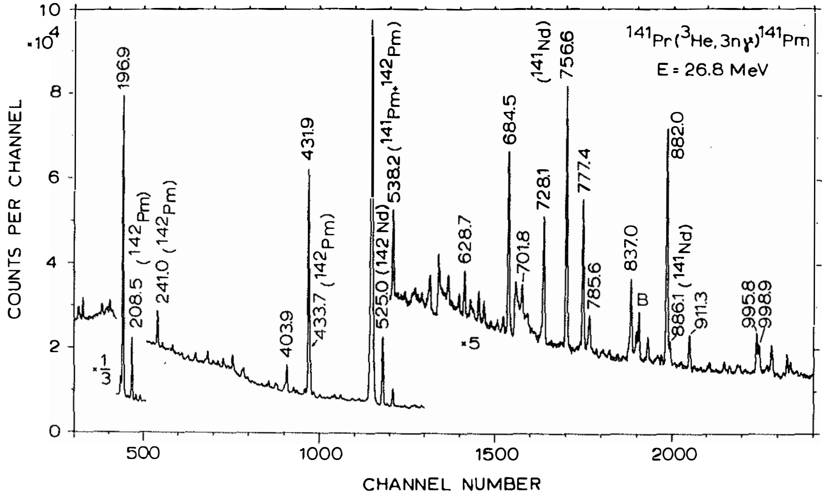

Fig. 1. A portion of a singles γ-ray spectrum arising from the ^{141}Pr(^{3}He,3nγ)^{141}Pm reaction measured at a 125^0 angle employing the 40 cm^3 Ge(Li) detector. Only prominent peaks are marked by energies; B = peaks caused by radioactivities or impurities in the target.

Two sets of γ-ray angular distribution experiments were made at angles of 90^0, 110^0, 125^0, 140^0, 150^0 and 161^0 with respect to the beam direction. The reactions and bombarding energies were the same as in the coincidence experiments. Some examples of experimental angular distributions of γ rays from the ^{142}Nd(p,2nγ)^{141}Pm reaction are shown in fig. 3.

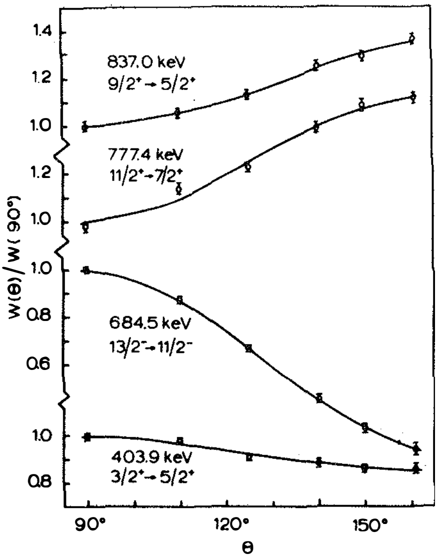

Fig. 3. Some typical γ-ray angular distributions from the $^{142}Nd(p,2n\gamma)^{141}$ reaction

Singles, prompt and delayed in-beam electron spectra were measured from the $^{141}Pr(^{3}He,3ne)$ reaction at an energy of 26.8 MeV. The conversion-electron spectra were normalized to γ-ray spectra with the aid of the 525.1 keV $4^{+} \rightarrow 2^{+}$ E2 transition in ^{142}Nd (from the reaction $^{141}Pr(^{3}He,pn)^{142}Nd$) and the 756.5 keV M4 transition in ^{141}Nd (from the reaction $^{141}Pr(^{3}He,2pn)^{141}Nd$). The multipolarities of the transitions were determined with the aid of conversion and angular distribution coefficients. The E2/M1 mixing ratio for a transition is given only if the conversion coefficient and the angular distribution results are in agreement.

Summaries of the γ-ray data and the measured α_K values are presented in tables 1 and 2.

Table 1. Energies E_γ, relative γ-ray intensities I_γ at 125^0 in the ^{142}Nd(p,2nγ)^{141}Pm and ^{141}Pr(^{3}He,3nγ)^{141}Pm reactions and assignments of the transitions in the ^{141}Pm level scheme. The uncertainties of the last figures are in parentheses.

E_γ (keV)	Relative γ intensity (p,2nγ) E = 20 MeV	(^{3}He,3nγ) E = 27 MeV	Assignment E_i - E_f
170.1 (3)		19(4)	
196.88(5)	1860(90)	1392(70)	196.9 - 0
197.5 (5)[a)]		6(4)[a)]	1510.8 - 1313.3
247.5 (4)	15(4)	8(3)	1414.5 - 1167.0
260.3 (4)		14(3)	1573.6 - 1313.3
324.53(15)	93(9)	25(4)	728.3 - 403.9
347.6 (4)		19(3)	
354.8 (5)		11(3)	
381.2 (3)		22(3)	1892.0 - 1510.8
391.3 (3)		18(3)	2361.4 - 1970.1
401.5 (3)		22(3)	2640.4 - 2238.9
403.85(10)	426(22)	106(10)	403.9 - 0
431.9 (3)	1000	1000	628.8 - 196.9
438.45(20)	107(10)	15(3)	438.5 - 0
531.4 (4)	37(7)	13(3)	728.3 - 196.9
538.2 (3)	184(24)	89(14)	1167.0 - 628.8
604.4 (4)	22(5)		1008.3 - 403.9
608.3 (3)	56(6)	33(4)	805.2 - 196.9
628.7 (3)	59(6)	63(6)	628.8 - 0
639.2 (5)		21(4)	2531.2 - 1892.0
640.2 (5)	24(5)		837.0 - 196.9
653.4 (5)		35(4)	2623.5 - 1970.1
661.7 (5)	24(5)	7(3)	858.6 - 196.9
684.49(10)	193(12)	305(18)	1313.3 - 628.8
701.8 (3)	28(6)	49(6)	2015.1 - 1313.3
707.6 (5)	17(3)	21(3)	
725.4 (4)	141(11)	19(5)	
728.1 (3)	102(8)	29(6)[a]	1132.0 - 403.9
728.1 (3)		206(14)	2238.9 - 1510.8

Table 1. (cont.)

E_γ (keV)	Relative γ intensity (p,2nγ) E = 20 MeV	(^{3}He,3nγ) E = 27 MeV	Assignment E_i - E_f
749.0 (4)	54(9)		1152.7 - 403.9
777.38(10)	340(24)	306(18)	974.3 - 196.9
785.6 (5)[b]	121(20)	77(11)	2098.9 - 1313.3
837.00(10)	387(27)	181(14)	837.0 - 0
858.55(15)	190(15)	54(8)	858.6 - 0
882.03(15)	177(14)	584(40)	1510.8 - 628.8
911.33(20)	172(14)	91(8)	1108.2 - 196.9
955.7 (6)[b]	72(14)	25(7)	1152.7 - 196.9
962.6 (5)	22(4)	10(3)	
995.8 (3)	40(6)	125(11)	1970.1 - 974.3
998.9 (4)	20(4)	74(7)	2509.7 - 1510.8
1037.2 (5)	52(8)	42(6)	1874.2 - 837.0
1067.9 (6)		32(5)	2381.2 - 1313.3
1108.2 (6)	24(5)	15(3)	1108.2 - 0
1112.6 (5)		46(7)	2623.5 - 1510.8
1163.0 (10)[b]	87(17)	64(12)	2137.3 - 974.3

a) From coincidence data; interfering lines in singles spectra.

b) Doublet peak.

Table 2. Experimental conversion coefficients α_K measured in the $^{141}Pr(^{3}He,3n)^{141}Pm$ reaction, angular distribution coefficients of transitions in the $^{142}Nd(p,2n\gamma)^{141}Pm$ and $^{141}Pr(^{3}He,3n\gamma)^{141}Pm$ reactions, and inferred transition multipolarities and E2/M1 mixing ratios. The uncertainties of the last figures are in parentheses.

E_γ (keV)	α_K ($\times 10^{-2}$)	$^{142}Nd(p,2n\gamma)^{141}Pm$ A_2/A_o	A_4/A_o	$^{141}Pr(^{3}He,3n\gamma)^{141}Pm$ A_2/A_o	A_4/A_o	Multi-polarity	δ(E2/M1)
196.9		-0.01(1)	0.00(1)	-0.01(2)	0.02(3)	M1[a]	
324.5		-0.11(3)	0.05(4)			(M1)	
403.9	2.5 (4)	-0.11(1)	0.02(2)	-0.07(3)	-0.04(4)	M1+E2	
431.9	7.7(15)	0.00(1)	0.02(2)	0.01(1)	0.01(1)	M2	
438.5		-0.07(7)	0.05(10)			E2[a]	
531.4		0.23(4)	-0.14(5)			(M1+E2)	-0.9(3)
538.2[b]	1.2(3)	-0.35(2)	≈0	-0.26(2)	≈0	M1+E2	
608.3	0.5(2)					(E2)	
628.7	1.4(2)			0.07(8)	0.11(12)	E3	
653.4	0.64(12)					E2(+M1)	
684.5	0.62(8)	-0.83(3)	0.09(2)	-0.71(3)	0.09(2)	M1+E2	-0.87(8)
701.8	0.61(11)			-0.66(6)	0.26(10)	M1+E2	-1.6 (3)
728.1	0.40(7)			0.07(2)	0.02(3)	E2	
777.4	0.38(6)	0.32(2)	-0.06(3)	0.18(2)	-0.00(2)	E2	
785.6		-0.35(3)	0.08(4)	-0.48(5)	0.05(9)	M1+E2	-0.19(8)
837.0	0.21(5)	0.24(2)	-0.00(2)			E2	
858.6	0.37(7)	0.30(2)	≈0			M1+E2	1.2 (2)
882.0	0.24(4)	0.27(4)	-0.06(6)	0.23(2)	-0.05(3)	E2	
911.3	0.16(5)	0.06(4)	0.08(5)			(E2)	
955.7		-0.20(6)	≈0			M1+E2	-0.07(5) or 4.0(3)
995.8	} 0.15(6)			0.42(9)	≈0	(E2)	
998.9							

a) Assignments from ref. 15.

b) Contains a contribution from ^{142}Pm, which is of E1 character (ref. 18).

The construction of the level scheme was based primarily on the $\gamma\gamma$ coincidence data, the transition intensities and on the excitation functions of the γ rays. The spins and parities of the states are based on conversion-electron measurements and angular distributions of the γ rays. The level scheme of ^{141}Pm is shown in fig. 4. The observed coincidences are marked by dots. The two lowest states in ^{141}Pm are $5/2^+$ and $7/2^+$ with main configurations of $d_{5/2}$ and $g_{7/2}$. At 403.9 and 438.5 keV Kennedy et al.[19] have reported $3/2^+$ and $(1/2)^+$ levels which are confirmed in this work. The excitation functions favour the spin assignment 1/2 for the 438.5 keV level.

An isomeric level of 0.59 ± 0.02 μs has been known[15] in ^{141}Pm at 628.8 keV and it has been assigned to the $h_{11/2}$ level mainly from the systematics of odd-mass Pm nuclei. Now we can confirm the spin assignment from the inferred M2 and E3 multipoles of the 432.1 and 628.7 keV transitions depopulating the 628.8 keV level.

Kennedy et al.[19] have reported a level at 728.3 keV decaying to the ground state and to the 403.9 keV level. We assign $5/2^+$ to this level which decays also to the 196.9 keV level. The decay mode 728.3 keV → 0 we cannot confirm because the strong 728.1 keV line has been placed twice in the level scheme of ^{141}Pm on the basis of the coincidence relationships.

The 974.3 keV level we have assigned as $11/2^+$. Eppley et al.[20] have reported a weak 974.3 keV → 0 transition, but we cannot find this γ ray, and our spin and parity assignment is strongly against the existence of this transition because it should be of an M3 character.

We have located several high-spin negative-parity levels in ^{141}Pm. At least the $13/2^-$ level at 1313.3 keV, the $15/2^-$ level at 1510.8 keV and the $(19/2)^-$ level at 2238.9 keV most probably belong to a band built on the $h_{11/2}$ state.

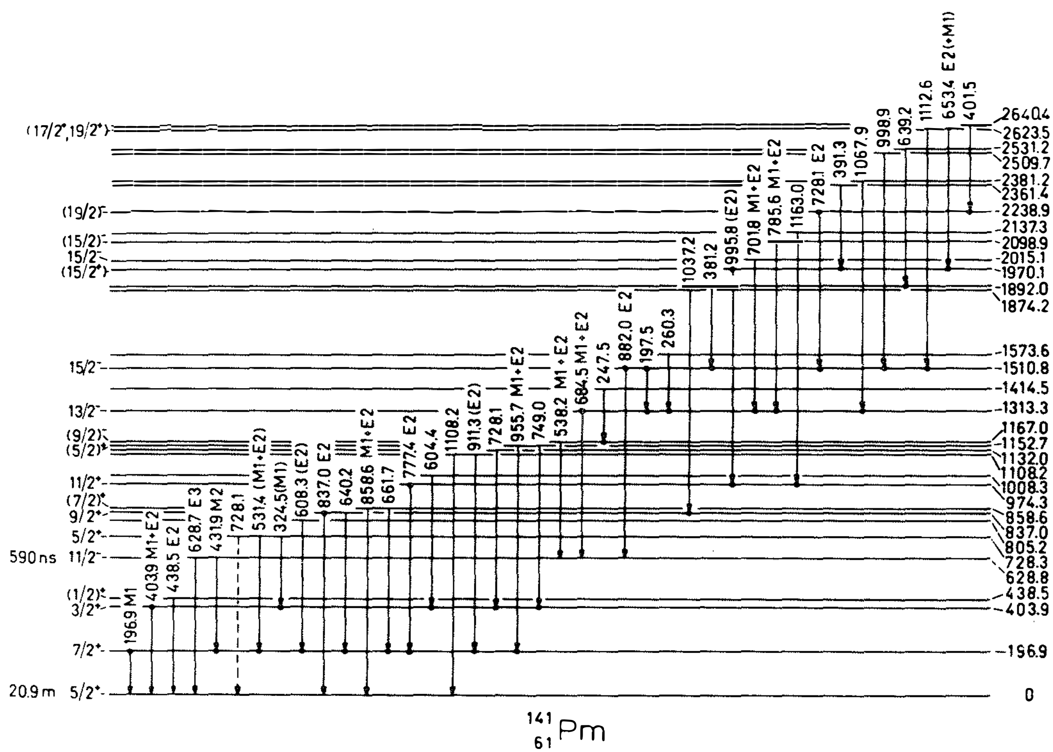

Fig. 4. Level scheme of ^{141}Pm based on the present study of the ^{142}Nd(p,2n)^{141}Pm and ^{141}Pr(^{3}He,3n)^{141}Pm reactions. Energies of levels and transitions are in keV. The observed $\gamma\gamma$ coincidence relations are marked by dots.

3.2. The nucleus ^{143}Pm

When we started our study we had knowledge of only six excited states in ^{143}Pm. From the β decay and from the $^{141}Pr(\alpha,2n\gamma)^{143}Pm$ reaction[21,22,23] the following levels were known: $7/2^+$ at 272, $11/2^-$ at 960, $3/2^+$ at 1057 and $(13/2)^-$ at 1664 keV. Furthermore, Wildenthal et al.[24] have proposed a $1/2^+$ level at 1170 and a $3/2^+$ level at 1400 keV from the $^{144}Sm(d,^3He)^{143}Pm$ and $^{142}Nd(^3He,d)^{143}Pm$ reactions. Recently Nagai et al.[25] have published their in-beam conversion-electron study. They suggest a spin $11/2^+$ to the 1664 keV level. The ground-state spin of ^{143}Pm has been determined to be 5/2 with the method of low-temperature nuclear orientation[26].

Singles γ-ray spectra were measured from the $^{144}Nd(p,2n\gamma)^{143}Pm$ reaction at energies E_p = 15.8, 17.8, 19.0, 19.6, 20.2 and 20.4 MeV and from the $^{145}Nd(p,3n\gamma)^{143}Pm$ reaction at E_p = 20.4 MeV. Some excitation functions of γ transitions from the first reaction are shown in fig. 5.

Gamma-gamma coincidence measurements were performed using 40 and 55 cm^3 Ge(Li) detectors at a proton energy of 20.2 MeV. Four of these coincidence spectra are shown in fig. 6.

The time measurements were performed by using 1.0 cm^3 Ge and 40 cm^3 Ge(Li) detectors. We measured the half-life 24.0 ± 1.0 ns for the $h_{11/2}$ level at 959.8 keV, and the 234.9 keV transition gave a half-life of $T_{1/2}$ = 10.3 ± 0.5 ns for the 1663.5 keV level. Both results are in agreement with the previous values measured by Fromm et al.[23].

The angular distribution experiments were made at angles of 90^0, 110^0, 125^0, 140^0, 150^0 and 161^0. The proton energy was 20.4 MeV. The angular distribution coefficients of the most intense single γ rays from the $^{144}Nd(p,2n\gamma)^{143}Pm$ reaction are presented in table 3.

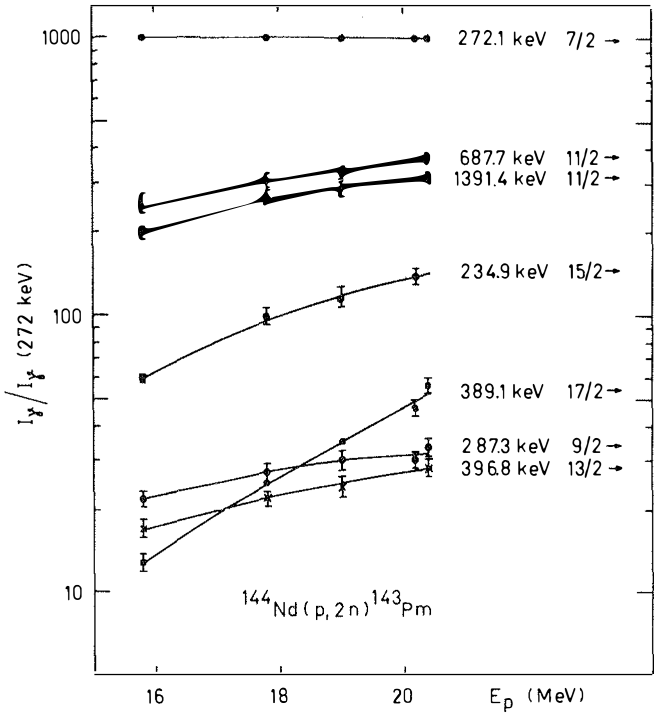

Fig. 5. Excitation functions of some γ transitions from the $^{144}Nd(p,2n)$ reaction

In-beam conversion-electron spectra were measured at E_p = 20.0 MeV. Fig. 7 presents a portion of a singles spectrum. The intensities of conversion electrons were normalized to γ-ray spectra with the aid of the 618.0 keV $4^+ \rightarrow 2^+$ transition in ^{144}Nd, present in the spectra from the $^{144}Nd(p,p')$ reaction. The experimental K conversion coefficient $\alpha_K(E2) - 5.7 \pm 0.8) \times 10^{-3}$ was used for normalization[27]. The multipolarities of the transitions were determined with the aid of conversion and angular distribution coefficients. The results of the γ-ray and electron data are presented in table 3.

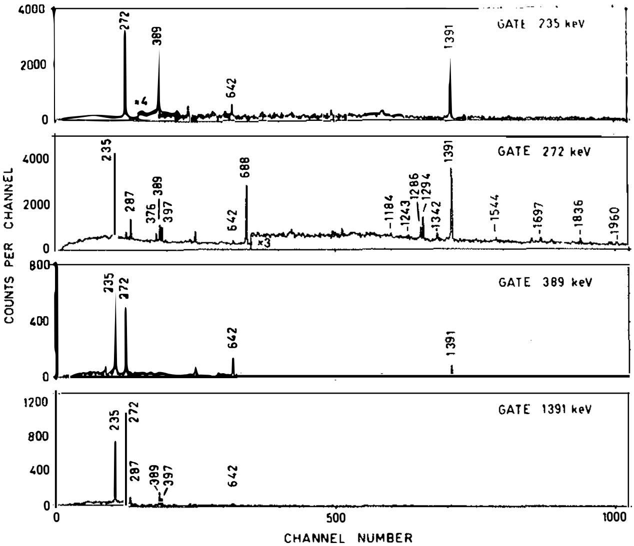

Fig. 6. Typical γγ coincidence spectra from the ^{144}Nd(p,2nγ)^{143}Pm reaction

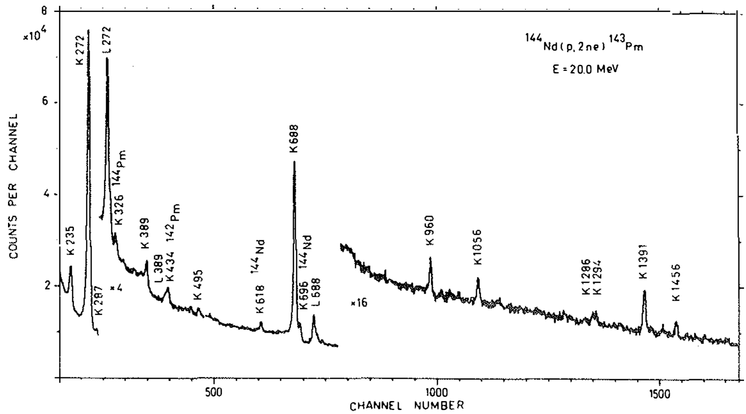

Fig. 7. A portion of an in-beam singles conversion-electron spectrum from the ^{144}Nd(p,2ne) reaction

Table 3. Energies E_γ, relative γ-ray intensities I_γ at 125°, conversion coefficients α_K, angular distribution coefficients and multipolarities of transitions in the ^{144}Nd(p,2nγ)^{143}Pm reaction. The uncertainties of the last figures are in parentheses.

E_γ (keV)	I_γ (E_p = 20.2 MeV)	α_K $\times 10^{-2}$	A_2/A_o	A_4/A_o	Multi-polarity	Assignment $E_i - E_f$, $J_i^\pi \to J_f^\pi$
83.41(8)	1.9 (10)					3013.3 - 2929.9, $(21/2) \to 19/2^-$
104.70(7)	2.4 (10)					
145.55(9)	4.5 (10)					
154.0(1)	1.9 (10)					
193.4(1)	3.5 (10)					
234.93(6)	130 (10)	8.6(9)			E2	1898.4 - 1663.5, $15/2^+ \to 11/2^+$
272.10(5)	1000	7.5(8)	-0.016(6)	-0.013(9)	M1+E2	272.1 - 0 , $7/2^+ \to 5/2^+$
287.32(6)	33(5)	2.2(3)	-0.21(2)	≈0	E1	1950.8 - 1663.5, $9/2^- \to 11/2^+$
296.0(1)	5.6(10)					
357.4(1)	4.8(6)					
376.54(10)	27(5)	1.1(5)	-0.21(3)	≈0	E1	1942.5 - 1566.0, $(7/2,9/2)^- \to (5/2,7/2)^+$
389.10(12)	45(5)	2.2(5)	-0.21(3)	≈0	M1(+E2)	2287.5 - 1898.4, $17/2^+ \to 15/2^+$
396.85(12)	25(5)	0.6(2)	-0.14(2)	-0.05(4)	E1	2060.3 - 1663.5, $13/2^- \to 11/2^+$
494.1(2)	19(5)	1.3(4)			(E2+M1)	
518.3(2)	13(4)					
642.4(2)	23(5)	<0.4	-0.16(3)	≈0	E1	2929.9 - 2287.5, $19/2^- \to 17/2^+$
687.2(4)	40(15) [a)]					
687.7(4)	310(50)	1.8(5)			M2	959.8 - 272.1, $11/2^- \to 7/2^+$
767.8(2)	18(4)					1824.3 - 1056.5, $(3/2,5/2) \to 3/2^+$
797.4(2)	10(3)					1853.9 - 1056.5, $(3/2,5/2) \to 3/2^+$
959.8(2)	70(10)	0.30(15)	0.04(2)	-0.03(3)	E3	959.8 - 0 , $11/2^- \to 5/2^+$

Table 3. (cont)

E_γ (keV)	I_γ (E_p = 20.2 MeV)	α_K $\times 10^{-2}$	A_2/A_o	A_4/A_o	Multi-polarity	Assignment $E_i - E_f$, $J_i^\pi - J_f^\pi$
983.2(2)	20(6)		0.12(1)	0.02(2)		
991.1(2)	9(3)					1950.8 - 959.8, $9/2^- \to 11/2^-$
1056.5(3)	110(15)	0.12(6)	-0.05(1)	-0.03(2)	E2(+M1)	1056.5 - 0 , $3/2^+ \to 5/2^+$
1173.1(3)	21(5)					1173.1 - 0 , $1/2^+ \to 5/2^+$
1184.3(3)	12(3)					1456.4 - 272.1
1242.7(3)	10(2)					1515.0 - 272.1, $(5/2,7/2)^+ \to 7/2^+$
1278.4(3)	16(3)					
1286.4(3)	40(8)	0.09(2)			E2(E1)	1558.5 - 272.1, $(3/2,5/2) \to 7/2^+$
1293.9(3)	68(10)	0.07(2)	-0.24(2)	-0.03(4)	E2+M1	1566.0 - 272.1, $(5/2,7/2)^+ \to 7/2^+$
1342.0(3)	30(7)					1614.1 - 272.1, $(3/2,5/2) \to 7/2^+$
1391.4(3)	260(50)	0.09(2)	0.20(1)	-0.05(2)	E2	1663.5 - 272.1, $11/2^+ \to 7/2^+$
1402.5(4)	30(5)	0.08(2)			E2	1402.5 - 0 , $(3/2,5/2)^+ \to 5/2^+$
1456.4(4)	115(15)	0.06(2)	0.22(1)	-0.03(2)	(E2,E1)	1456.4 - 0
1477.4(4)	32(8)	0.09(2)	0.39(4)	≈0	E2	2437.2 - 959.8, $15/2^- \to 11/2^-$
1515.0(4)	25(7)	0.10(3)			M1+E2	1515.0 - 0 , $(5/2,7/2)^+ \to 5/2^+$
1527.4(5)	15(5)					
1544.3(5)	18(6)					1816.4 - 272.1, $(3/2,5/2) \to 7/2^+$
1566.0(5)	28(6)	0.10(3)			M1+E2	1566.0 - 0 , $(5/2,7/2)^+ \to 5/2^+$
1667.4(5)	20(5)					
1697.5(5)	32(6)					1969.6 - 272.1
1735.7(6)	30(8)					2007.8 - 272.1
1824.8(6)	40(8)					1824.3 - 0 , $(3/2,5/2) \to 5/2^+$
1836.2(6)	50(10)					2108.3 - 272.1, $(3/2,5/2) \to 7/2^+$
1960.4(6)	35(10)					2232.5 - 272.1, $(3/2,5/2) \to 7/2^+$
1977.6(6)	38(10)					

The level scheme of ^{143}Pm is shown in fig. 8. All the levels were established by observed $\gamma\gamma$ coincidences except the 3013.3 level. The spins and parities of the states are based on conversion-electron measurements, angular distributions and excitation functions of the γ rays.

An isomeric level at 959.8 keV has been known in ^{143}Pm and it has been assigned to the $h_{11/2}$ state on the basis of (^3He,d) and (d,^3He) reactions[24]. We can confirm this spin because we obtained from the electron measurements an M2 and E3 multipolarity for the 687.7 and 959.8 keV transitions, respectively, which depopulate the 959.8 keV level.

Schibata et al.[22] have reported a $13/2^-$ state at 1664 keV. The spin was proposed on the basis of the E3 character of the 1392 keV transition from this level. Both their angular distribution and the conversion coefficients gave support to the $13/2^-$ assumption. However, we measured the conversion coefficient $\alpha_K = (0.9 \pm 0.2) \times 10^{-3}$ and the angular distribution coefficients $A_2/A_0 = 0.20 \pm 0.01$ and $A_4/A_0 = -0.05 \pm 0.02$ for the 1391.4 keV transition. All these coefficients support an E2 character for this transition and a spin $11/2^+$ for the 1663.5 keV level. The $11/2^+$ assignment is in agreement with the measurements of Nagai et al.[25].

Shibata et al.[22] and Nagai et al.[25] have proposed a level at 2054 keV which decays by the 389 keV γ ray. We cannot confirm this level because the 389.1 keV transition is in coincidence with the 234.9 keV γ ray which depopulates the isomeric level at 1898.4 keV ($T_{1/2} = 10.3 \pm 0.5$ ns).

We have observed several high-spin negative-parity states in ^{143}Pm. The $13/2^-$ level at 2060.3 keV, the $15/2^-$ level at 2437.2 leV and the $19/2^-$ level at 2929.9 keV most probably belong to a band built on the $h_{11/2}$ level. We also find a strong cascade connecting the positive-parity states $17/2^+$ (2287.5 keV), $15/2^+$ (1898.4 keV) and $11/2^+$ (1663.5 keV).

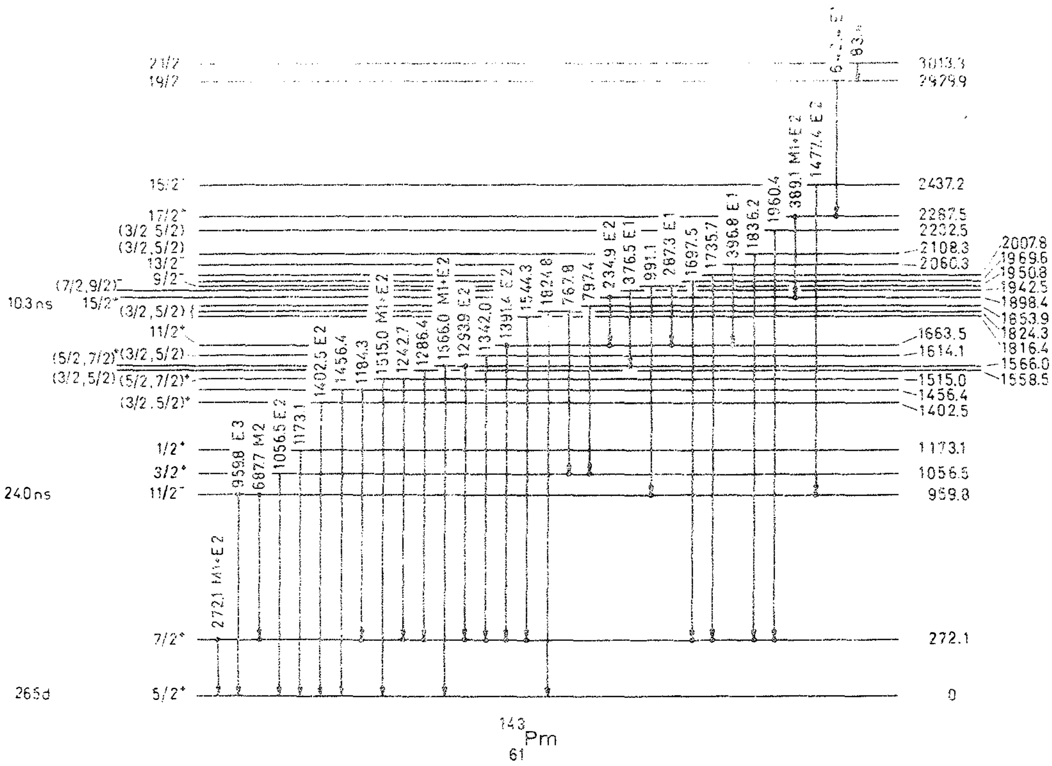

Fig. 8. Level scheme of ^{143}Pm based on the present study of the ^{144}Nd(p,2nγ), ^{144}Nd(p,2ne) and ^{145}Nd(p,3nγ) reactions. Energies of levels and transitions are in keV. The observed γγ coincidence relations are marked by dots.

During the course of this work Andrejtscheff et al.[28] have reported their study of ^{143}Pm by the ^{143}Nd(d,2n)^{143}Pm and ^{141}Pr(α,2n)^{143}Pm reactions. Their polarization experiments establish an E2 character for the 1391.4 keV transition. Their other results containing the level scheme of ^{143}Pm are consistent with ours except for the 1286.7 keV level. We observed that the 1286.4 keV γ ray is in coincidence with the 272.1 keV transition and we therefore suggest a 1558.5 keV level. The 3013.3 keV high-spin state that was suggested only on the basis of the excitation function is confirmed in ref. 28.

3.3. The nucleus ^{145}Pm

The level structure of the nucleus ^{145}Pm has been very poorly known From the β decay of ^{145}Sm only four levels were proposed[29,30]: $5/2^{(+)}$ ground state, $(7/2^+)$ at 61.2 keV, an uncertain level at 120.8 keV and $(3/2)^+$ at 492.3 keV. In a study[29] of the reactions ^{144}Nd(^{3}He,d)^{145}Pm and ^{144}Nd(α,t)^{145}Pm, the energies of 13 levels in ^{145}Pm were listed without any spin or parity assignments. During the course of this work Shibata et al.[31] have published their study of ^{145}Pm from the ^{145}Nd(p,nγ)^{145}Pm and ^{144}Nd(^{3}He,d)^{145} reactions. They located the missing $h_{11/2}$ isomer at 794.9 keV with a half-life of 18.3 ns and five other new levels. Recently Nagai et al.[25] have published their in-beam conversion-electron study of several nuclei. They have gained only a few new results on ^{145}Pm from the ^{145}Nd(p,ne)^{145}Pm reaction.

Singles γ-ray spectra were measured from the ^{146}Nd(p,2nγ)^{145}Pm reaction at bombarding energies E_p = 14.9, 15.8, 16.8, 17.0, 19.0 and 20.2 MeV. Fig. 9 shows a portion of a typical γ-ray spectrum measured at 125^o. Three-parameter ($\gamma\gamma$t) coincidence experiments were performed using two Ge(Li) detectors. The energy of the beam was E_p = 14.9 MeV. Three of these coincidence spectra are shown in fig. 10.

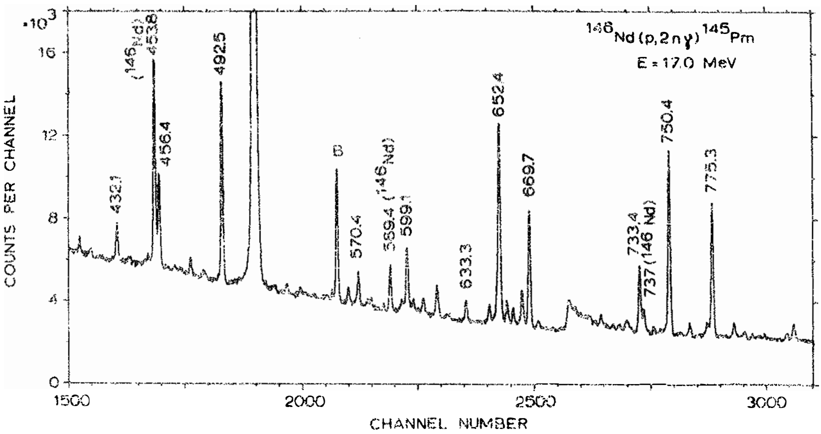

Fig. 9. A portion of a singles γ-ray spectrum arising from the $^{146}Nd(p,2n\gamma)$ ^{145}Pm reaction measured at a 125^{o} angle, employing the 7.5 cm^3 hyperpure Ge detector. Only prominent peaks are marked by energies; B = peaks caused by radioactivities or impurities in the target.

In the nanosecond lifetime experiment on ^{145}Pm, the 733.4 and 750.4 keV transitions gave a half-life of $T_{1/2}$ = 16.3 ± 1.5 ns for the 794.6 keV 11/2$^-$ level, which is consistent with the result of Shibata et al.[31]. The 61.2 keV transition gave a half-life of 2.5 ± 0.3 ns for the 61.2 keV level, consistent with the adopted value 2.62 ns from earlier measurements[29].

The angular distribution experiments were made at the same angles as those mentioned in the preceding section. The beam energy was 16.8 MeV.

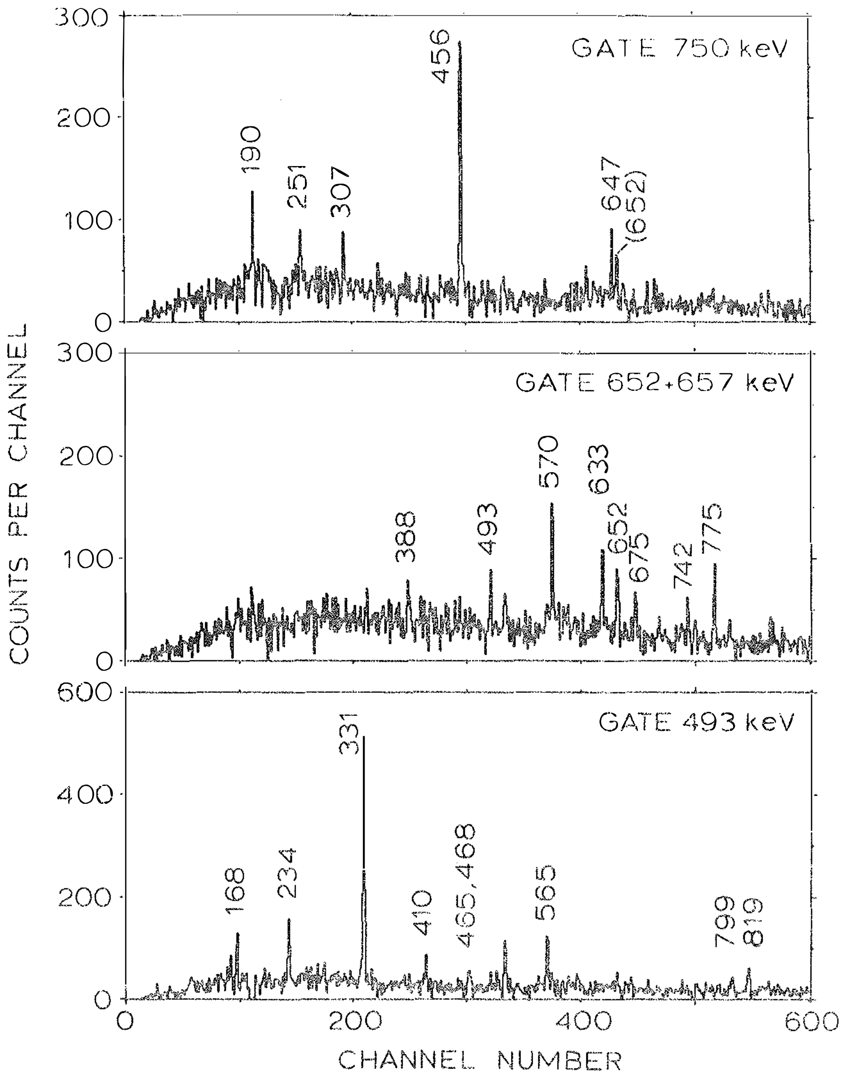

Fig. 10. Typical γγ coincidence spectra from the ^{146}Nd(p,2nγ)^{145}Pm reaction

Singles, prompt and delayed in-beam electron spectra were measured from the ^{146}Nd(p,2ne) reaction using an energy of 14.9 MeV. Fig. 11 shows an example of the singles electron spectra. The conversion-electron spectra were normalized to γ-ray spectra with the aid of the 750.4 keV transition which was supposed to be of a pure E2 character[25,31).

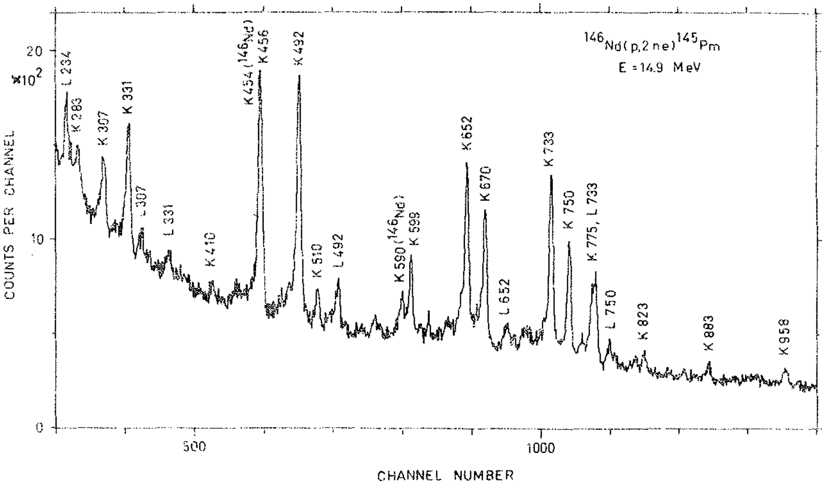

Fig. 11. A portion of in-beam singles conversion-electron spectra from the ^{146}Nd(p,2ne)^{145}Pm reaction

A summary of the γ-ray data and the measured conversion coefficients is presented in table 4. The multipolarities of the transitions were determined with the aid of conversion and angular distribution coefficients. The E2/M1 mixing ratio for a transition is given only if the conversion coefficient and the angular distribution results are in agreement.

Table 4. Energies E_γ, relative γ-ray intensities I_γ at 125°, experimental conversion coefficients α_K, K/L ratios, angular distribution coefficients and multipolarities of transitions from the $^{146}Nd(p,2n\gamma)^{145}Pm$ reaction. The uncertainties of the last figures are in parentheses.

E_γ (keV)	I_γ (E_p = 15.8 MeV)	α_K ($\times 10^{-2}$)	K/L	A_2/A_o	A_4/A_o	Multi-polarity	δ(E2/M1)	Assignment $E_i - E_f$
61.23(5)	410(50)			-0.05(1)	-0.03(2)	M1+E2		61.2 - 0
80.76(5)	35(5)							750.4 - 669.7
112.10(5)	8(2)							
122.80(5)	15(2)							(836.5 - 713.6)
146.9(2)	10(2)							
153.78(5)	21(3)							823.5 - 669.7
155.15(4)	27(3)							1502.0 - 1346.9
168.04(5)	63(5)							660.5 - 492.5
190.35(5)	106(10)			-0.15(3)	≈0	M1		1397.2 - 1206.8
223.50(8)	47(4)							883.8 - 660.5
234.00(6)	80(10)							726.5 - 492.5
246.5 (1)	20(4)							
251.48(7)	105(10)			-0.16(1)	0.09(2)			1648.7 - 1397.2
283.17(7)	43(4)	7.0(12)				M1+E2		1384.9 - 1101.8
307.26(8)	80(10)	6.2(9)		-0.26(3)	-0.12(5)	M1+E2	0.34(5)	1101.8 - 794.6
331.00(8)	190(15)	5.6(7)	6.8(6)			M1(+E2)		823.5 - 492.5
370.3(4)	26(7)							1206.8 - 836.5
388.1(4)	28(7)							1101.8 - 713.6
410.4(2)	60(10)	1.9(4)				E2(+M1)		1233.9 - 823.5
432.1(2)	120(12)	0.6(2)		-0.11(6)	≈0	E1		1101.8 - 669.7
456.4(2)	250(15)	2.5(4)		-0.07(2)	≈0	M1+E2	0.07(1)	1206.8 - 750.4
465.5(4)	35(8)							958.0 - 492.5

Table 4. (cont.)

E_γ (keV)	I_γ (E_p = 15.8 MeV)	α_K ($\times 10^{-2}$)	K/L	A_2/A_0	A_4/A_0	Multi-polarity	δ(E2/M1)	Assignment E_i - E_f
468.4(3)	35(8)							1291.9 - 823.5
492.5(3)	1000	1.7(2)	6.2(5)	-0.004(9)	0	M1(+E2)		492.5 - 0
493.2(5)	45(7)[a]							1206.8 - 713.6
510.4(4)[b]	90(15)[a]	1.7(4)				(M1+E2)		1346.9 - 836.5
529.4(3)	42(5)							1365.9 - 836.5
537.0(4)	50(7)							1206.8 - 669.7
545.5(4)	21(5)							1215.2 - 669.7
564.8(3)	134(14)	1.1(2)		-0.06(6)	0.09(9)	M1+E2		1057.3 - 492.5
570.4(3)	180(15)	0.3(1)		-0.09(8)	≈0	E1		1284.0 - 713.6
599.1(5)	660(50)	0.79(15)				(M1+E2)		660.5 - 61.2
608.6(4)	180(15)							669.7 - 61.2
616.4(4)	260(20)	0.38(12)		-0.04(2)	≈0	E1		
622.3(4)	50(7)							1291.9 - 669.7
633.3(3)	120(15)	0.4(2)		0.23(3)	0.03(5)	E2(+M1)		1346.9 - 713.6
646.8(4)	130(15)			0.18(6)	-0.05(8)	E2		1397.2 - 750.4
652.4(4)	95(15)[a]							1365.9 - 713.6
652.4(4)	1800(100)	0.46(15)	7.6(5)	0.25(1)	0.00(1)	M1+E2	0.63(3)	713.6 - 61.2
657.1(5)	105(10)			-0.29(6)	0.08(9)	M1(+E2)		1493.6 - 836.5
660.5(5)	160(15)			-0.19(5)	≈0	M1(+E2)		660.5 - 0
665.5(4)	240(20)			0.26(4)	≈0	E2(+M1)		1502.0 - 836.5
669.7(3)	940(50)	0.80(10)	6.8(8)	0.13(1)	-0.00(2)	M1+E2	0.44(7)	669.7 - 0
674.9(5)	40(10)							1388.5 - 713.6
711.1(4)	140(15)							
721.8(5)	50(10)							1558.3 - 836.5
733.4(3)	520(50)	2.0(3)		0.06(3)	≈0	M2		794.6 - 61.2

Table 4. (cont.)

E_γ (keV)	I_γ (E_p = 15.8 MeV)	α_K ($\times 10^{-2}$)	K/L	A_2/A_o	A_4/A_o	Multi-polarity	δ(E2/M1)	Assignment E_i - E_f
742.1(5)	50(10)							1455.7 - 713.6
750.4(3)	1540(80)	0.376[c]	6.2(12)	0.134(4)	-0.022(5)	E2[d]		750.4 - 0
762.3(4)	110(15)	0.56(12)				M1+E2		823.5 - 61.2
775.3(3)	1250(60)	0.45(10)		0.18(1)	-0.06(1)	E2		836.5 - 61.2
794.6(5)	25(10)[e]							794.6 - 0
799.4(5)	40(8)							1291.9 - 492.5
819.2(5)	120(15)							1311.7 - 492.5
822.7(5)	210(20)	0.37(10)				E2+M1		883.8 - 61.2
883.8(3)	250(30)	0.38(10)		0.31(3)	-0.05(5)	E2+M1	1.1(4)	883.8 - 0
958.0(4)	390(40)	0.30(10)		-0.06(3)	0.06(4)	M1+E2		958.0 - 0
1040.7(5)	140(15)							1101.8 - 61.2
1154.1(5)	42(8)							1215.2 - 61.2
1215.2(5)	150(15)							1215.2 - 0
1224.7(5)	90(15)							
1228.8(5)	140(20)							
1233.6(5)	115(15)							1233.9 - 0
1244.4(5)	155(20)							
1300.8(5)	160(20)							
1311.7(6)	65(10)							1311.7 - 0

a) From coincidence data; interfering lines in singles spectra.

b) From electron measurements.

c) Theoretical conversion coefficient (ref. 38) for E2 transition. Used for normalization.

d) Assignment from refs. 25 and 31.

e) From a delayed γ-ray spectrum; interfering lines in singles spectra.

The level scheme of ^{145}Pm is presented in fig. 12. All the levels shown in fig. 12 are based on the $\gamma\gamma$ coincidence data. We have confirmed all the levels in ^{145}Pm known from radioactive decay[29] and from the ^{145}Nd(p,nγ)^{145}Pm reaction[31], except that no sign of the tentative level[29] at 120.8 keV has been seen in this work.

New low-lying levels established in this work are a $(5/2, 7/2)^+$ level at 660.5 keV, a $7/2^+$ level at 669.7 keV, a level at 726.5 keV and a $5/2^+$ level at 823.5 keV. Preliminary results from the ^{144}Nd (^{3}He,d) and ^{144}Nd(α,t) reactions[32] give a spin assignment $1/2^+$ for the 726.5 and 1057.3 keV levels.

The isomeric $11/2^-$ level at 794.6 keV has been known[31] in ^{145}Pm. We have remeasured a 16.3±1.5 ns half-life for this level in agreement with the earlier result of Shibata et al.[31]. The isomer decays via E1, M2 and E3 transitions to the second $9/2^+$ level at 750.4 keV, to the $7/2^+$ level at 61.2 keV and to the $5/2^+$ ground state. The small E3 branch was not known before and it was identified in this work from the delayed γ-ray spectrum. The E3 branch has also been seen in a recent conversion-electron experiment[25]. The intensity reported in ref. 25 for this transition is about twice as large as ours. This may be due to the fact that, at least in our singles spectra, the 794 keV peak was a complex line and our intensity estimate was taken from the delayed spectra. The 44.1 keV E1 transition itself was not seen because of interference with strong x-ray peaks, but the transition has been placed because the following 750.4 keV transition has a delayed component with the same half-life as the $11/2^-$ level. Another possible E1 transition from the $11/2^-$ level to the first $9/2^+$ state at 713.6 keV was also searched for. An upper limit of 3 % of the total decay of the $11/2^-$ level was obtained for the intensity of the 794.6 $(11/2^-)$ $\rightarrow$ 713.6 $(9/2^+)$ E1 transition.

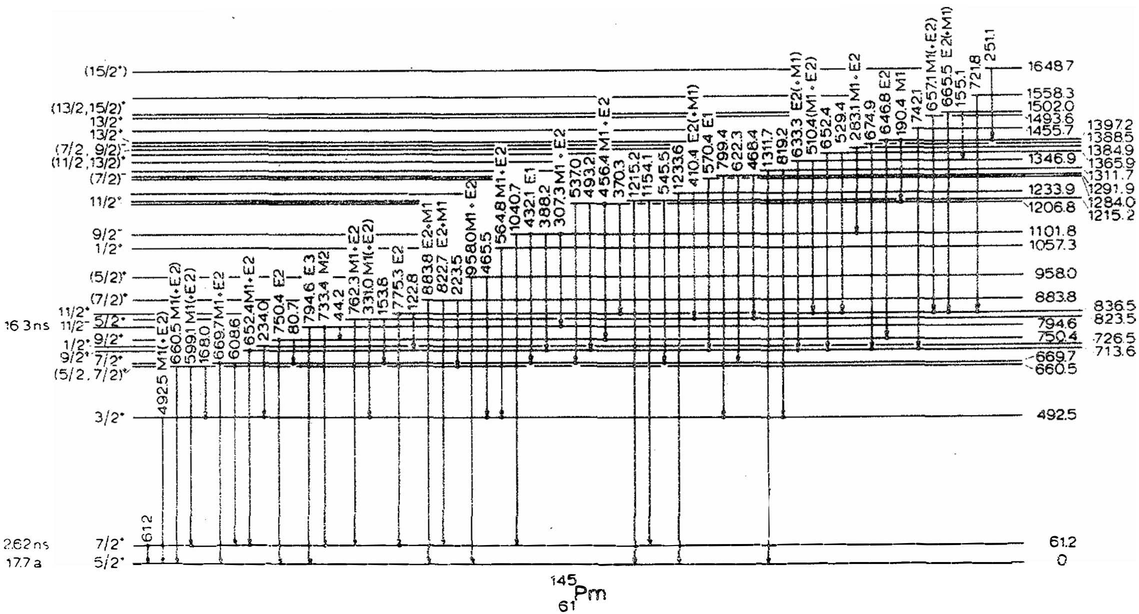

Fig. 12. Level scheme of ^{145}Pm based on the present study of the ^{146}Nd(p,2n)^{145}Pm reaction. Energies of levels and transitions are in keV. The observed $\gamma\gamma$ coincidence relations are marked by dots.

Nagai et al.[25] have reported an 835 keV transition from the $11/2^+$ 835 keV level to the $5/2^+$ ground state. This M3 transition we could not confirm.

Surprisingly, in ^{145}Pm we were not able to find any band structure of negative-parity levels based on the $h_{11/2}$ level at 794.6 keV as in ^{141,143}Pm. A strong cascade in ^{145}Pm establishes a positive-parity sequence of $9/2^+$, $11/2^+$, $13/2^+$ and $(15/2)^+$ levels at 750.4, 1206.8, 1397.2 and 1648.7 keV, respectively.

3.4. The nucleus ^{147}Pm

The structure of the low-lying levels of ^{147}Pm has been investigated by several authors[33-35] from the β decay of ^{147}Nd. However, only six excited states have been established: $5/2^+$ at 91, $3/2^+$ at 410, $(5/2^+)$ at 489, $5/2^+$ at 531, a level at 681 and $5/2^+$ at 686 keV. The ground state of ^{147}Pm has been proposed to be 7/2 on the basis of the paramagnetic resonance method[36]. No reaction data on ^{147}Pm have been published before our work.

We have measured singles γ-ray spectra from the ^{148}Nd(p,2nγ)^{147}Pm reaction at E_p = 12.1, 15.0, 15.8, 16.8, 17.8 and 20.2 MeV. Fig. 13 shows portions of representative γ-ray spectra measured at 125° with respect to the proton beam. Three-parameter (γγt) coincidence experiments were performed at E_p = 15.0 MeV using 40 cm^3 and 55 cm^3 Ge(Li) detectors. Three of these spectra are presented in fig. 14.

Nanosecond isomers in ^{147}Pm were measured with the aid of the small Ge and large Ge(Li) detectors using the rf method. For the half-life of the lowest excited state at 91.1 keV our result 2.6 ± 0.2 ns is in agreement with the previous value[37] of 2.57 ± 0.02 ns. The time distributions for the 649.2, 241.2 and 408.2 keV γ rays establish a half-life of 12 ± 2 ns for the 649.3 level. We have showed that level to be the missing $h_{11/2}$ isomeric state. Two time spectra measured employing the 55 cm^3 Ge(Li) detector are shown in fig. 15.

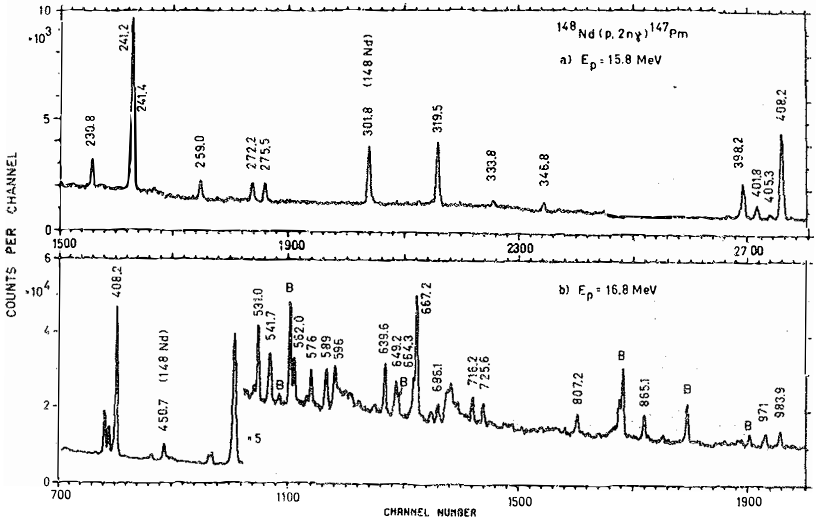

Fig. 13. Portions of singles γ-ray spectra from the $^{148}Nd(p,2n\gamma)^{147}Pm$ reaction measured employing a) the 1.0 cm^3 Ge detector and b) the 55 cm^3 Ge(Li) detector. Only prominent peaks are marked by energies; B = peaks caused by radioactivities or impurities in the target.

Angular distributions of γ rays were measured at the same angles as mentioned earlier at a proton energy of 16.8 MeV. The A_2/A_0 and A_4/A_0 coefficients are given in table 5, as well as the other γ-ray results. Because of the great complexity of the γ-ray spectra, only the distributions of the most intense single peaks were analyzed. The A_4/A_0 coefficient was assumed to be zero if its uncertainty was larger than $|A_4/A_0|$ and a χ^2 test gave a smaller value without the $P_4(\cos\theta)$ term.

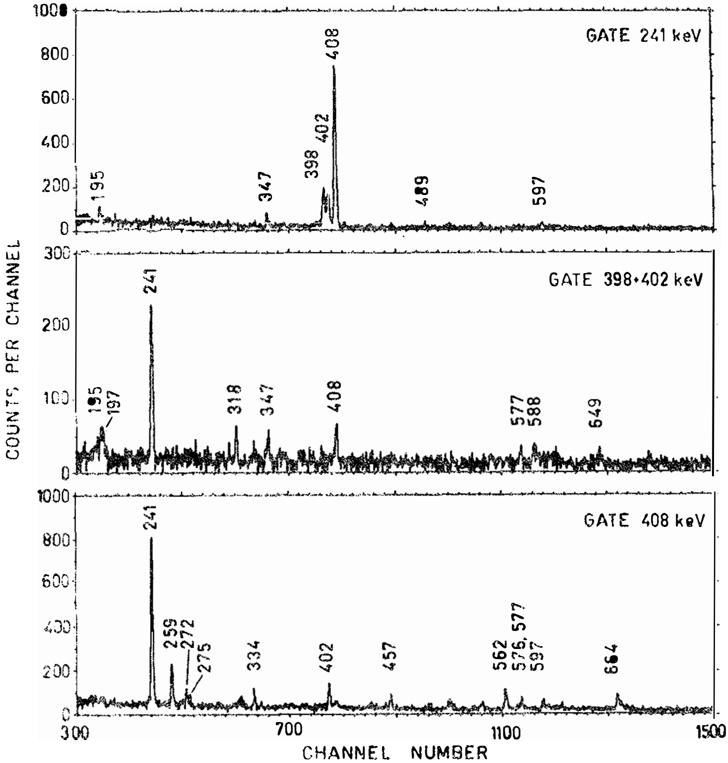

Fig. 14. γγ coincidence spectra from the $^{148}Nd(p,2n\gamma)^{147}Pm$ reaction. Spectra gated by the 241.2 and 241.4 keV γ rays, by the 398.24 and 401.85 keV γ rays and by the 408.20 keV γ ray are presented.

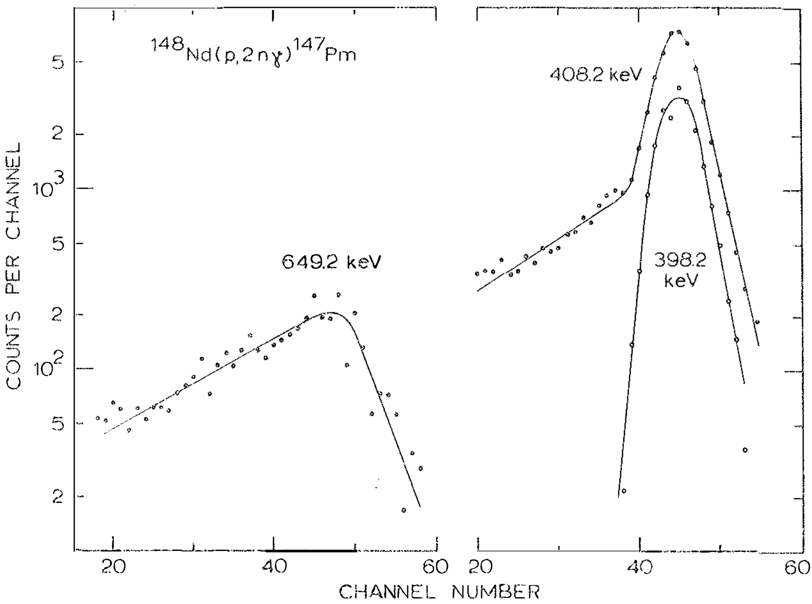

Fig. 15. Time distributions of γ rays from the $^{148}Nd(p,2n\gamma)$ reaction. The 649.2 keV γ ray shows only the delayed component, while the 408.20 keV γ ray is mainly prompt, and a delayed component is caused by the 241.2 keV transition between the 649.3 and 408.2 keV levels. The half-life of the 649.3 keV state is 12 ± 2 ns. The time calibration for the spectra is 1.10 ns/ch.

We have performed singles, prompt and delayed electron measurements from the $^{148}Nd(p,2ne)$ reaction at E_p = 15.0 MeV. Fig. 16 presents portions of singles and delayed spectra. The electron spectra were normalized to γ-ray spectra with the aid of the intense 301.8 keV $2^+ \rightarrow 0^+$ transition in ^{148}Nd, present in the spectra from the $^{148}Nd(p,p')$ reaction. The theoretical K conversion coefficient α_K (E2) = 0.0412 was used in normalization[38]. The measured α_K and K/L ratios are shown in table 5. The multipolarities of the transitions we have determined with the aid of conversion and angular distribution coefficients. The E2/M1 mixing ratio for a transition is given only if the conversion coefficient and the angular distribution results are in agreement. For example, the angular distribution of the 401.85 keV γ ray is better fitted with the 15/2(E2)11/2 sequence, but the measured $\alpha_K = 0.026 \pm 0.006$ is slightly larger than the theoretical[38] $\alpha_K(E2) = 0.0184$, and therefore the mixing ratio is not given. Some δ values, accurately known from directional correlation[33,38] and nuclear orientation[39] measurements, are also shown in table 5.

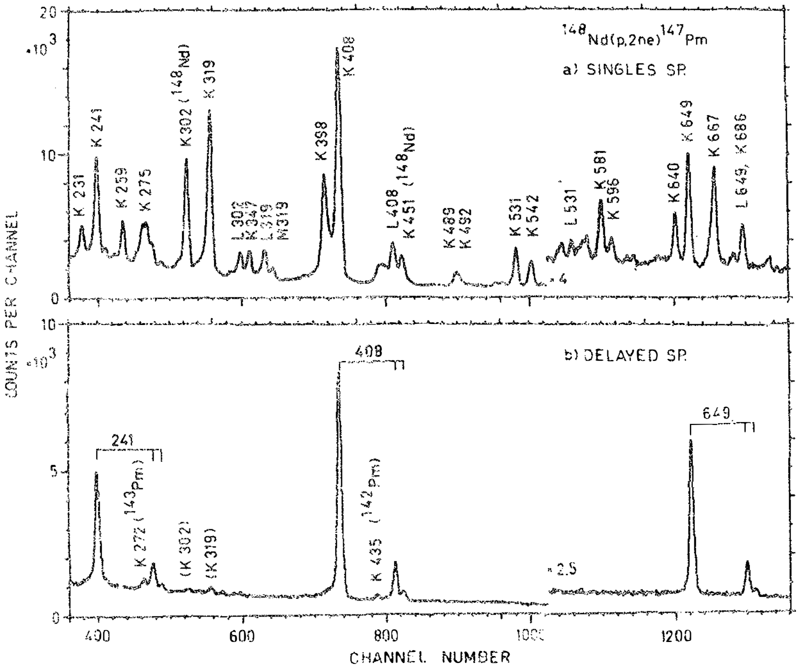

Fig. 16. In-beam conversion-electron spectra from the ^{148}Nd(p,2ne) reaction. a) Singles spectrum, b) delayed spectrum, which was measured during 6-30 ns after the beam pulse.

Table 5. Energies E_γ, relative γ-ray intensities I_γ at 125°, experimental conversion coefficients α_K, K/L ratios, angular distribution coefficients and multipolarities of transitions in the $^{148}Nd(p,2n\gamma)^{147}Pm$ reaction. The uncertainties of the last figures are in parentheses.

E_γ (keV)	I_γ (E_p=15 MeV)	α_K ($\times 10^{-2}$)	K/L	A_2/A_0	A_4/A_0	Multi-polarity	δ(E2/M1)	Assignment $E_i \to E_f$
91.10(4)	640(50)			-0.021(8)	≈0	M1+E2	0.13(2)[a]	91.1 - 0
120.49(6)	6(2)					M1+E2[a]	0.158(15)[a]	531.1 - 410.6
194.57(5)	21(2)							1245.8 - 1051.2
196.6(3)	16(4)[b]							686.1 - 489.3
230.77(8)	71(8)	10(2)	6.2(13)	-0.16(2)	≈0	M1(+E2)		641.3 - 410.6
241.2(2)	430(40)[b]	2.3(3)	6.9(11)			E1		649.3 - 408.2
241.4(3)	140(30)[b]	8(3)				M1,E2		730.7 - 489.3
247.0(2)	18(2)	2.2(4)				E1		1406.4 - 1159.5
259.01(8)	72(7)	6.5(12)		0.106(15)	0.06(2)	E2+M1	7.4(6)	667.2 - 408.2
272.2(2)	32(10)[b]							680.4 - 408.2
275.47(8)	70(6)	8.5(12)		-0.16(2)	≈0	M1+E2		686.1 - 410.6
318.0(3)	28(7)[b]							807.3 - 489.3
319.47(5)	400(20)	5.2(5)	7.0(10)	0.027(15)	≈0	M1+E2	-0.34(7)	410.6 - 91.1
333.82(10)	36(4)			-0.13(3)	≈0			1406.4 - 1072.5
346.81(10)	51(5)	4.4(5)		-0.043(14)	≈0	M1		1077.5 - 730.7
356.5(2)	17(3)							1434.0 - 1077.5
363.1(4)	20(5)[b]							1049.2 - 686.1
398.24(5)	360(20)	3.0(3)	7.5(12)	0.076(4)	-0.040(6)	M1+E2	0.30(1)	489.3 - 91.1
401.85(8)	144(12)	2.6(6)		0.266(11)	-0.09(2)	E2(+M1)		1051.2 - 649.3
405.34(12)	40(8)							1072.5 - 667.2
408.20(7)	1000	2.6(3)	7.0(9)	0.239(11)	-0.021(15)	M1+E2	0.57(3)	408.2 - 0
410.6(2)	30(8)							410.6 - 0
436.0(5)	17(5)[b]							1406.4 - 970.2
438.8(4)	20(5)[b]							1119.2 - 680.4
439.9(4)	20(5)[b]					M1+E2	0.6(1)[a]	531.1 - 91.1
447.0(5)	12(3)[b]							1119.2 - 667.2
457.0(5)	40(8)[b]							865.1 - 408.2
489.4(2)	84(12)	1.7(3)				M1(+E2)		489.3 - 0
492.3(2)	64(12)[b]	0.5(2)		-0.15(4)	≈0	E1		1159.5 - 667.2
518.1(5)	16(4)							1049.2 - 531.1
531.05(10)	206(15)	1.3(2)		+0.05(2)	-0.02(3)	M1+E2	-0.95(30)[c]	531.1 - 0
540.4(6)	46(15)[b]							
541.7(3)	140(20)[b]					E2[d]		632.8 - 91.1
562.0(2)	100(8)	0.24(5)		-0.12(3)	≈0	E1		970.2 - 408.2
572.6(3)	20(4)	0.28(6)				E1		1213.9 - 641.3
576.0(5)	24(6)[b]							984.0 - 408.2

Table 5. (cont.)

E_γ (keV)	I_γ (E_p=15 MeV)	α_K ($\times 10^{-2}$)	K/L	A_2/A_0	A_4/A_0	Multi-polarity	δ(E2/M1)	Assignment $E_i \rightarrow E_f$
576.6(5)	22(6)$^{b)}$							1627.8 - 1051.2
588.1(4)	32(6)$^{b)}$							1077.5 - 489.3
589.3(3)	91(15)$^{b)}$							680.4 - 91.1
595.0(4)	26(9)$^{b)}$	1.01$^{e)}$				M1+E2	±0.44$^{e)}$	686.1 - 91.1
596.6(4)	38(9)$^{b)}$	0.5(3)				E2(+M1)		1245.8 - 649.3
630.6(2)	36(3)							1041.2 - 410.6
639.60(15)	164(13)	0.59(8)		0.17(3)	-0.04(5)	E2		730.7 - 91.1
649.2(3)	96(8)	2.3(3)	5.1(8)			M2		649.3 - 0
664.3(3)	95(10)	0.51(13)		0.32(2)	0.10(3)	E2+M1	2.0(3)	1072.5 - 408.2
667.2(2)	350(20)	0.54(8)	6.0(12)	0.21(3)	-0.10(5)	E2		667.2 - 0
679.9(3)	50(12)	0.58(12)				E2(+M1)		
686.08(15)	75(7)	0.7(2)				M1+E2	-0.95(30)$^{c)}$	686.1 - 0
716.2(2)	84(8)	0.21(4)		-0.05(2)	≈ 0	E1		807.3 - 91.1
725.6(3)	43(6)	0.35(5)		0.26(3)	-0.08(5)	E2		1392.8 - 667.2
807.2(2)	76(8)	0.11(3)		-0.02(2)	≈ 0	E1		807.3 - 0
865.1(2)	103(9)	0.17(5)		-0.02(3)	≈ 0	E1(E2)		865.1 - 0
881.7(3)	38(6)							
947.3(4)	41(7)							
950.2(4)	25(5)							1041.2 - 91.1
970.3(5)	60(12)							970.2 - 0
971.5(5)	32(12)$^{b)}$							1382.1 - 410.6
983.9(3)	77(9)			-0.09(3)	≈ 0			984.0 - 0
1041.1(5)	25(5)							1041.2 - 0

a) Ref. 34.

b) From coincidence data; interfering lines in singles spectra.

c) Ref. 39.

d) Transition from the $1/2^+$ level (ref. 40) to the $5/2^+$ level.

e) Theoretical α_K using δ value of ref.33.

The level scheme of ^{147}Pm is presented in fig. 17. All the levels were established by observed $\gamma\gamma$ coincidences; in some cases the order of cascading γ rays was fixed by their intensity ratios. The spins and parities of the states are based on conversion-electron measurements, angular distributions and excitation functions of the γ rays.

The new $9/2^+$ level at 408.2 keV is the second excited state in ^{147}Pm. This level is populated by the E1 transition from the 649.3 keV state, which also decays to the ground state via an M2 transition. The spin and parity of $11/2^-$ have been established for this isomeric 649.3 keV level, which is obviously the $h_{11/2}$ quasiparticle state known in the other odd-A Pm nuclei. An $11/2^-$ level at 649 keV has been recently seen also in the ^{146}Nd(^{3}He,d) and ^{146}Nd(α,t)^{147}Pm experiments[40], which also give the spin $1/2^+$ for the 632.8 keV level. The angular distribution of the 398.24 keV γ ray did not give a δ value agreeing with directional correlation measurements[33,34] in the case of spin 5/2 for the 489.3 keV level. However, for the spin 7/2 our result $\delta = 0.30 \pm 0.01$ is in good agreement with the directional correlation result[34] δ^L(398.24 keV) = 0.31 ± 0.08, where the spin 7/2 was assumed for the 489.3 keV level. The spin assignment $7/2^+$ for the 489.3 keV level was confirmed by Al-Janebi et al.[41] in work published after our paper 1.

The half-lives of some excited states given in fig. 17 are from refs. 34 and 37, except that of the 649.3 keV level. None of the new levels at 182, 228.5, 275, 319.5 and 725 keV suggested in ref. 35 could be observed in the present study.

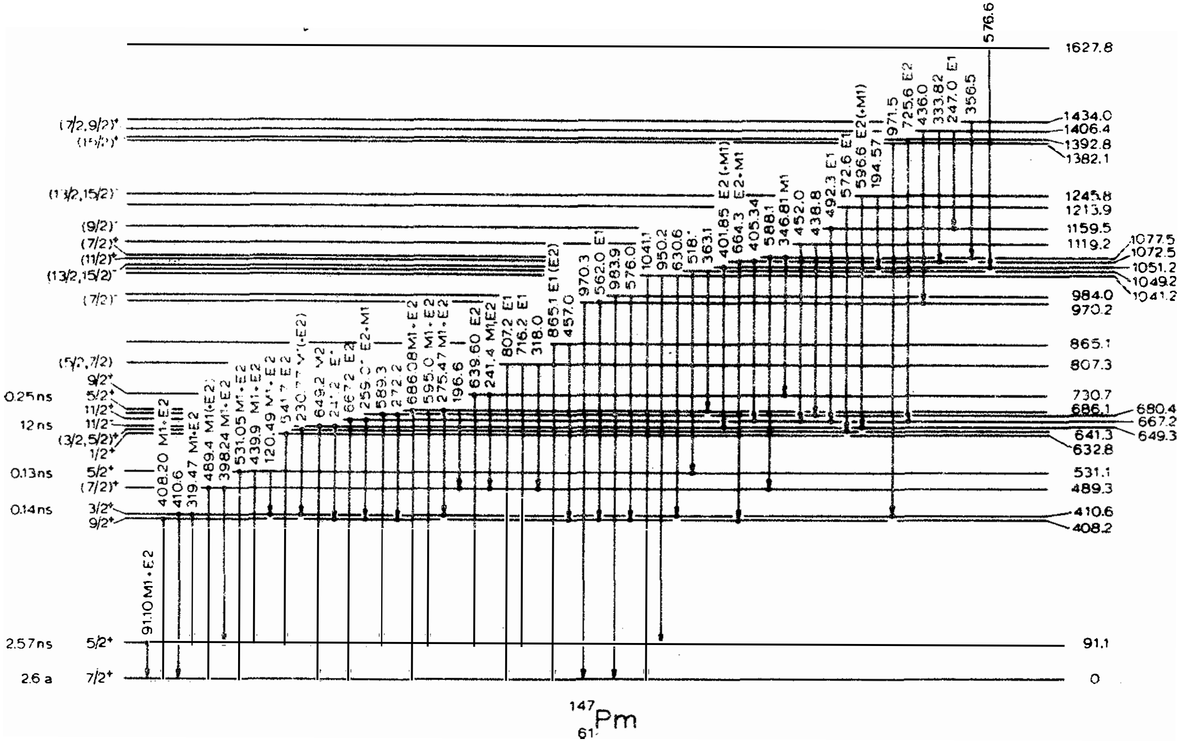

Fig. 17. Level scheme of ^{147}Pm based on the present study of the ^{148}Nd(p,2nγ) and ^{148}Nd(p,2ne) reactions. Energies of levels and transitions are in keV. The observed γγ coincidences are marked by dots.

3.5. The nucleus ^{149}Pm

The nuclear structure of ^{149}Pm has been investigated[42] in the decay of ^{149}Nd, and using ^{148}Nd(^{3}He,d) and ^{148}Nd(α,t) reactions[43]. The ground-state spin of ^{149}Pm has been measured by the atomic-beam resonance method[44] and found to be 7/2. The spins of some low-lying levels have been determined[42,43]. Also the isomeric $h_{11/2}$ state ($T_{1/2}$ = 35 μs) has been observed[42] in ^{149}Pm.

We have measured singles γ-ray spectra from the ^{150}Nd(p,2nγ)^{149}Pm reaction at proton energies of 12.1, 13.6, 14.3, 14.8 and 15.8 MeV. Fig. 18 presents a typical spectrum, which was measured at a 125^{o} angle, employing the 7.5 cm^{3} Ge detector.

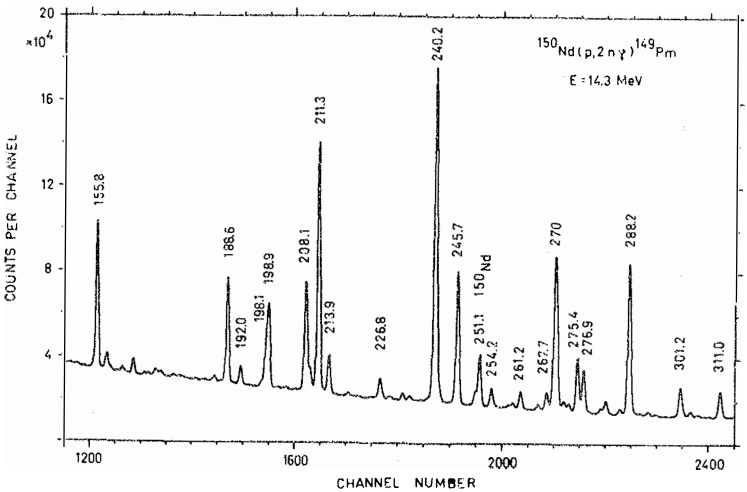

Fig. 18. A representative part of a singles γ-ray spectrum arising from the ^{150}Nd(p,2nγ)^{149}Pm reaction measured employing the 7.5 cm^{3} Ge detector. Only prominent peaks are marked by energies.

Three-parameter ($\gamma\gamma t$) coincidence experiments were performed using 55 cm^3 and 40 cm^3 Ge(Li) detectors. The energy of the proton beam was 13.6 MeV. Three typical coincidence spectra are shown in fig. 19. The density of the γ rays in singles spectra is very high and in many cases the γ-ray intensities were determined with the aid of the coincidence spectra, as can be seen in table 6.

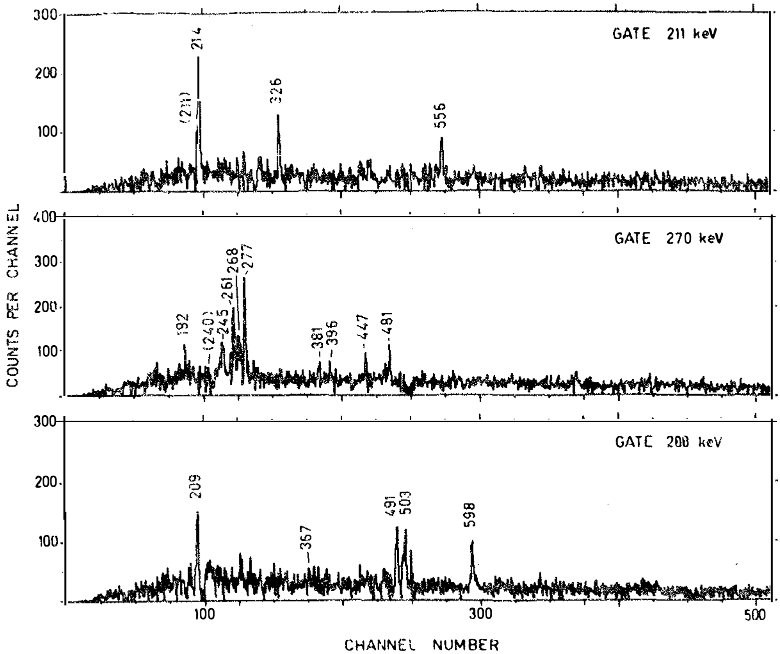

Fig. 19. Typical $\gamma\gamma$ coincidence spectra from the $^{150}Nd(p,2n\gamma)^{149}Pm$ reaction

A nanosecond lifetime experiment was performed using 1.0 and 7.5 cm^3 Ge detectors. The results for γ rays at 114.3 keV ($T_{1/2}$ = 2.7 ± 0.2 ns), at 188.6 and 74.3 keV ($T_{1/2}$ = 3.1 ± 0.2 ns) and at 270.1 and 155.8 keV

($T_{1/2}$ = 2.8 ± 0.2 ns) are in good agreement with the known half-lives[42] of the 114.3, 188.6 and 270.1 keV states.

The angular distribution experiments were performed at six angles between 90^0 and 161^0. In one run we used a Ge(Li) detector and a 15.8 MeV proton energy, in the other the 7.5 cm^3 detector and a 14.3 MeV proton energy. The A_2/A_0 coefficients are given in table 6, where a summary of γ-ray data is presented.

The level scheme of ^{149}Pm in fig. 20 is based on the γγ coincidence data, the transition intensities and on the excitation functions of the γ rays. The angular distributions and the excitation functions were used to determine the spins and parities of the levels. We suggest a spin $3/2^+$ for the 188.6 keV state in agreement with Straume et al.[43] and contradictory with ref. 42. To the 288.2 keV level we have given the spin values ($7/2^+$, $9/2^+$), of which the $9/2^+$ is most probable on the basis of the excitation function. For the 515.6 keV level we suggest a spin $(9/2)^-$ because the 275.4 keV γ transition is of an M1 + E2 character. The new levels at 497.8 and 510.0 keV have a spin $(11/2)^+$ and ($13/2^-$, $15/2^-$), respectively, on grounds of excitation functions, angular distribution coefficients and coincidence relations. Most of the levels above 400 keV have not been published earlier. However, many of these have now been observed also in the decay[45] of ^{149}Nd.

We have described the level structure of ^{149}Pm on the basis of a rotational picture because the ^{149}Pm nucleus is more deformed than the lighter Pm isotopes. In the other N = 88 nuclei ^{153}Tb (ref. 46) and ^{151}Eu (ref. 47), and also in the more deformed nucleus ^{151}Pm (ref. 48) rotational band structures have been observed. We are not able to see clear rotational bands in ^{149}Pm, but comparing the experimental and the calculated level order and transition rates, we can observe certain

Table 6. Energies E_γ, relative γ-ray intensities I_γ at 125°, angular distribution coefficients and multipolarities of transitions in the $^{150}Nd(p,2n\gamma)^{149}Pm$ reaction. The uncertainties of the last figures are in parentheses.

E_γ (keV)	I_γ (E_p = 14.3 MeV)	A_2/A_0	A_4/A_0	Multipolarity[b)]	Assignment $E_i - E_f$, $J^\pi_i - J^\pi_f$
58.81(5)	45(5)			E1	270.1 - 211.3, $7/2^- - 5/2^+$
74.3 (1)	155(30)				188.6 - 114.3, $3/2^+ - 5/2^+$
97.04(5)	25(5)	0.05(3)	-0.02(4)	M1 + E2	211.3 - 114.3, $5/2^+ - 5/2^+$
114.35(5)	1000	-0.04(1)	≈0	M1 + E2	114.3 - 0 , $5/2^+ - 7/2^+$
126.59(6)	9(2)	-0.12(8)	≈0	E1	396.7 - 270.1, $5/2^+ - 7/2^-$
137.01(6)	15(3)				425.3 - 288.2, $(5/2,7/2)^+ - (7/2,9/2)^+$
155.85(6)	210(20)	-0.06(1)	-0.02(1)	E1	270.1 - 114.3, $7/2^- - 5/2^+$
185.42(8)	10(2)				396.7 - 211.3, $5/2^+ - 5/2^+$
188.58(8)	205(20)			E2	188.6 - 0 , $3/2^+ - 7/2^+$
191.97(8)	36(6)			E2	462.1 - 270.1, $3/2^- - 7/2^-$
198.1(1)	45(8)[a)]				558.1 - 360.0, $(7/2,9/2) - 7/2^+$
198.9(1)	200(40)			M1	387.5 - 188.6, $1/2^+ - 3/2^+$
208.15(9)	260(30)	-0.03(2)	≈0	M1	396.7 - 188.6, $5/2^+ - 3/2^+$
209.2(2)	50(10)				497.8 - 288.2, $(11/2)^+ - 7/2^+$
211.27(10)	610(50)	0.03(1)	≈0	M1 + E2	211.3 - 0 , $5/2^+ - 7/2^+$
213.96(10)	98(10)	0.13(2)	0.03(3)	M1 + E2	425.3 - 211.3, $(5/2,7/2)^+ - 5/2^+$
226.80(12)	56(6)				415.5 - 188.6, $3/2^+ - 3/2^+$
240.19(12)	1050(50)			M2	240.2 - 0 , $11/2^- - 7/2^+$
241.2(3)	40(15)[a)]				666.5 - 425.3
245.5(3)	80(20)[a)]				515.6 - 270.1, $(9/2)^- - 7/2^-$
245.7(3)	370(30)	-0.01(1)	0.01(2)	(M1 + E2)	360.0 - 114.3, $7/2^+ - 5/2^+$

250.3(2)	42(8)				808.7 - 558.1
254.17(12)	65(8)				650.8 - 396.7, (5/2,7/2) - $5/2^+$
261.25(12)	54(8)				771.2 - 510.0
267.68(15)	78(7)	-0.13(3)	≈0	M1	537.8 - 270.1, $5/2^-$ - $7/2^-$
269.8(3)	430(50)	0.17(2)	0.02(2)	(M1 + E2)	510.0 - 240.2, ($13/2^-$,$15/2^-$)-$11/2^-$
270.1(3)	380(50)	0.08(1)	≈0	E1	270.1 - 0 , $7/2^-$ - $7/2^+$
272.0(1)	44(8)				
273.2(1)	24(5)			M1,E2	387.5 - 114.3, $1/2^+$ - $5/2^+$
275.50(15)	235(20)	-0.19(1)	≈0	M1 + E2	515.6 - 240.2, $(9/2)^-$ - $11/2^-$
276.95(15)	185(15)	-0.04(2)	-0.02(2)		547.0 - 270.1, (5/2,7/2) - $7/2^-$
281.3(1)	22(4)				778.9 - 497.8
282.4(1)	61(5)	0.08(2)	≈0	M1 + E2	396.7 - 114.3, $5/2^+$ - $5/2^+$
288.22(15)	650(50)	0.32(1)	0.02(1)	M1 + E2	288.2 - 0 , $(7/2,9/2)^+$ - $7/2^+$
301.2(2)	130(30)				415.5 - 114.3, $3/2^+$ - $5/2^+$
301.2(2)	35(10) a)				716.3 - 415.5
311.05(15)	145(15)	0.10(1)	0.02(1)	M1 + E2	425.3 - 114.3, $(5/2,7/2)^+$ - $7/2^+$
326.5(1)	56(8)			E1	537.8 - 211.3, $5/2^-$ - $5/2^-$
349.2(1)	20(5)			E1	537.8 - 188.6, $5/2^-$ - $3/2^+$
360.1(2)	70(12)				360.0 - 0 , $7/2^+$ - $7/2^+$
361.4(2)	27(6) a)				721.4 - 360.0
367.2(2)	25(12)				655.2 - 288.2, $7/2^-$ - $(7/2,9/2)^+$
380.8(2)	50(8)				650.8 - 270.1, (5/2,7/2) - $7/2^-$
396.4(3)	7(3)				396.7 - 0 , $5/2^+$ - $7/2^+$

Table 6. (cont.)

E_γ (keV)	I_γ (E_p = 14.3 MeV)	A_2/A_0	A_4/A_0	Multipolarity[b)]	Assignment $E_i - E_f$, $J_i^\pi - J_f^\pi$
396.4(3)	58(2)[a)]				666.5 - 270.1
423.6(2)	90(10)			E1	537.8 - 114.3, $5/2^- - 5/2^+$
425.4(2)	80(15)				425.3 - 0 , $(5/2,7/2)^+ - 7/2^+$
426.3(2)	80(15)				666.5 - 240.2
432.8(2)	15(5)				547.0 - 114.3, $(5/2,7/2) - 5/2^+$
439.4(2)	30(7)				650.8 - 211.3, $(5/2,7/2) - 5/2^+$
444.1(5)	90(20)	0.13(3)	-0.03(4)		558.1 - 114.3, $(7/2,9/2) - 5/2^+$
444.1(3)	10(3)			E1	655.2 - 211.3, $7/2^- - 5/2^+$
446.7(3)	63(12)	0.18(4)	-0.13(6)		716.8 - 270.1
448.7(3)	105(15)	0.25(5)	0.07(7)		808.7 - 360.0
450.1(3)	30(6)				
455.3(2)	45(8)				666.5 - 211.3
462.3(2)	25(5)				650.8 - 188.6, $(5/2,7/2) - 3/2^+$
480.6(2)	82(10)	-0.13(4)	0.05(6)		750.7 - 270.1
490.7(2)	137(12)	0.26(3)	0.07(4)		778.9 - 288.2
497.8(2)	330(20)	0.24(2)	≈0	(E2)	497.8 - 0 , $(11/2)^+ - 7/2^+$
502.8(2)	90(12)	-0.08(7)	≈0		791.0 - 288.2
531.2(3)	82(12)				771.2 - 240.2
538.5(3)	28(10)				778.9 - 240.2
540.8(3)	50(12)			E1	655.2 - 114.3, $7/2^- - 5/2^+$
547.8(3)	32(7)				
556.5(5)	50(15)				767.8 - 211.3
597.6(5)	130(20)				885.8 - 288.2
606.5(4)	55(12)				
635.0(5)	50(10)				
651.4(5)	72(15)				
654.9(5)	75(15)			E1	655.2 - 0 , $7/2^- - 7/2^+$
787.1(5)	63(12)				
790.1(5)	45(9)				
799.7(5)	85(10)				
812.8(5)	35(7)				

a) From coincidence data.

b) Based on ref. 42 and the present data.

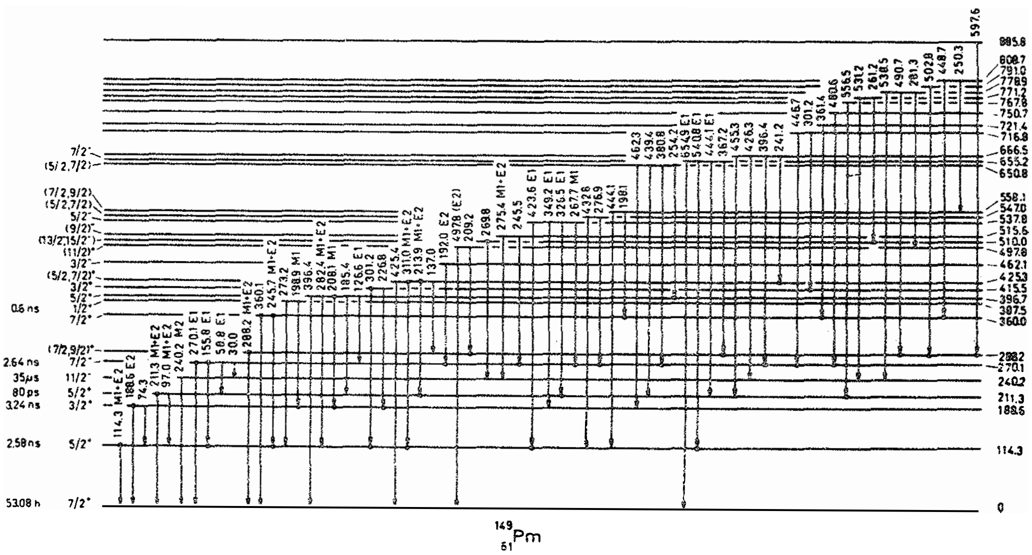

Fig. 20. Level scheme of ^{149}Pm based on the present study of the ^{150}Nd(p,2n)^{149}Pm reaction. Energies of levels and transitions are in keV. The observed coincidence relations are marked by dots.

levels to be correlated. In section 5.1 these bands are discussed in detail.

Bäcklin et al.[49] have suggested the $5/2^-$ level at 537.8 keV and the $7/2^-$ level at 655.2 keV to be the band head and the first rotational state of the $5/2^-$ [532] Nilsson state. In addition to these levels we have interpreted the other negative-parity states to be formed from the $h_{11/2}$ state.

Another way to describe the level structure of ^{149}Pm, besides the above rotational approach, is to explain that excited states are created of quadrupole vibrations of the core nucleus with the last odd proton coupled to them (cf. 4.1.4).

4. THEORETICAL MODELS AND CALCULATIONS

4.1. Intermediate-coupling model

4.1.1. Description of the model

In this part of the work I shall report on the theoretical models that we have used to describe the level structure of odd-A Pm nuclei.

Since the excited states of the doubly even Nd nuclei (A-1) show a vibrational character it seems possible to describe each odd-mass Pm nucleus in terms of the neighbouring doubly even Nd nucleus plus the last odd proton in a shell-model single-particle state. This coupled system consists of a doubly even core susceptible of quadrupole vibrations plus the last odd proton which has several single-particle states available to it. It is further assumed that the single-particle states of the odd proton are neither weakly nor strongly coupled to the quadrupole vibrations of the core, and it is taken into account that a single-particle state may be partly occupied. The above picture is an intermediate-coupling approach in the unified nuclear model outlined by Bohr and Mottelson[50,51] and afterwards developed by Choudhury[52]. Such an approach has been used by various authors[1,2,41,53-56] to study the properties of the low-lying levels of odd-mass nuclei in the neighbourhood of the Pm nuclei. The first parameter of the intermediate-coupling model is the phonon energy $\hbar\omega$, associated with the collective surface vibrations of the core. The second parameter is the strength of the coupling between the single-particle motion and the core vibrations. The remaining parameters are the energies of the proton states.

In subsect. 4.1.2 is presented a brief description of the basic formulae needed in our calculation. We have programmed these formulae of the model for the PDP-11/45 computer at JYFL. The results of our calculations are given in subsects. 4.1.4-7 and they are compared with our experimental results.

4.1.2. Mathematical formulation

The total Hamiltonian for the system of a doubly even core plus an extra nucleon is assumed to be separable into three parts,

$$(1) \qquad H = H_c + H_p + H_{int},$$

where H_c, H_p and H_{int} are the Hamiltonians associated, respectively, with the harmonic quadrupole vibrations of the core, the motion of the odd nucleon in an effective average potential and the surface-particle interaction. H_{int} is given by

$$(2) \qquad H_{int} = -\sqrt{\pi/5}\ \xi\ \hbar\omega \sum_{i,\mu} [b^{\mu} + (-1)^{\mu} b^{+}_{-\mu}] Y_{2\mu}(\theta_i,\phi_i),$$

where $\hbar\omega$ is the phonon excitation energy of the core, b^{μ} and b^{+}_{μ} the annihilation and creation operators for the quadrupole phonon with z-component μ and $Y_{2\mu}$ a spherical harmonic. The dimensionless parameter

(3) $$\xi = k\sqrt{5/(2\pi\hbar\omega C)}$$

has been introduced for the interaction strength, where C is the surface deformation parameter and the coupling constant k is the average of radial integrals. The wave functions for the odd-proton nuclei will be expanded in the basis

(4) $$|j, NR; IM> = \sum_{m_j, M_R} <jm_j RM_R|IM>|jm_j>|NRM_R>,$$

where the N-phonon state of the core with total angular momentum R and projection M_R along the z-axis is coupled with the single-particle state $|jm_j>$ to give a total angular momentum I and its projection M. The basis eigenvectors satisfy the eigenvalue equation

(5) $$(H_c + H_p)|j,NR;IM> = \left[\hbar\omega(N + \tfrac{5}{2}) + E_j\right]|j,NR;IM>$$

where E_j is the energy of the single particle in the quantum state of angular momentum j (other quantum numbers not indicated).

The only off-diagonal matrix elements of the total Hamiltonian are given by the interaction part (ref. 2)

(6) $$<j',N'R';IM|H_{int}|j,NR;IM> = -\frac{1}{2}\,\xi\hbar\omega(-1)^{I + j + j' - 1/2}$$
$$\times \sqrt{(2j + 1)(2j' + 1)} \begin{Bmatrix} j & R & I \\ R' & j' & 2 \end{Bmatrix} \begin{pmatrix} j' & 2 & j \\ -\frac{1}{2} & 0 & \frac{1}{2} \end{pmatrix}$$
$$\times \left[(-1)^{R'}<N'R'||b^{+}||NR> + (-1)^{R}<NR||b^{+}||N'R'>\right]\delta^{\ell+\ell'}_{\text{even}} \times (u_j u_{j'} - v_j v_{j'}),$$

where { } and ( ) are 6j- and 3j-symbols. The reduced matrix elements of the creation operator differ by a factor $(-1)^{R+R'}$ from the values tabulated by Raz[57]. The factor $u_j u_{j'} - v_j v_{j'}$ is added to the formula of ref. 2 and here u_j and v_j represent the quasiparticle non-occupation and occupation amplitudes in the state j, respectively. The selection rules are $\Delta N = 1$, $\Delta R \leq 2$, $\Delta j \leq 2$ and $\Delta \ell = 0$ or 2.

The eigenvalues and the expansion coefficients of the eigenvectors are obtained by diagonalizing the total Hamiltonian whose diagonal and off-diagonal matrix elements are given in eqs.(5) and (6). The eigenvectors of the total Hamiltonian are then a linear combination of the basis eigenvectors and can be expressed as

$$(7) \qquad |E^{(\alpha)};IM\rangle = \sum_{j,N,R} c_\alpha(\ell j,NR;I)\,|j,NR;IM\rangle ,$$

where $c_\alpha(\ell j,NR;I)$ are the expansion coefficients and E the eigenvalues.

The above wave functions will be used to calculate the magnetic and electric transition rates. For the coupled system consisting of a single particle and the quadrupole oscillations of the surface of the core the magnetic dipole operator expressed in the spherical tensor representation is

$$(8) \qquad \mathcal{M}(M1,\mu) = \sqrt{3/4\pi}\,[g_\ell \ell_\mu + g_s s_\mu + g_R R_\mu]\,\mu_N .$$

From the general definition of the reduced transition probability

$$(9) \qquad B(\lambda;\alpha I \rightarrow \beta I') = \frac{1}{2I+1} \sum_{MM'\mu} |\langle E^{(\beta)};I'M'|\mathcal{M}(\lambda,\mu)|E^{(\alpha)};IM\rangle|^2$$

one obtains for the magnetic-dipole case[2]

$$(10)\quad B(M1;\alpha I \to \beta I') = \frac{3}{4\pi}\mu_N^2(2I'+1)\Bigg|\sum_{\ell jj'NR} c_\beta(\ell j',NR;I')c_\alpha(\ell j,NR;I)$$

$$\times\Bigg\{(-1)^{R+I+j'+\ell}\begin{Bmatrix} j' & j & 1\\ I & I' & R\end{Bmatrix}\sqrt{(2j+1)(2j'+1)}\Bigg[(-1)^{j-1/2}\begin{Bmatrix}\ell & \ell & 1\\ j & j' & \frac{1}{2}\end{Bmatrix}$$

$$\times g_\ell\sqrt{\ell(\ell+1)(2\ell+1)} + (-1)^{j-1/2}\begin{Bmatrix}\frac{1}{2} & \frac{1}{2} & 1\\ j & j' & \ell\end{Bmatrix} g_s\sqrt{3/2}\Bigg] \times (u_j u_{j'} + v_j v_{j'})$$

$$+ (-1)^{R+I'+j}\begin{Bmatrix}R & R & 1\\ I & I' & j\end{Bmatrix} g_R\sqrt{R(R+1)(2R+1)}\quad\delta_{jj'}\Bigg\}\Bigg|^2,$$

where μ_N denotes the nuclear magneton. The g factors for orbital angular momentum, spin and the core are denoted by g_ℓ, g_s and $g_R = Z/A$, respectively.

The electric quadrupole operator is given by

$$(11)\quad \mathcal{M}(E2,\mu) = \frac{3}{4\pi} ZeR_0^2\sqrt{\frac{\hbar\omega}{2C}}\Big[(-1)^\mu b^{-\mu} + b^+_\mu\Big] + \sum_i\Big(e_i + \frac{Ze}{A^2}\Big)r_i^2 Y_2(\hat{r}_i),$$

where the summation is extended over the extra-core protons ($e_i = e_p$). So, if there is one proton outside the core, we obtain for the electric-quadrupole reduced transition probability the formula[2]

$$(12)\quad B(E2;\alpha I \to \beta I') = (2I'+1)\Bigg|\sum_{\substack{\ell,\ j,\ N,\ R\\ \ell',j',N',R'}} c_\beta(\ell' j',N'R';I')c_\alpha(\ell j,NR;I)$$

$$\times\Bigg\{\frac{3}{4\pi}ZeR_0^2\sqrt{\frac{\hbar\omega}{2C}}(-1)^{j+I'}\begin{Bmatrix}R & R' & 2\\ I' & I & j\end{Bmatrix}\Big[(-1)^{R'}\langle NR||b^+||N'R'\rangle +$$

$$(-1)^R\langle N'R'||b^+||NR\rangle\Big]\,\delta_{\ell\ell'}\delta_{jj'} + \sqrt{\frac{5}{4\pi}}\quad\Big(e_p + \frac{Ze}{A^2}\Big)\langle \ell j'|r^2|\ell j\rangle\delta^{\ell+\ell'}_{even}(-1)^{R+I+1/2}$$

$$\times\sqrt{(2j+1)(2j'+1)}\begin{Bmatrix}j' & j & 2\\ I & I' & R\end{Bmatrix}\begin{pmatrix}j' & 2 & j\\ -\frac{1}{2} & 0 & \frac{1}{2}\end{pmatrix}(u_j u_{j'} - v_j v_{j'})\delta_{NN'}\delta_{RR'}\Bigg\}\Bigg|^2,$$

where the symbols are the same as above. For the radial matrix element $<\ell'j'|r^2|\ell j>$ we have used in our calculation the Weisskopf approximation $<|r^2|> = \frac{3}{5}R_0^{\ 2}$.

A multipole moment calculated from a nuclear model serves as another test of the theory. Here are given general expressions for the magnetic dipole and electric quadrupole moments in terms of the calculated coefficients of the nuclear wave functions. The magnetic dipole moment for the state $|E;IM>$ is defined in units of μ_N as

$$(13) \qquad \mu = <E;II\left|\sqrt{4\pi/3}\,\mathcal{M}(M1,\mu{=}0)\right|E;II> = \left[\frac{4\pi}{3}\,\frac{I}{I+1}\,B(M1;I\rightarrow I)\right]^{1/2}$$

In an analogous way the electric quadrupole moment is defined in units of eb as

$$(14) \qquad Q = <E;II\left|\sqrt{16\pi/5}\,\mathcal{M}(E2,\mu{=}0)\right|E;II> = \left[\frac{16\pi}{5}\,\frac{I(2I-1)}{(I+1)(2I+3)}\,B(E2;I\rightarrow I)\right]^{1/2}$$

It thus follows that the computer program written to calculate B(M1) and B(E2) values can be used directly to obtain dipole and quadrupole moments.

The wave functions previously obtained have been used to calculate spectroscopic factors for a stripping reaction leading from the core nucleus to a state of spin I = j. The spectroscopic factor is the overlap integral between the parent and the nuclear system composed of the daughter nucleus and the stripped nucleons. Therefore the spectroscopic factor is the absolute square of that coefficient in its wave function which corresponds to a pure particle state multiplied by u_j^2,

$$(15) \qquad S_\alpha(\ell,j) = u_j^2 |c_\alpha(j,00;j)|^2.$$

In subsect. 4.1.7 these calculated spectroscopic factors are presented for odd-A Pm nuclei together with the corresponding experimental values from stripping reactions.

We have now obtained the basic formulae for the present calculation. The corresponding expressions for H_{int}, B(M1) and B(E2) are identical to those given in ref. 2 except for a multiplicative factor in the particle part involving u_j and v_j.

4.1.3. Assumptions made in the calculation

The calculation of the low-energy nuclear properties of the ^{141,143,145,147,149}Pm nuclei is performed using the formulation given in the preceding subsection. We assume that the above nuclei can be described as doubly even cores of 60 protons and 80, 82, 84, 86 and 88 neutrons, respectively. For the 61st proton the five states $g_{7/2}$, $d_{5/2}$, $h_{11/2}$, $d_{3/2}$ and $s_{1/2}$ are available. The cores perform quadrupole surface vibrations and are coupled to the single-particle states. Core states with more than three phonons are excluded from the calculations. The quadrupole energies are taken from the spectra of the corresponding even Nd nuclei (the energy of the first excited state). This energy $\hbar\omega$ is then slightly adjusted as a parameter. The next parameters are the energy differences $\Delta_j = E_j - E_{5/2}$ (or $\Delta_j = E_j - E_{7/2}$), instead of the five single-particle energies. The last parameter is the dimensionless coupling strength ξ which is varied within reasonable limits to obtain the best fit to the experimental spectra. The particle (u_j) and hole (v_j) amplitude for the state j are taken from (^{3}He,d) and (α,t) reactions[24,31,43,58].

Table 7 gives the values for the parameters that have been used in the calculations. The u and v values are taken from experiments whenever possible and the lacking values are linear interpolations from the neighbouring Pm nuclei. Such experimental values are now available for the odd nuclei $^{143-149}Pm$.

Table 7. Values of the parameters used in the calculation of energy levels of odd-mass Pm nuclei

Parameter	^{141}Pm	^{143}Pm	^{145}Pm	^{147}Pm	^{149}Pm
ξ	4.0	2.0	4.5	10.5	9.9
$\hbar\omega$ (keV)	770	1550	690	450	300
$\varepsilon_{7/2}$ (keV)	348	300	101	0	0
$\varepsilon_{5/2}$ (keV)	0	0	0	45	128
$\varepsilon_{3/2}$ (keV)	1556	1660	1365	1050	302
$\varepsilon_{1/2}$ (keV)	3140	2875	4000	4500	4500
$u_{g_{7/2}}$	0.49	0.56	0.62	0.64	0.76
$u_{d_{5/2}}$	0.71	0.73	0.73	0.75	0.76
$u_{d_{3/2}}$	1.00	1.00	0.92	0.72	0.59
$u_{s_{1/2}}$	0.99	0.98	0.86	0.77	0.77
$u_{h_{11/2}}$	0.91	0.89	0.90	0.82	0.75
$v_{g_{7/2}}$	0.87	0.83	0.78	0.77	0.65
$v_{d_{5/2}}$	0.70	0.68	0.68	0.66	0.64
$v_{d_{3/2}}$	0.10	0.30	0.38	0.69	0.81
$v_{s_{1/2}}$	0.14	0.25	0.51	0.64	0.64
$v_{h_{11/2}}$	0.41	0.45	0.44	0.56	0.66

4.1.4. Energy levels and eigenfunctions

The Hamiltonian given by eq. (1) in subsection 4.1.2 is diagonalized for each I. I varies between 1/2 and 15/2 for positive-parity levels and between 3/2 and 19/2 for negative-parity states. As a result of the diagonalization procedure we obtain the energy eigenvalues and expansion coefficients of the eigenvectors for every value of I. As an example, the largest matrices to be diagonalized are 26 x 26 for I = 7/2 and 5/2.

Figs. 21-25 show the experimental and calculated level scheme of the odd-A Pm nuclei which have been obtained in the present work. In the fitting procedure the energies of the three lowest excited states were brought as close to the experimental values as was practical (except for ^{149}Pm, see below). We chose this procedure instead of least-squares fitting, because the character of the lowest levels is well known. The agreement between the calculated and experimental value is then <1 keV for the three lowest states in all the Pm nuclei except ^{145}Pm. In ^{145}Pm one should take a larger value for ξ to get a better agreement but then the first $3/2^+$ level goes too far down. The experimental and theoretical levels have been connected in the figures with dashed lines. The spin order has been the main argument in this identification, but in some cases the electromagnetic decay properties have been taken into account.

In figs. 21-25 calculated levels are shown in the following way: for ^{141}Pm all levels <1300 keV and the lowest $13/2^+$ and $15/2^+$ states; for ^{143}Pm all levels <3000 keV and the lowest $13/2^+$ and $15/2^+$ states; for ^{145}Pm all levels <1200 keV and in the region 1200 - 1600 keV only states with $I > 9/2^+$; for ^{147}Pm all levels <1100 keV and for ^{149}Pm all levels <700 keV.

Tables 8-12 list the amplitudes of the basis states for selected energy levels in every Pm nucleus. Wave functions are of a rather mixed character, and the expansion coefficients larger than 0.01 have been listed in tables 8-12. In the present tables the basis states are denoted by $|\ell_j; NR\rangle$, where ℓ_j is the single-particle state, N is the number of phonons and R the angular momentum of the core.

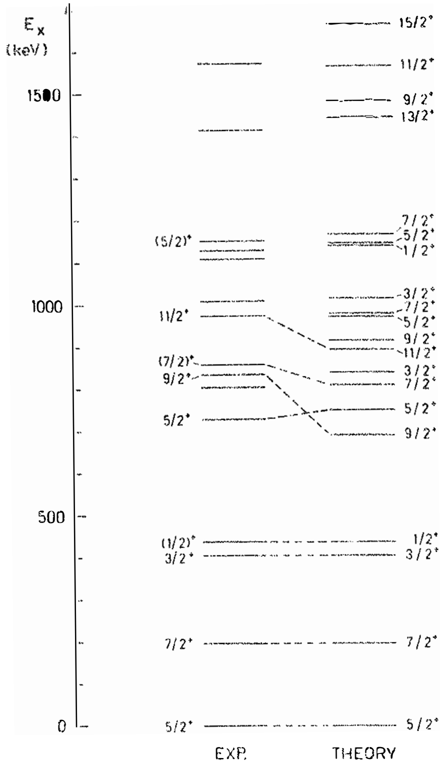

$^{141}_{61}Pm_{80}$

Fig. 21.

Figs. 21-25.

Comparisons between the experimental positive-parity energy levels and the theoretical calculations using the intermediate-coupling model

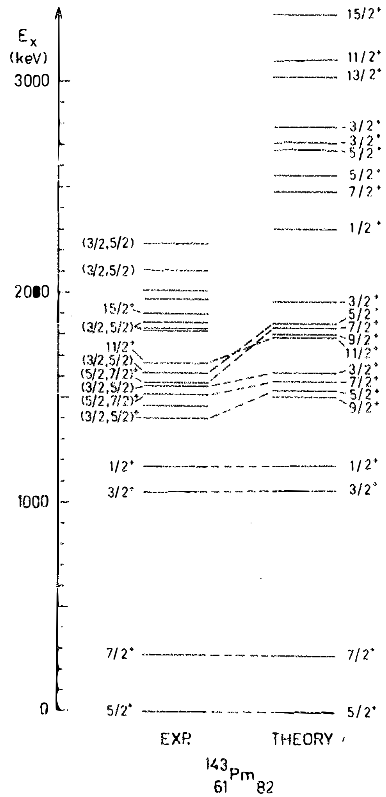

E_x
(keV)
3000
2000
1000
0
(3/2,5/2)
(3/2,5/2)
15/2⁺
(3/2,5/2)
11/2⁺
(3/2,5/2)
(5/2,7/2)⁺
(3/2,5/2)
(5/2,7/2)⁺
(3/2,5/2)⁺
1/2⁺
3/2⁺
7/2⁺
5/2⁺
15/2⁺
11/2⁺
13/2⁺
3/2⁺
3/2⁺
5/2⁺
5/2⁺
7/2⁺
1/2⁺
3/2⁺
5/2⁺
7/2⁺
9/2⁺
11/2⁺
3/2⁺
7/2⁺
5/2⁺
9/2⁺
1/2⁺
3/2⁺
7/2⁺
5/2⁺
EXP.
THEORY
$^{143}_{61}Pm_{82}$

Fig. 22.

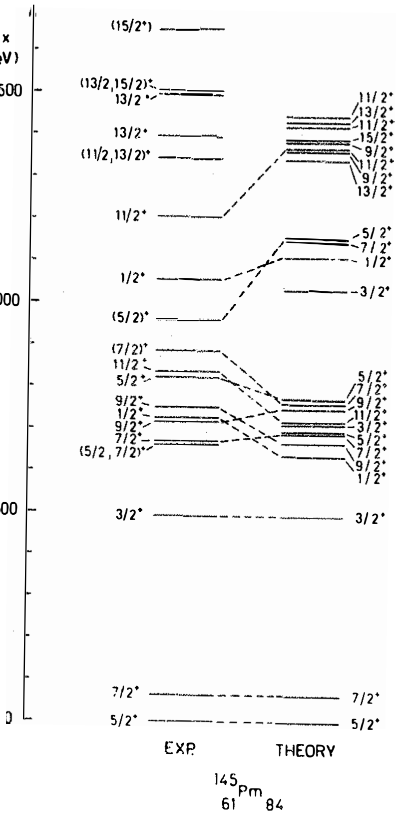

Ex
(keV)
1500
1000
500
0
(15/2+)
(13/2,15/2)+
13/2+
13/2+
(11/2,13/2)+
11/2+
1/2+
(5/2)+
(7/2)+
11/2+
5/2+
9/2+
1/2+
9/2+
7/2+
(5/2,7/2)+
3/2+
7/2+
5/2+
11/2+
13/2+
11/2+
15/2+
9/2+
11/2+
9/2+
13/2+
5/2+
7/2+
1/2+
3/2+
5/2+
7/2+
9/2+
11/2+
3/2+
5/2+
7/2+
9/2+
1/2+
3/2+
7/2+
5/2+
EXP.
THEORY
145 Pm 61 84

Fig. 23.

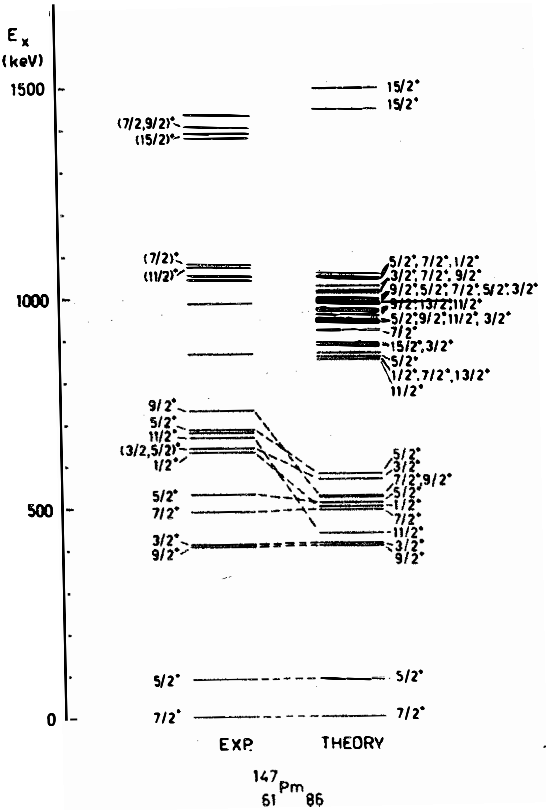

E_x (keV)
1500
1000
500
0
(7/2,9/2)⁺
(15/2)⁺
(7/2)⁺
(11/2)⁺
9/2⁺
5/2⁺
11/2⁺
(3/2,5/2)⁺
1/2⁺
5/2⁺
7/2⁺
3/2⁺
9/2⁺
5/2⁺
7/2⁺
15/2⁺
15/2⁺
5/2⁺, 7/2⁺, 1/2⁺
3/2⁺, 7/2⁺, 9/2⁺
9/2⁺, 5/2⁺, 7/2⁺, 5/2⁺, 3/2⁺
3/2⁺, 13/2⁺, 11/2⁺
5/2⁺, 9/2⁺, 11/2⁺, 3/2⁺
7/2⁺
15/2⁺, 3/2⁺
5/2⁺
1/2⁺, 7/2⁺, 13/2⁺
11/2⁺
5/2⁺
3/2⁺
7/2⁺, 9/2⁺
5/2⁺
1/2⁺
7/2⁺
11/2⁺
3/2⁺
9/2⁺
5/2⁺
7/2⁺
EXP.
THEORY
$^{147}_{61}Pm_{86}$

Fig. 24.

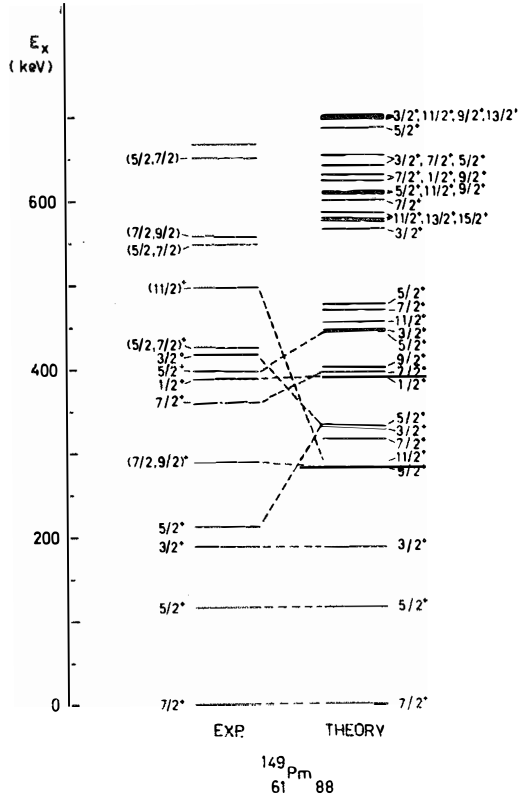

Ex
(keV)
600
400
200
0
(5/2,7/2)
(7/2,9/2)
(5/2,7/2)
(11/2)+
(5/2,7/2)+
3/2+
5/2+
1/2+
7/2+
(7/2,9/2)+
5/2+
3/2+
5/2+
7/2+
3/2+, 11/2+, 9/2+, 13/2+
5/2+
3/2+, 7/2+, 5/2+
7/2+, 1/2+, 9/2+
5/2+, 11/2+, 9/2+
7/2+
11/2+, 13/2+, 15/2+
3/2+
5/2+
7/2+
11/2+
3/2+
5/2+
9/2+
7/2+
1/2+
5/2+
3/2+
7/2+
11/2+
9/2+
3/2+
5/2+
7/2+
EXP.
THEORY
149 Pm 61 88

Fig. 25.

Table 8. Expansion coefficients of the eigenvectors for selected states in the ^{141}Pm nucleus.

$\|\ell_j\ ;\ NR\rangle$	E(keV) ; I^{π}							
	$0;5/2^+$	$197;7/2^+$	$404;3/2^+$	$438;1/2^+$	$728;5/2^+$	$837;9/2^+$	$858;7/2^+$	$974;11/2^+$
$\|s_{1/2}\ ;\ 00\rangle$				0.3263				
$\|s_{1/2}\ ;\ 12\rangle$	0.1330		-0.1717		-0.0488			
$\|s_{1/2}\ ;\ 20\rangle$				0.1741				
$\|s_{1/2}\ ;\ 22\rangle$	-0.0200		0.1199		0.1664			
$\|s_{1/2}\ ;\ 24\rangle$		0.0355				0.1796	0.0675	
$\|s_{1/2}\ ;\ 30\rangle$				-0.0378				
$\|s_{1/2}\ ;\ 32\rangle$	0.0148		-0.0493		-0.0238			
$\|s_{1/2}\ ;\ 33\rangle$							-0.0183	
$\|s_{1/2}\ ;\ 34\rangle$						-0.0198		
$\|s_{1/2}\ ;\ 36\rangle$								0.0488
$\|d_{3/2}\ ;\ 00\rangle$			-0.5368					
$\|d_{3/2}\ ;\ 12\rangle$	0.1316	0.1711	0.3203	-0.3337	-0.0361		0.0375	
$\|d_{3/2}\ ;\ 20\rangle$			-0.2040					
$\|d_{3/2}\ ;\ 22\rangle$	0.0118	0.0435	-0.0313	0.1913	0.0717		-0.1037	
$\|d_{3/2}\ ;\ 24\rangle$	-0.0795	-0.0473			0.0927	0.1717	0.0826	0.2339
$\|d_{3/2}\ ;\ 30\rangle$								
$\|d_{3/2}\ ;\ 32\rangle$	0.0141	0.0210	0.0751	-0.0931	-0.0152			
$\|d_{3/2}\ ;\ 33\rangle$			0.0124				0.0208	
$\|d_{3/2}\ ;\ 34\rangle$	0.0161				-0.0760		0.0475	0.0406
$\|d_{3/2}\ ;\ 36\rangle$						-0.1038		-0.0602
$\|d_{5/2}\ ;\ 00\rangle$	0.9716				0.0579			
$\|d_{5/2}\ ;\ 12\rangle$	-0.0347	-0.0991	0.5183	0.8188	0.9585	0.9432	0.9715	
$\|d_{5/2}\ ;\ 20\rangle$	0.0431				-0.0453			
$\|d_{5/2}\ ;\ 22\rangle$	0.0553	-0.0323	0.0369	-0.0926	-0.0403		0.0176	
$\|d_{5/2}\ ;\ 24\rangle$	0.0131	-0.0390	-0.1982		-0.0492	-0.0448	-0.0342	-0.1003
$\|d_{5/2}\ ;\ 30\rangle$					0.0390			
$\|d_{5/2}\ ;\ 32\rangle$			0.0473	0.0850	0.0363	0.0513	0.0200	
$\|d_{5/2}\ ;\ 33\rangle$			0.0268	0.0404	0.0445	-0.0411		0.0175
$\|d_{5/2}\ ;\ 34\rangle$	-0.0125		0.0449		0.0399	0.0436	0.0330	-0.0348
$\|d_{5/2}\ ;\ 36\rangle$		0.0203				0.0133	0.0200	-0.0497
$\|g_{7/2}\ ;\ 00\rangle$		0.3787					0.0594	
$\|g_{7/2}\ ;\ 12\rangle$	0.0698	0.4034	-0.4166		0.0782	0.1327	0.0821	0.8655
$\|g_{7/2}\ ;\ 20\rangle$		0.0881					-0.0110	
$\|g_{7/2}\ ;\ 22\rangle$	0.0258	-0.0171	-0.1060		-0.0527	0.0171	-0.0143	0.1977
$\|g_{7/2}\ ;\ 24\rangle$	0.0320	0.0917	0.1110	-0.1269	0.0540	0.0907	0.1161	0.3436
$\|g_{7/2}\ ;\ 30\rangle$							-0.0106	
$\|g_{7/2}\ ;\ 32\rangle$		0.0259	-0.0551			0.0180		0.0794
$\|g_{7/2}\ ;\ 33\rangle$				0.0270	0.0169	-0.0183	-0.0288	0.0238
$\|g_{7/2}\ ;\ 34\rangle$			0.0103	0.0181	0.0165	0.0185		0.0209
$\|g_{7/2}\ ;\ 36\rangle$	-0.0171				0.0321	0.0422	0.0339	0.0996

Coefficients larger than 0.01 are given in the table.

Table 9. Expansion coefficients of the eigenvectors for selected states in the ^{143}Pm nucleus.

	E(keV) ; I^{π}								
$\vert \ell_j$; NR>	0;5/2$^+$	272;7/2$^+$	1056;3/2$^+$	1173;1/2$^+$	1663;11/2$^+$	1898;15/2$^+$	1402;(5/2$^+$)	1515;(7/2$^+$)	1558;(3/2$^+$)
$\vert s_{1/2}$; 00>				0.4480					
$\vert s_{1/2}$; 12>	0.0923		0.1762				-0.0146		0.0862
$\vert s_{1/2}$; 20>				0.1140					
$\vert s_{1/2}$; 22>			-0.0702				0.1184		0.0537
$\vert s_{1/2}$; 24>		0.0128						0.0444	
$\vert s_{1/2}$; 30>				-0.0146					
$\vert s_{1/2}$; 32>			0.0177						
$\vert s_{1/2}$; 33>									
$\vert s_{1/2}$; 34>									
$\vert s_{1/2}$; 36>					0.0206				
$\vert d_{3/2}$; 00>			0.7646						0.2279
$\vert d_{3/2}$; 12>	0.0657	0.0885	-0.2742	-0.2717			-0.0206	0.0164	-0.0629
$\vert d_{3/2}$; 20>			0.0940						
$\vert d_{3/2}$; 22>			0.0269	0.0992			0.0306	-0.0556	0.0987
$\vert d_{3/2}$; 24>	-0.0275	-0.0134			0.1264		0.0323	0.0469	
$\vert d_{3/2}$; 30>									
$\vert d_{3/2}$; 32>			-0.0216	-0.0339					
$\vert d_{3/2}$; 33>							-0.0113		0.0243
$\vert d_{3/2}$; 34>							-0.0277	0.0152	
$\vert d_{3/2}$; 36>					-0.0205	0.1353			
$\vert d_{5/2}$; 00>	0.9920						0.0353		
$\vert d_{5/2}$; 12>	-0.0313	-0.0321	-0.3970	0.8338			0.9886	0.9941	0.8756
$\vert d_{5/2}$; 20>	0.0107						-0.0234		
$\vert d_{5/2}$; 22>	0.0158			-0.0503				0.0234	-0.0137
$\vert d_{5/2}$; 24>			0.0925		-0.0367		-0.0243	-0.0318	0.0435
$\vert d_{5/2}$; 30>							0.0120		
$\vert d_{5/2}$; 32>			-0.0101	0.0274			0.0112		
$\vert d_{5/2}$; 33>							0.0169		0.0134
$\vert d_{5/2}$; 34>			-0.0143				0.0132		
$\vert d_{5/2}$; 36>					-0.0101	-0.0417			
$\vert g_{7/2}$; 00>		0.9789						0.0298	
$\vert g_{7/2}$; 12>	0.0261	0.1786	0.3517		0.9727		0.0301		0.3893
$\vert g_{7/2}$; 20>		0.0152						-0.0125	
$\vert g_{7/2}$; 22>			0.0395		0.0910		-0.0211		0.0444
$\vert g_{7/2}$; 24>		0.0176	-0.0428	-0.0501	0.1625	0.9719	0.0225	0.0306	0.0242
$\vert g_{7/2}$; 30>									
$\vert g_{7/2}$; 32>			0.0114		0.0171				
$\vert g_{7/2}$; 33>									
$\vert g_{7/2}$; 34>						0.0973			0.0122
$\vert g_{7/2}$; 36>					0.0214	0.1608			

Coefficients larger than 0.01 are given in the table.

Table 10. Expansion coefficients of the eigenvectors for selected states in the ^{145}Pm nucleus.

	E(keV) ; I^{π}								
$\vert \ell_j$; NR>	0;5/2$^+$	61;7/2$^+$	492;3/2$^+$	660;5/2$^+$	670;7/2$^+$	713;9/2$^+$	726;1/2$^+$	750;9/2$^+$	836;11/2$^+$
$\vert s_{1/2}$; 00>							0.1253		
$\vert s_{1/2}$; 12>	0.0469		-0.0650						
$\vert s_{1/2}$; 20>							0.0642		
$\vert s_{1/2}$; 22>			0.0431	0.0553					
$\vert s_{1/2}$; 24>		0.0136			0.0204	0.0652		-0.0144	
$\vert s_{1/2}$; 30>							-0.0160		
$\vert s_{1/2}$; 32>			-0.0157						
$\vert s_{1/2}$; 33>					-0.0120				
$\vert s_{1/2}$; 34>						-0.0113			
$\vert s_{1/2}$; 36>									0.0215
$\vert d_{3/2}$; 00>			-0.4845						
$\vert d_{3/2}$; 12>	0.0898	0.1248	0.2152	0.0294			-0.1461		
$\vert d_{3/2}$; 20>			-0.1432						
$\vert d_{3/2}$; 22>		0.0155		0.0706	-0.0828		0.1124		
$\vert d_{3/2}$; 24>	-0.0288	-0.0252		-0.0314	0.0663	0.1278		0.0521	0.1757
$\vert d_{3/2}$; 30>									
$\vert d_{3/2}$; 32>			0.0382				-0.0373		
$\vert d_{3/2}$; 33>					0.0119			0.0233	
$\vert d_{3/2}$; 34>				-0.0271	0.0225	0.0111		0.0196	0.0148
$\vert d_{3/2}$; 36>						-0.0440			-0.0367
$\vert d_{5/2}$; 00>	0.9895			0.0793					
$\vert d_{5/2}$; 12>	-0.0882	-0.0326	0.5399	0.9699	0.9838	0.9581	0.9601	-0.2264	
$\vert d_{5/2}$; 20>	0.0145			-0.0494					
$\vert d_{5/2}$; 22>	0.0119	-0.0145	0.0258	0.0312	0.0689	-0.0326	-0.1287	0.0408	
$\vert d_{5/2}$; 24>		-0.0157	-0.0837	-0.0795	-0.0838	-0.0909			-0.0370
$\vert d_{5/2}$; 30>				0.0113					
$\vert d_{5/2}$; 32>			0.0240	0.0126	0.0118	0.0192	0.0267		
$\vert d_{5/2}$; 33>						-0.0109	0.0169		
$\vert d_{5/2}$; 34>			0.0119		0.0122				-0.0176
$\vert d_{5/2}$; 36>								-0.0124	-0.0213
$\vert g_{7/2}$; 00>		0.9630			0.0489				
$\vert g_{7/2}$; 12>	0.0306	0.2283	-0.6116	0.1687	-0.0565	0.2091		0.9285	0.9530
$\vert g_{7/2}$; 20>		0.0314			-0.0243				
$\vert g_{7/2}$; 22>	0.0148		-0.1026					-0.1617	0.1156
$\vert g_{7/2}$; 24>	0.0167	0.0346	0.0679	0.0540	0.0251	0.0663	-0.0676	0.2291	0.2000
$\vert g_{7/2}$; 30>									
$\vert g_{7/2}$; 32>			-0.0370			0.0113		0.0249	0.0355
$\vert g_{7/2}$; 33>				0.0100	-0.0164	-0.0127	0.0150	-0.0111	
$\vert g_{7/2}$; 34>				0.0161		0.0126	0.0182	-0.0219	0.0185
$\vert g_{7/2}$; 36>				0.0108	0.0161	0.0257		0.0333	0.0404

Coefficients larger than 0.01 are given in the table.

Table 11. Expansion coefficients of the eigenvectors for selected states in the ^{147}Pm nucleus.

$\|\ell_j$; NR>	E(keV) ; I^{π}								
	0;7/2$^+$	91;5/2$^+$	408;9/2$^+$	410;3/2$^+$	489;7/2$^+$	531;5/2$^+$	633;1/2$^+$	667;11/2$^+$	731;9/2$^+$
$\|s_{1/2}$; 00>							0.0673		
$\|s_{1/2}$; 12>		0.0339							
$\|s_{1/2}$; 20>							0.0384		
$\|s_{1/2}$; 22>		-0.0122							
$\|s_{1/2}$; 24>									0.0477
$\|s_{1/2}$; 30>							-0.0143		
$\|s_{1/2}$; 32>									
$\|s_{1/2}$; 33>									
$\|s_{1/2}$; 34>									-0.0145
$\|s_{1/2}$; 36>									
$\|d_{3/2}$; 00>				-0.1415					
$\|d_{3/2}$; 12>	-0.0473	0.0314		-0.0185	0.0248	-0.0323	-0.0312		
$\|d_{3/2}$; 20>				-0.0450					
$\|d_{3/2}$; 22>	-0.0169			-0.0189	-0.0507	-0.0468	0.0250		
$\|d_{3/2}$; 24>			-0.0302					-0.0658	0.0384
$\|d_{3/2}$; 30>				-0.0160					
$\|d_{3/2}$; 32>									
$\|d_{3/2}$; 33>			-0.0193		-0.0159				
$\|d_{3/2}$; 34>								-0.0206	
$\|d_{3/2}$; 36>									-0.0104
$\|d_{5/2}$; 00>		0.9530				-0.0148			
$\|d_{5/2}$; 12>	-0.0160	-0.2929		0.0454	0.2821	0.0370	0.9365		0.9444
$\|d_{5/2}$; 20>		0.0346							
$\|d_{5/2}$; 22>		-0.0120	0.0114	-0.0211	0.0574	-0.0148	-0.3340		-0.1301
$\|d_{5/2}$; 24>		0.0363	-0.0129		-0.0882			-0.0189	-0.2874
$\|d_{5/2}$; 30>									
$\|d_{5/2}$; 32>					0.0104		0.0464		0.0353
$\|d_{5/2}$; 33>							-0.0297		0.0129
$\|d_{5/2}$; 34>									
$\|d_{5/2}$; 36>									0.0485
$\|g_{7/2}$; 00>	0.9064				-0.3797				
$\|g_{7/2}$; 12>	0.4036	0.0278	0.8784	0.8890	0.7352	0.9536		0.8973	
$\|g_{7/2}$; 20>	0.0614				0.2459				
$\|g_{7/2}$; 22>	-0.0491		-0.2593	0.3995	-0.2292	0.1129		0.1978	0.0221
$\|g_{7/2}$; 24>	0.0777		0.3782	0.1138	0.3005	0.2594	0.0225	0.3699	0.0160
$\|g_{7/2}$; 30>					-0.0365				
$\|g_{7/2}$; 32>	0.0186		0.0630	0.0577	0.1134	0.0218		0.0538	
$\|g_{7/2}$; 33>			-0.0221	-0.0804		-0.0525		0.0497	
$\|g_{7/2}$; 34>			-0.0813	0.0396	-0.0379	0.0409			
$\|g_{7/2}$; 36>			0.0732		0.0412	0.0197		0.0933	

Coefficients larger than 0.01 are given in the table.

Table 12. Expansion coefficients of the eigenvectors for selected states in the ^{149}Pm nucleus.

$\vert \ell_j$; NR>	E(keV) ; I^π								
	0;7/2$^+$	114;5/2$^+$	188;3/2$^+$	211;5/2$^+$	288;9/2$^+$	360;7/2$^+$	387;1/2$^+$	415;3/2$^+$	497;11/2$^+$
$\vert s_{1/2}$; 00>							0.0456		
$\vert s_{1/2}$; 12>		0.0239							
$\vert s_{1/2}$; 20>							0.0285		
$\vert s_{1/2}$; 22>		-0.0107							
$\vert s_{1/2}$; 24>						0.0109			
$\vert s_{1/2}$; 30>							-0.0121		
$\vert s_{1/2}$; 32>									
$\vert s_{1/2}$; 33>						-0.0133			
$\vert s_{1/2}$; 34>									
$\vert s_{1/2}$; 36>									
$\vert d_{3/2}$; 00>			0.7361					0.4109	
$\vert d_{3/2}$; 12>	-0.0925	-0.0587	0.3555	0.1348			0.1515	0.3439	
$\vert d_{3/2}$; 20>			0.1101						
$\vert d_{3/2}$; 22>	0.0179	0.0334	0.0144	-0.1286		0.0673	0.0379	-0.0348	
$\vert d_{3/2}$; 24>	-0.0196			0.0289	-0.0602	-0.0400			-0.1299
$\vert d_{3/2}$; 30>								0.0186	
$\vert d_{3/2}$; 32>			0.0260	0.0291		-0.0145	0.0244	0.0183	
$\vert d_{3/2}$; 33>				0.0197	0.0222	0.0236		0.0121	
$\vert d_{3/2}$; 34>				-0.0124	0.0193	0.0259			0.0182
$\vert d_{3/2}$; 36>					-0.0115				-0.0299
$\vert d_{5/2}$; 00>		0.9064		0.2063					
$\vert d_{5/2}$; 12>	0.0856	-0.3418	0.1182	-0.1065		0.8582	0.8795	0.0283	
$\vert d_{5/2}$; 20>		0.0568		-0.0545					
$\vert d_{5/2}$; 22>		-0.0346	-0.0660	0.0669	-0.0694	0.2381	-0.3926	0.0370	
$\vert d_{5/2}$; 24>	-0.0260	0.0435		0.0595		-0.3179		0.0297	0.1017
$\vert d_{5/2}$; 30>					0.0752				
$\vert d_{5/2}$; 32>		-0.0143	0.0104	0.0139		0.0652	0.0587		
$\vert d_{5/2}$; 33>			-0.0136	0.0145		-0.0127			
$\vert d_{5/2}$; 34>				-0.0264	0.0197	-0.0503	-0.0562	-0.0160	
$\vert d_{5/2}$; 36>					-0.0217	0.0338			-0.0354
$\vert g_{7/2}$; 00>	0.9349					-0.1423			
$\vert g_{7/2}$; 12>	-0.3222	-0.2134	-0.5279	0.9167	0.9131	-0.1425		0.7389	0.9245
$\vert g_{7/2}$; 20>	0.0455					0.1602			
$\vert g_{7/2}$; 22>	-0.0294		0.1330	-0.1102	0.2135			-0.3399	-0.1596
$\vert g_{7/2}$; 24>		0.0633	-0.0536	-0.2049	-0.3129	-0.1325	-0.1796	-0.1948	
$\vert g_{7/2}$; 30>									-0.2909
$\vert g_{7/2}$; 32>	-0.0101		-0.0264	0.0258	0.0473	-0.0348		0.0404	0.0438
$\vert g_{7/2}$; 33>				-0.0243	-0.0147	-0.0216	-0.0570	-0.0625	0.0243
$\vert g_{7/2}$; 34>				0.0345	-0.0463	-0.0351	0.0462	0.0459	
$\vert g_{7/2}$; 36>					0.0467	0.0531			0.0536

Coefficients larger than 0.01 are given in the table.

4.1.5. Electromagnetic transition rates

We can now calculate the electromagnetic transition rates with the aid of the wave functions obtained in the preceding subsection. The calculation for the M1 and E2 transition rates have been performed using the general expressions given by eqs. (10) and (12). In the present calculation of B(M1) transition rates we have used the values of gyromagnetic ratios $g_\ell = 1$, $g_s = 0.7\ g_s^{free}$ and $g_R = Z/A$ for the orbital angular momentum, the spin and the core, respectively. In the calculation of B(E2) transition rates the stiffness parameter C for each nucleus is needed. These C values were derived from the experimental $2_1^+ \rightarrow 0_1^+$ reduced transition probabilities in the neighbouring Nd isotones assuming that those nuclei could be described by pure harmonic oscillator motion[59] with

$$(16) \qquad B(E2;\ 0^+ \rightarrow 2^+) = 5\ \frac{\hbar\omega}{2C}\ \left(\frac{3}{4\pi}\ ZeR_0^{\ 2}\right)^2$$

The following values were obtained: C(^{141}Pm) = 124 MeV, C(^{143}Pm) = 303 MeV, C(^{145}Pm) = 115 MeV, C(^{147}Pm) = 57 MeV and C(^{149}Pm) = 26 MeV. For the radial matrix element in eq. (12) we have used the approximation $<|r^2|> = \frac{3}{5}R_0^{\ 2}$ and $R_0 = 1.2\ A^{1/3}$ fm. In order to take into account polarization effects of the core[2,60] we have used the effective proton charge $e_p = 2e$.

The results of our calculation of B(M1) and B(E2) transition rates are presented in tables 13-17. In addition to the B(M1) and B(E2) values are given λ_{tot} and branching ratios of certain levels. In addition to the experimental branching ratios in tables 13-17, we also give theoretical values which have been obtained with the aid of theoretical B(M1) and B(E2) transition rates and experimental transition energies in the Pm isotopes. The small branches given by the calculation are ignored if they are not known experimentally. Table 15

Table 13. Electromagnetic transition rates and branching ratios in ^{141}Pm. The uncertainties of the last figures are in parentheses.

E_i ; I_i^{π} (keV)	E_f ; I_f^{π} (keV)	E_{γ} (keV)	B(M1) ($\times 10^{-3} \mu_N^2$) a)	B(E2) ($e^2 fm^4$) a)	λ_{tot} (1/s)	Branching ratio Exp	Branching ratio Theory a)
196.9 ; $7/2^+$	0 ; $5/2^+$	196.9	2.9×10^{-6}	35.0	1.264×10^{7}	1	1.000
403.9 ; $3/2^+$	0 ; $5/2^+$	403.9	307.8	666.0	3.656×10^{11}	1	0.999
438.5 ; $(1/2)^+$	0 ; $5/2^+$	438.5	-	1427.4	2.823×10^{10}	1	0.997
728.3 ; $5/2^+$	0 ; $5/2^+$	728.1	0.39	992.7	2.505×10^{11}	0.26(3) b)	0.481
	196.9 ; $7/2^+$	531.4	8.90	10.1	2.402×10^{10}	0.21(2)	0.046
	403.9 ; $3/2^+$	324.5	409.3	0.618	2.461×10^{11}	0.53(6)	0.473
837.0 ; $9/2^+$	0 ; $5/2^+$	837.0	-	1032.7	5.176×10^{11}	0.94(4)	0.930
	196.9 ; $7/2^+$	640.2	7.12	46.3	3.896×10^{10}	0.06(1)	0.070
858.6 ; $(7/2)^+$	0 ; $5/2^+$	858.6	3.22	972.4	5.894×10^{10}	0.89(7)	0.817
	196.9 ; $7/2^+$	661.7	21.3	23.2	1.120×10^{11}	0.11(2)	0.155
974.3 ; $11/2^+$	196.9 ; $7/2^+$	777.4	-	1147.5	3.975×10^{11}	1	0.999
1152.7 ; $(5/2)^+$	196.9 ; $7/2^+$	955.7	3.84	549.2	5.932×10^{11}	0.57(1)	0.359
	403.9 ; $3/2^+$	749.0	1.65	689.4	2.104×10^{11}	0.43(1)	0.127
1970.1 ; $(15/2)^+$	974.3 ; $11/2^+$	995.8	-	2093.9	2.501×10^{12}	1	1.000

a) Calculated in the present work using the intermediate-coupling model.

b) Ref. 19.

Table 14. Electromagnetic transition rates and branching ratios in ^{143}Pm. The uncertainties of the last figures are in parentheses.

E_i ; I_i^{π} (keV)	E_f ; I_f^{π} (keV)	E_γ (keV)	B(M1) ($\times 10^{-3}\mu_N^2$) a)	B(E2) (e^2fm^4) a)	λ_{tot} (1/s)	Branching ratio Exp	Branching ratio Theory a)
272.1 ; $7/2^+$	0 ; $5/2^+$	272.1	0.00035	5.54	1.021×10^7	1	1.000
1056.5 ; $3/2^+$	0 ; $5/2^+$	1056.5	694.6	298.7	1.442×10^{13}	1	0.992
1173.1 ; $1/2^+$	0 ; $5/2^+$	1173.1	-	1088.8	2.951×10^{12}	1	0.999
1402.5 ; $(3/2, 5/2)^+$	0 ; $5/2^+$	1402.5	0.192	831.7	5.515×10^{12}	1	0.999
1515.0 ; $(5/2, 7/2)^+$	0 ; $5/2^+$	1515.0	0.583	848.6	8.298×10^{12}	0.72(7)	0.984
	272.1 ; $7/2^+$	1242.7	3.985	0.539	1.365×10^{11}	0.28(3)	0.016
1558.5 ; (3/2, 5/2)	272.1 ; $7/2^+$	1286.4	-	185.4	7.968×10^{11}	1	0.077
1566.0 ; $(5/2, 7/2)^+$	0 ; $5/2^+$	1566.0	0.020	0.168	3.287×10^9	0.29(3)	0.00095
	272.1 ; $7/2^+$	1293.9	0.192	775.1	3.437×10^{12}	0.71(7)	0.999
1614.1 ; (3/2, 5/2)	272.1 ; $7/2^+$	1342.0	1.623	760.9	4.110×10^{12}	1	0.968
1663.5 ; $11/2^+$	272.1 ; $7/2^+$	1391.4	-	851.5	5.418×10^{12}	1	0.999

a) Calculated in the present work using the intermediate-coupling model.

Table 15. Electromagnetic transition rates and branching ratios in ^{145}Pm. The uncertainties of the last figures are in parentheses.

E_i ; I_i^{π} (keV)	E_f ; I_f^{π} (keV)	E_{γ} (keV)	B(M1) ($\times 10^{-3} \mu_N^2$) a)	B(E2) ($e^2 fm^4$) a)	λ_{tot} (1/s)	Branching ratio Exp	Theory a)	Theory b)
61.2 ; $7/2^+$	0 ; $5/2^+$	61.2	9.01×10^{-3}	4.65	4.122×10^{4}	1	1.000	
492.5 ; $3/2^+$	0 ; $5/2^+$	492.5	343.5	466.8	7.387×10^{11}	1	0.983	
660.5 ; $5/2^+$	0 ; $5/2^+$	660.5	0.107	949.9	1.462×10^{11}	0.18(2)	0.809	
	61.2 ; $7/2^+$	599.1	1.46	32.3	8.559×10^{9}	0.75(6)	0.047	
	492.5 ; $3/2^+$	168.0	309.9	19.6	2.586×10^{10}	0.07(1)	0.143	
669.7 ; $7/2^+$	0 ; $5/2^+$	669.7	3.42×10^{-4}	1004.0	1.650×10^{11}	0.84(4)	0.875	0.719
	61.2 ; $7/2^+$	608.6	5.88	2.98	2.363×10^{10}	0.16(2)	0.125	0.280
713.6 ; $9/2^+$	61.2 ; $7/2^+$	652.4	0.508	1005.0	1.473×10^{11}	1	0.935	
726.5 ; $1/2^+$	492.5 ; $3/2^+$	234.0	247.5	106.1	5.590×10^{10}	1	0.174	
750.4 ; $9/2^+$	0 ; $5/2^+$	750.4	-	978.8	2.841×10^{11}	0.98(5)	0.814	0.971
	669.7 ; $7/2^+$	80.7	20.08	1.22	1.857×10^{8}	0.02(1)	9.0×10^{-4}	0.029
823.5 ; $5/2^+$	61.2 ; $7/2^+$	762.3	3.37	866.1	2.983×10^{11}	0.34(4)	0.792	0.184
	492.5 ; $3/2^+$	331.0	45.1	119.8	2.939×10^{10}	0.59(5)	0.078	0.735
	669.7 ; $7/2^+$	153.8	5.85	4.85	3.750×10^{8}	0.06(1)	9.9×10^{-4}	0.080
836.5 ; $11/2^+$	61.2 ; $7/2^+$	775.3	-	1057.2	3.613×10^{11}	0.99(5)	0.999	0.997
	713.6 ; $9/2^+$	122.8	1.20	0.088	3.914×10^{7}	0.010(1)	1.1×10^{-4}	0.003
883.8 ; $(7/2)^+$	0 ; $5/2^+$	883.8	0.026	5.36	3.840×10^{9}	0.49(5)	0.009	0.680
	61.2 ; $7/2^+$	822.7	0.450	925.7	4.300×10^{11}	0.44(4)	0.977	0.319
	660.5 ; $5/2^+$	223.5	10.78	1.21	2.119×10^{9}	0.09(1)	0.005	
958.0 ; $(5/2)^+$	0 ; $5/2^+$	958.0	7.75	0.064	1.200×10^{11}	0.92(9)	0.375	0.971
	492.5 ; $3/2^+$	465.5	0.672	1168.0	3.233×10^{10}	0.08(1)	0.101	0.029
1057.3 ; $1/2^+$	492.5 ; $3/2^+$	564.8	131.1	1179.7	4.984×10^{11}	1	0.881	
1206.8 ; $11/2^+$	669.7 ; $7/2^+$	537.0	-	1367.9	7.452×10^{10}	0.13(1)	0.669	0.030
	713.6 ; $9/2^+$	493.2	0.150	597.8	2.159×10^{10}	0.12(9)	0.194	0.293
	750.4 ; $9/2^+$	456.4	2.49	25.9	4.800×10^{9}	0.67(4)	0.043	0.199
	836.5 ; $11/2^+$	370.3	11.32	37.0	1.043×10^{10}	0.07(2)	0.094	0.478

a) Calculated in the present work using the intermediate-coupling model.

b) Calculated by Paar using the cluster-vibration model (ref. 61).

Table 16. Electromagnetic transition rates and branching ratios in ^{147}Pm. The uncertainties of the last figures are in parentheses.

E_i ; I_i^{π} (keV)	E_f ; I_f^{π} (keV)	E_{γ} (keV)	B(M1) ($\times 10^{-3} \mu_N^2$) a)	B(E2) ($e^2 fm^4$) a)	λ_{tot} (1/s)	Branching ratio Exp	Branching ratio Theory a)
91.1 ; $5/2^+$	0 ; $7/2^+$	91.1	0.019	2.68	2.852×10^5	1	1.000
408.2 ; $9/2^+$	0 ; $7/2^+$	408.2	6.32	1668.2	3.063×10^{10}	1	0.999
410.6 ; $3/2^+$	0 ; $7/2^+$	410.6	-	1527.9	2.175×10^{10}	0.07(1)	0.613
	91.1 ; $5/2^+$	319.5	23.92	3.26	1.374×10^{10}	0.93(9)	0.387
489.3 ; $7/2^+$	0 ; $7/2^+$	489.4	1.25	971.0	3.583×10^{10}	0.19(2)	0.855
	91.1 ; $5/2^+$	398.2	3.41	156.6	5.700×10^9	0.81(7)	0.136
531.1 ; $5/2^+$	0 ; $7/2^+$	531.0	10.0	993.5	7.752×10^{10}	0.89(9)	0.966
	91.1 ; $5/2^+$	439.9	0.96	2.22	1.483×10^9	0.09(2)	0.018
	410.6 ; $3/2^+$	120.5	37.27	376.2	1.159×10^9	0.03(1)	0.014
632.8 ; $1/2^+$	91.1 ; $5/2^+$	541.7	-	1584.1	9.014×10^{10}	1	0.991
641.3 ; $(3/2, 5/2)^+$	410.6 ; $3/2^+$	230.8	0.67	0.45	1.468×10^8	1	2.4×10^{-4}
667.2 ; $11/2^+$	0 ; $7/2^+$	667.2	-	1435.7	2.316×10^{11}	0.83(7)	0.970
	408.2 ; $9/2^+$	259.0	22.38	226.3	7.160×10^9	0.17(2)	0.030
686.1 ; $5/2^+$	0 ; $7/2^+$	686.1	0.092	0.71	6.579×10^8	0.40(4)	0.003
	91.1 ; $5/2^+$	595.0	23.86	1109.8	1.894×10^{11}	0.14(3)	0.944
	410.6 ; $3/2^+$	275.5	0.19	0.95	7.530×10^7	0.37(4)	3.7×10^{-4}
	489.3 ; $7/2^+$	196.6	71.23	28.0	9.536×10^9	0.08(2)	0.047
730.7 ; $9/2^+$	91.1 ; $5/2^+$	639.6	-	1420.9	1.855×10^{11}	0.54(5)	0.873
	489.3 ; $7/2^+$	241.4	46.12	12.6	1.143×10^{10}	0.46(7)	0.054

a) Calculated in the present work using the intermediate-coupling model.

Table 17. Electromagnetic transition rates and branching ratios in ^{149}Pm. The uncertainties of the last figures are in parentheses.

E_i ; I_i^{π} (keV)	E_f ; I_f^{π} (keV)	E_γ (keV)	B(M1) ($\times 10^{-3} \mu_N^2$) a)	B(E2) ($e^2 fm^4$) a)	λ_{tot} (1/s)	Branching ratio Exp	Theory a)	Theory b)
114.3 ; $5/2^+$	0 ; $7/2^+$	114.3	0.35	224.6	1.459×10^7	1	1.000	1.000
188.6 ; $3/2^+$	0 ; $7/2^+$	188.6	-	995.9	2.903×10^8	0.57(5)	0.097	5.3×10^{-4}
	114.3 ; $5/2^+$	74.3	371.8	140.6	2.684×10^9	0.43(8)	0.902	0.99
211.3 ; $5/2^+$	0 ; $7/2^+$	211.3	6.01	1506.5	1.771×10^9	0.96(8)	0.573	0.79
	114.3 ; $5/2^+$	97.0	82.0	10.3	1.317×10^9	0.04(1)	0.426	0.21
288.2 ; $(7/2, \underline{9/2})^+$	0 ; $7/2^+$	288.2	4.50	2298.8	7.472×10^9	1	0.999	0.99
360.0 ; $7/2^+$	0 ; $7/2^+$	360.1	6.75	29.2	5.761×10^9	0.16(2)	0.196	0.41
	114.3 ; $5/2^+$	245.7	80.6	2241.7	2.349×10^{10}	0.84(7)	0.800	0.58
387.5 ; $1/2^+$	114.3 ; $5/2^+$	273.2	-	2217.8	4.118×10^9	0.11(2)	0.872	0.02
	188.6 ; $3/2^+$	198.9	3.35	287.9	5.734×10^8	0.89(15)	0.121	0.98
396.7 ; $5/2^+$	0 ; $7/2^+$	396.4	3.46	5.26	3.858×10^9	0.02(1)	0.071	0.20
	114.3 ; $5/2^+$	282.4	31.5	1515.6	1.579×10^{10}	0.18(1)	0.290	0.70
	188.6 ; $3/2^+$	208.1	216.0	125.0	3.432×10^{10}	0.77(9)	0.631	0.04
	211.3 ; $5/2^+$	185.4	0.24	59.0	4.290×10^7	0.03(1)	7.9×10^{-4}	0.04
415.5 ; $3/2^+$	114.3 ; $5/2^+$	301.2	63.7	0.21	3.064×10^{10}	0.70(12)	0.431	
	188.3 ; $3/2^+$	226.8	53.0	752.5	1.143×10^{10}	0.30(3)	0.161	
425.3 ; $(5/2, \underline{7/2})^+$	0 ; $7/2^+$	425.4	2.19	1692.5	3.173×10^{10}	0.24(4)	0.702	0.39
	114.3 ; $5/2^+$	311.0	10.3	140.8	5.953×10^9	0.43(4)	0.132	0.25
	211.3 ; $5/2^+$	213.9	31.9	208.8	5.608×10^9	0.29(3)	0.124	0.16
	288.2 ; $9/2^+$	137.0	42.2	328.4	1.929×10^9	0.04(1)	0.043	0.20
497.8 ; $11/2^+$	0 ; $7/2^+$	497.8	-	2141.6	7.987×10^{10}	0.87(5)	0.955	0.97
	288.2 ; $9/2^+$	209.2	22.9	198.3	3.787×10^9	0.13(2)	0.045	0.03
515.6 ; $(9/2)^-$	240.2 ; $11/2^-$	275.4				0.75(6)		0.62
	270.1 ; $7/2^-$	245.5				0.25(6)		0.38

a) Calculated in the present work using the intermediate-coupling model.
b) Calculated in the present work using the axial particle-rotor model.

for ^{145}Pm lists also branching ratios that have been calculated on the cluster-vibration model (CVM) by Paar[61]. The branching ratios for ^{149}Pm given in table 17 have been calculated using the axial-rotor model[62,63]. Both of these models are described in sections 4.2 and 4.3, respectively.

4.1.6. Magnetic dipole and electric quadrupole moments

The magnetic dipole and electric quadrupole moments for the ground state and several of the low-lying levels have been calculated for each of the Pm nuclei. The calculations have been performed using eqs. (13) and (14) and the same values of the parameters and eigenfunctions as in the calculation of the electromagnetic transition rates. The results of our calculations and the available experimental data on the ground states and the first excited states are presented in table 18. The experimental data are very poor, but in those cases where experimental values are available the agreement with theoretical values is quite good. In table 18 there are also given the values that have been obtained using the gyromagnetic ratio $g_s = 5.58$ and the charge $e_p = e$ of the free proton. As can be seen, the calculations with the effective parameters $g_s = 3.91$ and $e_p = 2e$ give better results.

4.1.7. Spectroscopic factors

The method of calculation of the spectroscopic factors was given in subsect. 4.1.2. In table 19 the calculated spectroscopic factors $S_{\ell j}$ for a stripping reaction leading from the core nucleus to a state of

Table 18. Magnetic dipole moments and electric quadrupole moments of ground and first excited states of odd-mass Pm nuclei. The uncertainties of the last figures are in parentheses.

Nucleus	E (keV)	I^{π}	μ (μ_N) calc. g_s = 5.587 a)	μ (μ_N) calc. g_s = 3.91 a)	μ (μ_N) exp.	Q (eb) calc. e_p = e a)	Q (eb) calc. e_p = 2e a)	Q (eb) exp.
^{141}Pm	0	$5/2^+$	4.67	3.85		-0.049	-0.048	
	196.9	$7/2^+$	1.74	2.33		0.65	0.72	
^{143}Pm	0	$5/2^+$	4.76	3.93		-0.043	-0.050	
	272.1	$7/2^+$	1.72	2.36		0.28	0.34	
^{145}Pm	0	$5/2^+$	4.76	3.93		-0.12	-0.13	
	61.2	$7/2^+$	1.71	2.35		0.35	0.38	
^{147}Pm	0	$7/2^+$	1.71	2.34	+2.62(8) b)	0.70	0.72	+0.7(2) b)
	91.1	$5/2^+$	4.69	3.87	+3.6 (1) b)	-0.43	-0.44	0.6(3) b)
^{149}Pm	0	$7/2^+$	1.74	2.36	+3.3 (5) c)	-0.66	-0.68	
	114.3	$5/2^+$	4.38	3.66	2.22(26) c)	-0.62	-0.64	

a) Calculated in the present work using the intermediate-coupling model.

b) Ref. 64.

c) Ref. 42.

Table 19. Calculated and experimental spectroscopic factors $S_{\ell j}$ for a stripping reaction leading from the core nucleus to a state of spin I in odd-mass Pm nucleus.

I^{π}	^{141}Pm calc.	^{141}Pm exp.	^{143}Pm calc.	^{143}Pm exp.[a)]	^{145}Pm calc.	^{145}Pm exp.[b)]	^{147}Pm calc.	^{147}Pm exp.[c)]	^{149}Pm calc.	^{149}Pm exp.[d)]
$5/2^{+}_{1}$	0.48		0.52	0.52	0.53	0.54	0.51	0.39	0.48	0.40
$7/2^{+}_{1}$	0.18		0.29	0.32	0.36		0.34	0.21	0.50	0.27
$3/2^{+}_{1}$	0.29		0.58		0.20		0.01	0.007	0.19	0.01
$1/2^{+}_{1}$	0.10		0.19	1.12	0.01		0.003	0.61	0.001	0.14
$11/2^{-}_{1}$	0.57		0.73	0.71	0.53	0.81	0.34	0.70	0.51	0.36

a) Ref. 24.
b) Ref. 31.
c) Ref. 58.
d) Ref. 43.

spin I in Pm are shown. Also all experimental data available from stripping reactions to levels in Pm nuclei are given there. In those cases where the experimental values are available the agreement with the calculated values is very good for ground states and the first excited states. Also for the $11/2^-$ state the agreement is quite well but for the $1/2^+$ states there are very large discrepancies between experiment and the present calculation. The $s_{1/2}$ single-particle component must be much larger than in our theoretical wave functions (tables 8-12) where the main component is $|d_{5/2}; 12>$.

The $S_{\ell j}$ values for the $11/2^-$ states were calculated by coupling the $h_{11/2}$ single-particle state to the quadrupole vibrations; the octupole vibrations were neglected. The agreement is very good although the calculation was simple.

4.2. Description of the cluster-vibration model

In the previous section I have discussed the particle-vibration model with intermediate coupling when one particle has several single-particle states available. In the present section I shall describe briefly the cluster-vibration model (CVM) of Paar[3,4]. The calculations in this section were performed by Paar using our experimental results for Pm nuclei.

In the cluster-vibration model nuclei are described by a core and a cluster of a few particles or holes in the valence shell or subshell. Here we apply the CVM to odd $_{61}$Pm isotopes under the assumption of a Z = 64 subshell closure which persists even for nuclei three protons off (Z = 61). The cluster consists of three proton holes in the Z = 50 - 64 shell. The Z = 64 closure has been demonstrated by Kleinheinz et al.[5].

The Hamiltonian of the cluster-vibration model is

$$H = H_{SM}^{(n)} + H_{VIB} + H_{RES}^{(n)} + H_{PVC}^{(n)}$$

Here $H_{SM}^{(n)}$ describes the motion of n free valence-shell particles (holes) (in this case n = 3), H_{VIB} represents the quadrupole phonons and H_{RES} is the residual interaction between the valence-shell particles (holes) of the cluster. The term $H_{PVC}^{(n)}$ represents the interaction between each of the n particles (holes) of the cluster and the vibration; it is the usual particle-vibration coupling summed over all particles (holes) of the cluster. The effective strength of the particle-vibration interaction is denoted here by a in units of MeV. (The previously mentioned $\xi = 2\sqrt{5}\ a/\hbar\omega$.) The residual interaction $H_{RES}^{(n)}$ is taken here in its simplest form with only the pairing force.

In order to obtain the spectrum and wave functions, the following parameters are necessary: single-particle (hole) energies, phonon energy, pairing strength and particle(hole)-vibration coupling strength. In calculating the positive-parity states in Pm nuclei the following single-hole position was used[61]: $\varepsilon(g_{7/2}^{-1}) - \varepsilon(_{5/2}^{-1}) = 0.4$ MeV. For the phonon energy $\hbar\omega_2 = 1$ MeV was used and for the pairing strength G = 0.2 MeV; these two values are not adjusted to Pm isotopes but are taken as average values used for the CVM in medium-heavy nuclei in the region Z ≈ 50.

The basis states for diagonalizing the Hamiltonian are $|[(j_1^{-1}j_2^{-1})\ J_{12}, j_3^{-1}]\ J,NR;I\rangle$. The first part in this basis state represents a three-hole valence-shell cluster; N and R are the number and angular momentum of phonons. The cluster angular momentum J and the phonon angular momentum R are coupled to the total angular momentum I. By diagonalizing the CVM Hamiltonian in this basis the energy spectra and wave functions are obtained.

In fig. 26 the calculated CVM spectra are presented, obtained for the parameters given above and for different values of the particle-vibration coupling strength a. In the zeroth-order approximation the lowest states are the clusters $(d^{-3}_{5/2})5/2$, $[(d^{-2}_{5/2})0, g^{-1}_{7/2}]7/2$ and $(d^{-3}_{5/2})3/2, 9/2$ in this order (see the spectrum for a = 0 in fig.26). The distance between the clusters $(d^{-3}_{5/2})5/2$ and $(d^{-3}_{5/2})3/2, 9/2$ is given by pairing. With the increase of the particle-vibration coupling strength a the theoretical $7/2^+_1$ state, which in the present parametrization for a = 0 lies above the $5/2^+_1$ state, is lowered with respect to $5/2^+_1$. For a ≈ 0.5 they cross and $7/2^+_1$ becomes the ground state. This appears as a consequence of the matrix elements $\langle g^{-1}_{7/2}||Y_2||g^{-1}_{7/2}\rangle > \langle d^{-1}_{5/2}||Y_2||d^{-1}_{5/2}\rangle$, which appear in the corresponding matrix elements of the particle-vibration interaction. The gap between the doublet $5/2^+_1$, $7/2^+_1$ and the neighbouring higher states $3/2^+_1$, $9/2^+_1$, which is due to pairing, persists with the increase of the particle-vibration coupling strength a. The $3/2^+_1$ state is lower than the $9/2^+_1$; this is due to the effect of the so called I = j-1 anomaly in the CVM (refs. 4, 65, 66), which leads to a lowering of the state $|(j^{-3})I = j-1\rangle$. However, due to the presence of close-lying clusters involving the $g_{7/2}$ configuration (the lowest are $[(d^{-2}_{5/2})2, g^{-1}_{7/2}]9/2$ and $[(d^{-2}_{5/2})4, g^{-1}_{7/2}]9/2$), for large a the $9/2^+_1$ state is more strongly pushed down than the $3/2^+_1$. For a ≈ 0.7 the $9/2^+_1$ and $3/2^+_1$ states cross and for a > 0.7, the $9/2^+_1$ lies below the $3/2^+_1$ (see fig. 26). Furthermore, for the cluster states discussed so far, in the zeroth-order approximation there is a one-phonon multiplet based on the $(d^{-3}_{5/2})5/2$ cluster state:

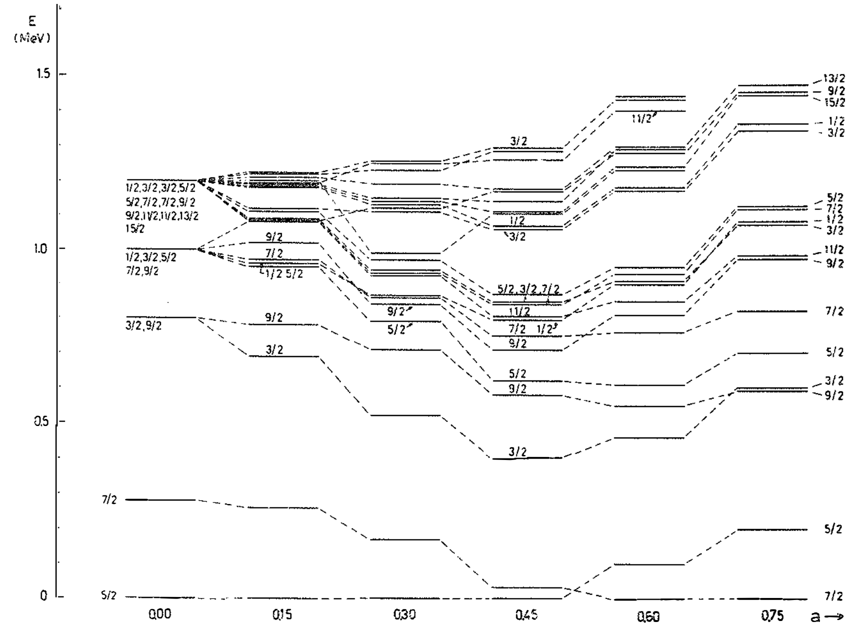

Fig. 26. Calculated positive-parity spectra for Z = 64-3 nuclei as a function of the particle-vibration coupling strength a. For parametrization see the text.

$|(d^{-3}_{5/2})5/2, 1\ 2; I = 1/2, 3/2, 5/2, 7/2, 9/2\rangle$, and the seniority-three cluster states $d^{-2}_{5/2}\ g^{-1}_{7/2}$: $[(d^{-2}_{5/2})2, g^{-1}_{7/2}]I = 3/2, 5/2, 7/2, 9/2, 11/2$; $[(d^{-2}_{5/2})4, g^{-1}_{7/2}]I = 1/2, 3/2, 5/2, 7/2, 9/2, 13/2, 15/2$. For $a > 0.3$, a group of states $5/2^+_2, 7/2^+_2, 9/2^+_2, 11/2^+_1, 3/2^+_2, 1/2^+_1, 7/2^+_3, 5/2^+_3$ is formed above and close to the doublet $3/2^+_1, 9/2^+_1$. Above this group of states there is a gap of a few hundred keV. Additional admixtures in the wave functions of the low-lying positive-parity states calculated in the present work are due to 4 hole - 1 particle clusters (with respect to the $Z = 64$ closure). Especially, the contributions of $|(d^{-4}_{5/2})0, d_{3/2}; 3/2^+_2\rangle$ and $|(d^{-4}_{5/2})0, s_{1/2}; 1/2^+\rangle$ states are sizeable.

For negative-parity states the 4 hole - 1 particle clusters should be included. The CVM calculation was performed by approximating the 4 hole - 1 particle cluster by a 2 hole - 1 particle cluster, and taking the $g_{7/2}$, $d_{5/2}$ configuration space for holes and only the $h_{11/2}$ configuration for particles. In this way the lowest calculated negative-parity state is $11/2^-$ followed by a group consisting of states $7/2^-$, $9/2^-$, $11/2^-$, $15/2^-$.

Comparing with the experimental spectra, it appears that for $a \approx 0.4$ the theoretical results qualitatively resemble $^{141}_{61}Pm_{80}$ and $^{145}_{61}Pm_{84}$, and for $a \approx 0.7$, $^{147}_{61}Pm_{86}$.

More detailed calculations have been performed so far only for ^{145}Pm (see ref. 61). By using the calculated wave functions, the branching ratios were calculated and compared with the experimental values in table 15. In this calculation the usual values for the effective charges and gyromagnetic ratios were used[4]: $e^{SP} = 1.5\ e$, $e^{VIB} = 2.5\ e$, $g_R = Z/A$, $g_\ell = 1$, $g_s = 0.7\ g_s^{free} = 3.91$.

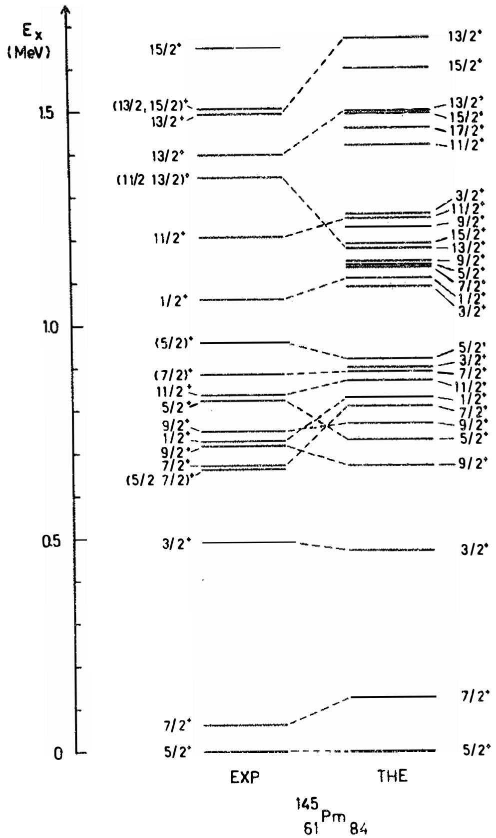

Fig. 27. Experimental and calculated positive-parity states of ^{145}Pm. The calculation was made on the cluster-vibration model with $a = 0.35$. Above 1.25 MeV only the calculated states with $I \geq 11/2$ are presented.

However, for the transition $7/2_1^+ \rightarrow 5/2_1^+$ it is necessary to include also the tensor component $g_p(Y_2 \otimes S)$ in the M1 operator because it gives the main contribution in this case. In the zeroth-order approximation ($a = 0$) the $7/2_1^+ \rightarrow 5/2_1^+$ E2 transition is of the spin-flip type and therefore hindered, while for the standard M1 operator the $7/2_1^+ \rightarrow 5/2_1^+$ M1 transition is ℓ-forbidden. Therefore, the additional tensor term in the M1 operator is important. By including the tensor term the result is $B(M1;\ 7/2_1^+ \rightarrow 5/2_1^+) = 0.057\ \mu_N^2$. On the other hand $B(E2;\ 7/2_1^+ \rightarrow 5/2_1^+) = 44\ e^2fm^4$ (cf. table 15). In this way, the calculated half-life is $T_{1/2}(7/2_1^+) = 3$ ns, in agreement with the experimental value of 2.6 ± 0.1 ns.

For more detailed results calculated using the cluster-vibration model, see ref. 61.

4.3. Interpretation of band structure in ^{149}Pm on the basis of the axial particle-rotor and the triaxial particle-rotor models

With increasing neutron number in the Pm nuclei the energy of the quadrupole phonon decreases, as was seen in the previous subsect. 4.1.4. So it can be supposed that (quasi-)rotational bands appear in the low-lying spectrum of the ^{149}Pm nucleus because in the nucleus ^{151}Pm the rotational bands are quite obvious. In the present section I shall review the results for ^{149}Pm that we have obtained applying the axial and triaxial particle-rotor models.

At first I describe the calculation using the axial particle-rotor model. This model is presented in some detail in refs. 62 and 63.

A comprehensive description of the particle-rotor model is given in ref. 8. The total Hamiltonian in this model consists of the particle motion and the collective rotation of a nucleus:

$$H_{mod} = H_{qp} + H_{qp\ rot}$$

The rotational part is further divided into three different contributions,

$$H_{qp\ rot} = H_I + H_{rpc} + H_j,$$

where H_I is associated with the adiabatic rotor, H_{rpc} with the Coriolis interaction and H_j is the recoil term.

The single-particle energies which are needed in the particle part of the Hamiltonian (H_{qp}) are calculated with Woods-Saxon potentials. The single-particle Hamiltonian (H_{WS}) contains nine parameters. Six of them are so-called potential parameters, $2 \times \{r_o, a_\perp, a_z\}$, and the remaining variables are the two potential depths V_o and the spin-orbit strength λ. In our calculations these potential parameters were: $r_o = 1.28$ fm, $a = a_z = a_\perp = 0.76$ fm, $V_o = V_{\ell s} = 54.5$ MeV, $r_{\ell s} = 1.09$ fm, $a_{\ell s} = a_{z\ell s} = a_{\perp\ell s} = 0.60$ fm and $\lambda = 17$.

The nuclear shape is expressed with the quadrupole and hexadecapole deformations $\eta_2 = (4/3)\varepsilon_2$ and $\eta_4 = \varepsilon_4$, respectively. In addition to these deformation parameters, the model contains only two free parameters: the rotational parameter A and the attenuation factor k for the Coriolis Hamiltonian (H_{rpc}). We have taken the following values for these parameters: $\eta_2 = 0.15$ and 0.20, $\eta_4 = 0$, A = 50 and 25 keV, and k = 1.0.

More detailed knowledge about the diagonalization of the model Hamiltonian can be obtained from refs. 62 and 63. The formulae for the B(M1) and B(E2) transition rates are also given there.

Fig. 28 presents the calculated and experimental level structure of ^{149}Pm. We have not performed any iteration to get this level order;

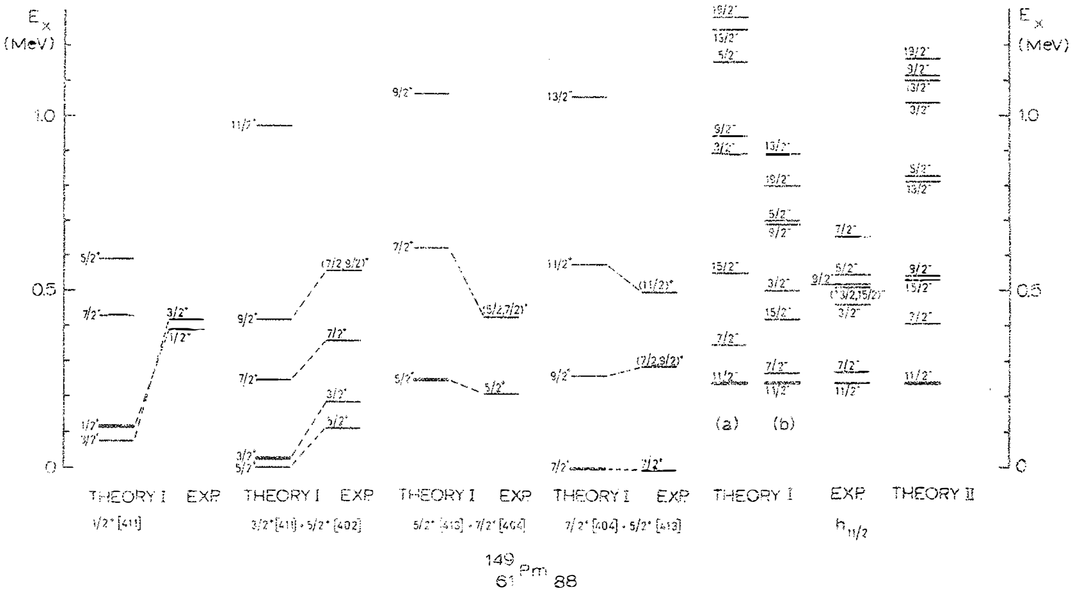

Fig. 28. Experimental and calculated level structure of ^{149}Pm. Theory I represents the theoretical results from the axial particle-rotor model and theory II from the triaxial particle-rotor model. For parametrization of both models see the text.

only two different deformations [η_2 = 0.15 and 0.20, (a) and (b) in fig. 28] have been considered for the negative-parity band. In table 22 the decay properties of some states are shown as predicted by this model.

The triaxial particle-rotor model of Meyer-ter-Vehn consists of an odd nucleon coupled to a rotating triaxial core. A comprehensive description of this model is given in ref. 7. The free parameters of the model are the deformation β ($0.1 < \beta < 0.2$), the asymmetry parameter γ ($0^0 < \gamma < 60^0$) and the Fermi energy λ_F. β and γ will be determined from the lowest excited states of the adjacent even nucleus, and λ_F will be estimated from the Nilsson level scheme. The other parameters k, Δ and J_0 are smooth functions of the mass A; k is the strength of the deformed field of the core ($k = 206/A^{1/3}$ MeV), Δ is the pairing potential and J_0 is the inertia parameter. We have tested the validity of this model in all odd-A Pm nuclei for the level family based on the unique-parity $h_{11/2}$ state. Fig. 28 shows the theoretical negative-parity states of ^{149}Pm, together with the experimentally known levels.

The compatibility between experiment and the triaxial rotor model is satisfactory. The level order agrees with experiment when the parameters are $\gamma = 21.4^0$, $\beta = 0.212$, $\Delta = 0.91$ MeV and $\tilde{\lambda}_F = 1.0$. The Fermi energy λ_F is given in the form $\tilde{\lambda}_F = (\lambda_F - \varepsilon_1)/(\varepsilon_2 - \varepsilon_1)$, where ε_i with $i = 1,2,...j + 1/2$ are the single-particle energies of the j shell. These were obtained after a fitting procedure. However, the energy fit is rather poor and gets worse when the excitation energy increases. The situation in the other Pm nuclei is similar with respect to the energy fit, and this is evidence that the rigid triaxial rotor is not a good description of the odd-A Pm nuclei investigated in this work. It seems to be necessary to take into account the idea of a variable moment of inertia which could lower the energies of the high-spin members of the bands[67].

The negative-parity states of the other Pm nuclei are shown in figs. 31 and 32. They show the experimental and calculated level schemes using both the intermediate-coupling model [theory (a)] and the triaxial rotor model [theory (b)].

5. DISCUSSION AND CONCLUSIONS

5.1. Positive-parity states

Fig. 29 presents our experimental results on level schemes of odd-A Pm isotopes measured in the present work. Fig. 29 shows only those levels for which the spin has been determined. The corresponding levels have been connected with dashed lines. The comparisons between the experimental and the theoretical results obtained using the intermediate-coupling model are given in figs. 21-25. As can be seen from fig. 29, the $5/2^+$ level is the ground state in $^{141-145}$Pm but becomes the first excited state in ^{147}Pm and ^{149}Pm. At the same time the first $7/2^+$ excited state in $^{141-145}$Pm crosses the $5/2^+$ level and becomes the ground state in ^{147}Pm and ^{149}Pm. In the IMC calculation the spin of the ground state is obtained correctly because it is chosen to agree with experiment. Tables 8-12 also show that the ground and first excited states of all the Pm isotopes investigated in the present work are highly pure. The $5/2^+$ states have $d_{5/2}$ admixtures larger than 95 %, and in the $7/2^+$ states the $g_{7/2}$ components are also >95 % in all the isotopes. The spectroscopic factors obtained from stripping reactions and given in table 19 also verify these assumptions.

The second excited state in all the isotopes except ^{147}Pm is $3/2^+$. This $3/2^+$ state has $d_{3/2}$ as its main component in ^{143}Pm and ^{149}Pm, but the other isotopes have also comparable $d_{5/2}$ and $g_{7/2}$

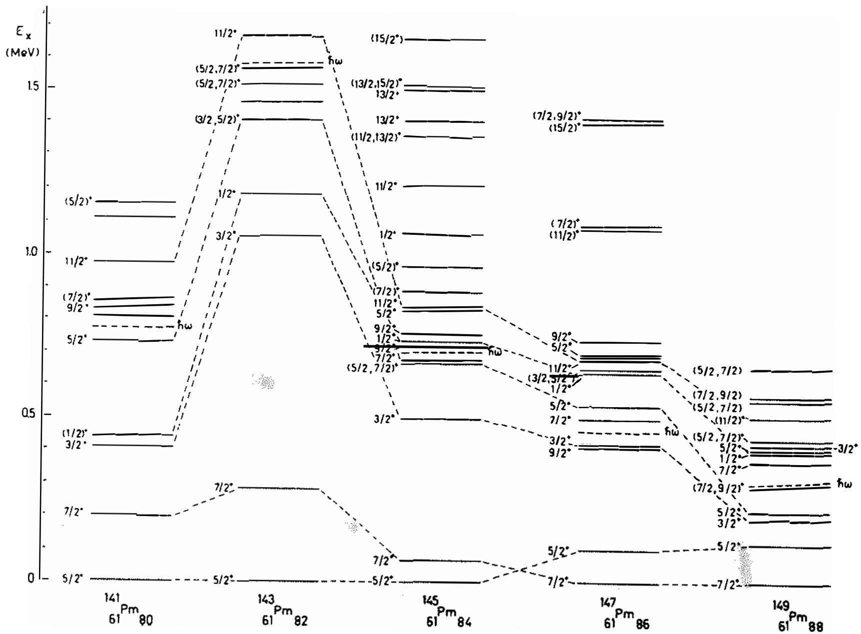

Fig. 29. Systematics of the experimental positive-parity levels in the odd-mass Pm nuclei

components. In ^{147}Pm a $9/2^+$ state becomes the second excited state. This $9/2^+_1$ state belongs to the $g_{7/2}$ multiplet and has a higher energy in the other Pm isotopes. There is also another $9/2^+_2$ state observed experimentally in ^{145}Pm and ^{147}Pm but it belongs to the $d_{5/2}$ multiplet. In ^{145}Pm these $9/2^+$ states have an energy difference of only about 40 keV, and according to the decay properties the member of the $g_{7/2}$ multiplet is higher in energy.

The third excited state in ^{141}Pm and ^{143}Pm is $1/2^+$ consisting of about 14 % of $s_{1/2}$ and about 68 % of $d_{5/2}$ admixtures in ^{141}Pm, and of about 21 % of $s_{1/2}$ and about 69 % of $d_{5/2}$ admixtures in ^{143}Pm. The other three Pm isotopes have also a $1/2^+$ state, but it is higher in energy and these $1/2^+$ states consist of over 93 % of $d_{5/2}$ components in each case.

If one looks at figs. 21-25 one can draw the conclusion that the agreement is excellent between experimental and theoretical level schemes as regards the energies and spin order of the states discussed above. There are also a few discrepancies between theory and experiment. In ^{149}Pm the $5/2^+_1$ state comes too low in energy but this can be explained by a rotational structure, and the energy of the $5/2^+_2$ state is in agreement with the results of the axial rotor-model. In ^{149}Pm the first experimental $11/2^+$ state is too high in energy compared with the IMC-model calculation but this can again be explained by a rotational band structure. In ^{147}Pm the calculated energy of the $11/2^+$ state is 200 keV too low, in ^{145}Pm the $1/2^+$ comes 100 keV too low, and in ^{141}Pm the calculated level order of $9/2^+_1$ and $5/2^+_2$ states is exchanged.

The cluster-vibration model (CVM) described in section 4.2 gives level schemes similar to those of the IMC model. In section 4.2 I already discussed the level sequences in general and the particle-vibration strength in each Pm nucleus. The detailed calculation for

^{145}Pm by using the CVM model (ref. 61) gives results comparable with those of the IMC model, but the $1/2^+$ state does not come so low. Experimentally there are nine states in ^{145}Pm in the region of 0.7 - 0.9 MeV. Eight of the nine calculated states of the multiplet seem to have their experimental counterparts. The exception is the $3/2^+$ state at 0.9 MeV. If we compare these theoretical results of the CVM (fig. 27) to those of the IMC model (fig. 23), we see that both calculations give the same spins but the level order is different. However, in general there are no appreciable differences between the results of these two particle-vibration models.

To interpret the level structure of ^{149}Pm we have applied the axially symmetric particle-rotor model to both positive- and negative-parity states, and the triaxial particle-rotor model to the negative-parity states. Here I discuss the positive-parity states on the basis of the band structure given by the axial particle-rotor model[62,63]. According to the Nilsson scheme for odd-proton nuclei with Z = 61, there are $5/2^+$[413], $3/2^+$[411], $7/2^+$[404], $5/2^+$[402] and $1/2^+$[411] levels available for the lowest excitations in the region of deformation parameter β = 0.1 - 0.2. We have taken the parameters needed in this model (cf. 4.3) as averages used for small deformations and we have calculated the level structure shown in fig. 28. We have selected the experimental states to correspond to the theoretical levels according to the B(M1) and B(E2) transition rates. We have interpreted the four mixed rotational bands in ^{149}Pm (fig. 28) accordingly. The suggested bands are : the $7/2^+$[404] ground-state band consisting of the $7/2^+$ ground state, the 288.2 keV $(9/2)^+$ state and the 497.8 keV $11/2^+$ state. This band is mixed with the $5/2^+$ [413] band whose ground state is the 211.3 keV $5/2^+$ state and the first rotational state is the 425.3 keV $(7/2)^+$ level. To the $3/2^+$[411] band mixed with the $5/2^+$[402] band belong the 114.3 keV $5/2^+$, 188.6 keV $3/2^+$, 360.0 keV $7/2^+$ and 588.1 keV $(9/2^+)$ states. The 387.5 keV $1/2^+$ and the 415.5 keV $3/2^+$ states we have proposed to belong to the $1/2^+[411]$ band; this is, however, very uncertain, because there are no supporting transitions. In another N = 88 nucleus, ^{153}Tb, the $7/2^+[404]$, $5/2^+[413]$, $3/2^+[411]$ bands and, furthermore, a $5/2^+[402]$ band have been observed[46] as has been also a $5/2^+[413]$ band[47] in ^{151}Eu. The $3/2^+[411]$ and $5/2[413]$ rotational bands are identified in the more deformed ^{151}Pm nucleus[48].

We can conclude that the level structure of ^{149}Pm to some extent can be explained on the basis of its vibrational character and partly on the basis of its rotational character. The rotational character can be seen especially in negative-parity states which seem to have a larger deformation.

5.2. Negative-parity states

Fig. 30 shows all negative-parity states observed experimentally in the present work. In addition, there are shown negative-parity states in ^{139}Pm obtained from ref. 68. In all of these Pm nuclei the lowest negative-parity level is an isomeric $11/2^-$ state with decreasing energy as the number of neutrons decreases and increases from N = 82. The other states have spins of $5/2^-$ to $19/2^-$. The levels with high spin values are populated weakly in (p,2n) and (^{3}He,3n) reactions due to the low bombarding energy.

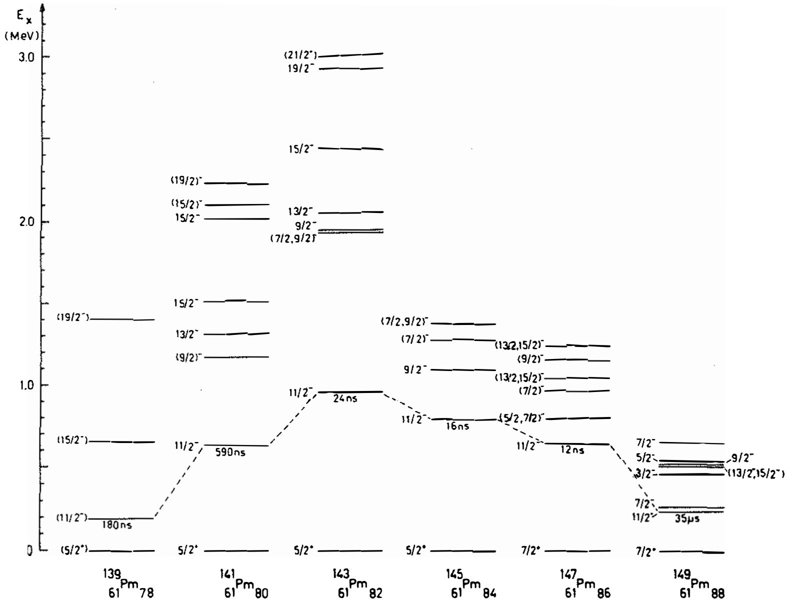

Fig. 30. Systematics of the experimental negative-parity levels in the odd-mass Pm nuclei

The Fermi level in slightly deformed Pm nuclei is near low-Ω orbits of the $h_{11/2}$ proton shell. It is therefore possible that decoupled bands could be built on the $11/2^-$ levels. These band structures have in general been interpreted using the triaxial rotor model (cf. 4.3). For these moderate deformations the Coriolis force decouples the particle from the core, and for high-spin states the particle and core angular momenta are nearly aligned, which gives rise to the typical $\Delta I = 2$ bands. Such band structures have been found in several lighter odd-proton nuclei: ${}^{125-133}_{57}La$ (ref. 69), ${}^{135,137}_{59}Pr$ (refs. 70, 71) and ${}^{139}_{61}Pm$ (ref. 68) and also in heavier ${}^{147,149,151}_{63}Eu$ (refs. 72, 73). In ^{141}Pm and ^{143}Pm the $13/2^-$ level is lowered below the $15/2^-$ level, showing that the structure is not of the decoupled type. In ^{147}Pm we cannot say surely which one of the $13/2^-$ or $15/2^-$ levels is lower in energy.

In figs. 31 and 32 the experimental negative-parity level schemes are compared with the calculated states from the triaxial particle-rotor TPR [theory (b)] and the IMC model [theory (a)]. In fig. 28 there are also results of the axial particle-rotor calculation (theory Ia, b). The parameters that are needed in the TPR model are given in the figure captions. The parameters in the IMC model are the same as those used with positive-parity states. The agreement between experiment and both theories is rather poor. In the TPR model the lowest states agree quite well but the higher spin states go too high. Therefore the VMI (variable-moment-of-inertia) prescription, as applied by Toki and Faessler[67], should be extended to the present model. This procedure lowers the states at higher energy in agreement with experiment.

The changed order of the $13/2^-$ and $15/2^-$ levels in ^{141}Pm, as mentioned before, can be explained[74] if a triaxial shape is allowed for the N = 80 core. The theory indicates that the level spectrum would

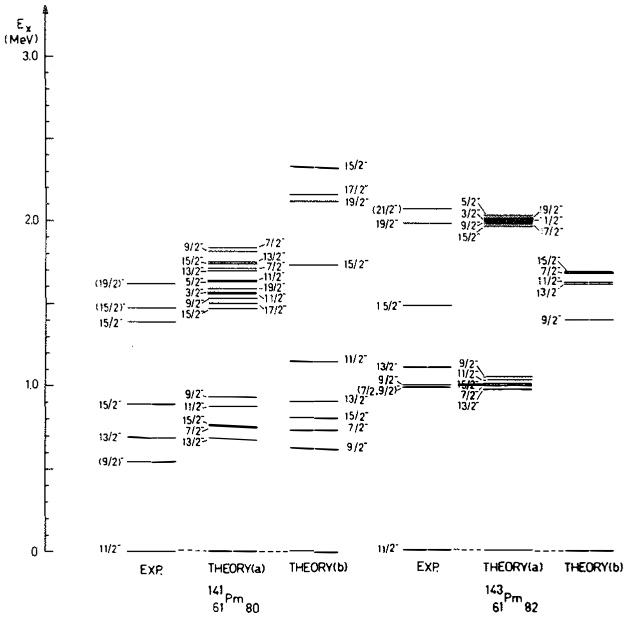

Fig. 31. Comparisons between the experimental negative-parity levels and the theoretical calculations. Theory (a) means the intermediate-coupling model calculations. For parametrization see the text. Theory (b) means the triaxial particle-rotor model calculations. The following parameters were used: ^{141}Pm (γ = 30°, β = 0.151, Δ = 0.96 MeV, $\tilde{\lambda}_F$ = 1.0); ^{143}Pm (γ = 35°, β = 0.101, Δ = 0.94 MeV, $\tilde{\lambda}_F$ = 1.0).

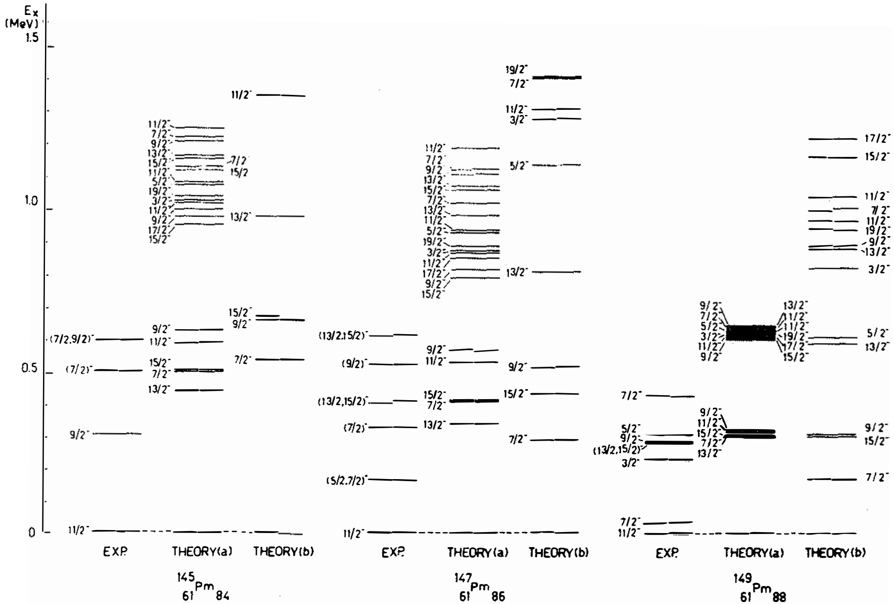

Fig. 32. Same as fig. 31, but the following parameters were used for theory (b): ^{145}Pm (γ = 25^o, β = 0.150, Δ = 0.93 MeV, $\tilde{\lambda}_F$ = 1.0); ^{147}Pm (γ = 20^o, β = 0.173, Δ = 0.92 MeV, $\tilde{\lambda}_F$ = 1.0); ^{149}Pm (γ = 21.4^o, β = 0.212, Δ = 0.91 MeV $\tilde{\lambda}_F$ = 1.0)

change gradually from a decoupled level order at $\gamma = 0^{0}$ to a strongly coupled level order at $\gamma = 60^{0}$ when passing through the triaxial plane[7]. This transition to a triaxial shape seems to happen in Pr and Pm nuclei at N = 80 when the neutron number increases below the N = 82 shell. This is analogous to the case of Ir, Au and Tl nuclei below the Z = 82 closed shell, where the $h_{9/2}$ particle families also change gradually from a decoupled type to a strongly coupled level system and the $11/2^{-}$ level is lowered below the $13/2^{-}$ level in ^{191}Au (ref. 75).

In the IMC model the level spectrum of negative-parity states was calculated by coupling only the $h_{11/2}$ quasiparticle to the quadrupole vibrations of the core. Therefore for the negative-parity states it would be necessary to take into account also the octupole vibrations of the core, although the energy of the octupole vibration quantum is twice as large as the energy of quadrupole phonons.

Furthermore, a rotational description is needed expecially for ^{149}Pm, where the $5/2^{-}$ level at 537.8 keV and $7/2^{-}$ level at 655.2 keV are supposed to be the band head and the first excited state of the rotational band built on the $5/2^{-}$[532] Nilsson state.

5.3. Electromagnetic transition rates

Experimental data on transition rates between the $\pi g_{7/2}$ and $\pi d_{5/2}$ states in odd-A Pm nuclei are collected in table 20. Also given are the E2 enhancements and M1 hindrances, relative to the Weisskopf single-particle estimates. Without a tensor term in the M1 operator (see below), M1 transitions between single-particle states for which the orbital angular momenta differ by two units are strictly forbidden, so that the transitions $g_{7/2} \leftrightarrows d_{5/2}$ are pure E2 in this picture.

Table 20. Experimental data on $\pi g_{7/2} \leftrightarrows \pi d_{5/2}$ transitions in odd-A Pm nuclei. The uncertainties of the last figures are in parentheses.

Nucleus	E_γ (keV)	$T_{1/2}$(exp) (ns)	E2 admixture %	B(M1) ($\times 10^{-3}\ \mu_N^2$)	B(E2) (e^2fm^4)	H(M1) a)	E(E2) b)	$T_{1/2}$ calc. c) (ns)
^{141}Pm	196.9	< 1 [d)]	-	> 4.2	-	< 430	-	44.3
^{143}Pm	272.1	1.06(8) [e)]	32(15) [f)]	1.15(46)	105(42)	1560(600)	2.4 (8)	62.2
^{145}Pm	61.2	2.6 (1)	0.14(5) [g)]	8.75(25)	47(15)	204(70)	1.05(35)	2226
^{147}Pm	91.1	2.6(1)	1.6 (4) [h)]	6.44(16)	182(45)	278(70)	3.97(10)	794
^{149}Pm	114.3	2.6(1)	2.8 (8) [i)]	4.79(14)	145(41)	373(106)	3.1 (9)	22.8

a) Hindrance factor H = $T_{1/2}$ (exp)/$T_{1/2}$ (W.e.). W.e. is the Weisskopf single-particle estimate.

b) Enhancement factor E = $T_{1/2}$ (W.e.)/$T_{1/2}$ (exp).

c) Calculated using the intermediate-coupling model; corrected for internal conversion.

d) Estimated from our measurements.

e) Ref. 21.

f) From α_K and δ^2 measured in the present work.

g) Ref. 29.

h) Ref. 34.

i) Ref. 42.

However, the $g_{7/2} \leftrightarrows d_{5/2}$ transitions are observed to be mainly of an M1 character, although strongly retarded. Generally, ℓ-forbidden M1 transitions have been found to be hindered by more than a factor of a hundred as compared with the single-particle estimate. This can be seen in table A in Appendix 1, where all experimental data on $g_{7/2} \leftrightarrows d_{5/2}$ transition rates in the region Z = 57 - 63 and N = 80 - 88 are presented. Therefore, for ℓ-forbidden transitions the tensor term $g_p(Y_2 \otimes S)$ of the M1 operator is considered to be important[76,77]. As we mentioned earlier in connection with the calculation for ^{145}Pm by Paar[61], a half-life of 3 ns is obtained for the $7/2^+$ state by including the tensor term, while the experimental $T_{1/2}$ is 2.6 ns. In the ICM-model calculation the tensor component is not included, and the calculated results disagree with the experimental half-lives (cf. table 20).

Experimental half-life values for other excited states than the $7/2_1^+$ or $5/2_1^+$ are available only for ^{147}Pm and ^{149}Pm. In table 21 we compare the experimental B(M1) and B(E2) values for ^{147}Pm with the IMC calculation. The corresponding results for ^{149}Pm are given in table 22; in addition there are also the calculated values predicted by the axial particle-rotor model. As a general conclusion we can say that the theoretical B(M1) and B(E2) values do not agree well with the experimental results, but for the branching ratios of γ rays (cf. tables 13-17 and 21) the situation is much better. The agreement between experiment and the IMC model is very good for ^{141}Pm and ^{143}Pm. One can say the same for ^{145}Pm, except for the $(7/2)_3^+$ 883.8 keV level. For ^{147}Pm the agreement is good except for the 641.3 keV $3/2_2^+$ and 686.1 keV $5/2_3^+$ levels. For ^{149}Pm both the IMC model and ASR model give similar branching ratios which are in good agreement with experiment . Which one of the models is better cannot be said on these grounds. The CVM model removes the disagreement

Table 21. Experimental and theoretical reduced transition probabilities B(M1), B(E2) and branching ratios in ^{147}Pm. The uncertainties of the last figures are in parentheses. Theoretical α_t values from ref. 38 are used when experimental values are not available.

Level energy (keV)	$T_{1/2}$ [a] (ns)	Transition energy (keV)	Multipolarity	B(M1) exp. ($\times 10^{-3}\ \mu_N^2$)	B(M1) th.[e] ($\times 10^{-3}\ \mu_N^2$)	B(E2) exp. (e^2fm^4)	B(E2) th.[e] (e^2fm^4)	Branching ratios exp.[f]	Branching ratios th.[e]
91.1	2.57	91.1	M1 + 1.6 % E2 [b]	6.4 (9)	0.019	182(25)	2.7	1	1
410.6	0.14	319.5	M1 + 11 % E2	6.7 (9)	23.9	118(16)	3.3	0.93(9)	0.39
		410.6	E2 [c]	-	-	23(3)	1528	0.07(1)	0.61
531.1	0.13	120.5	M1 + 0.2 % E2 [c]	4.3 (6)	37.3	8.5(12)	376	0.03(1)	0.014
		439.9	M1 + 27 % E2 [b]	0.21(3)	0.96	5.9(8)	2.2	0.09(2)	0.018
		531.05	M1 + 47 % E2 [d]	0.91(13)	10.0	42(6)	993	0.89(9)	0.97
686.1	0.25	196.6	M1 + 3.8 % E2 [c]	1.06(14)	71.2	15.7(22)	28.0	0.08(2)	0.047
		275.5	M1 + 1.9 % E2 [c]	1.7 (2)	0.19	6.3(9)	0.95	0.37(4)	3.7×10^{-4}
		595.0	M1 + 16 % E2	0.26(4)	23.9	2.1(3)	1110	0.14(3)	0.94
		686.1	M1 + 47 % E2	0.065(9)	0.092	1.8(2)	0.71	0.40(4)	0.003

a) Refs. 34 and 37.

b) Ref. 34.

c) Ref. 41.

d) Ref. 39.

e) Calculated in the present work using the intermediate-coupling model.

f) Present work

Table 22. Experimental and theoretical reduced transition probabilities B(M1) and B(E2) in ^{149}Pm.
The uncertainties of the last figures are in parentheses.

Level energy (keV)	$T_{1/2}$ (ns) c)	Transition energy (keV)	Multipolarity c)	B(M1) exp. (x 10^{-3} μ_N^2)	B(E2) exp. (e^2fm^4)	B(M1) (x 10^{-3} μ_N^2) a)	B(E2) (e^2fm^4) a)	B(M1) (x 10^{-3} μ_N^2) b)	B(E2) (e^2fm^4) b)
114.3	2.58	114.3	M1 + 2.8 % E2	4.8(7)	145(25)	0.35	225	0.45	55
188.6	3.24	74.3	M1 + 33 % E2	3.4(7)	4400(700)	372	141	1323	9.4
		188.6	E2 + <18 % M1	<0.08	> 130	-	996	-	18
211.3	0.08	97.0	M1 + < 6 % E2	>23	< 2500	82	10	51	50
		211.3	M1 + 14 % E2	32 (9)	1700(500)	6.0	1506	24	486
387.5	0.6	198.9	M1 + <20 % E2	>7.4	<10850	3.3	288	64	1790
		273.2	E2	-	72(24)	-	2218	-	86

a) Calculated in the present work using the intermediate-coupling model.
b) Calculated in the present work using the axial particle-rotor model.
c) Ref. 42.

for ^{145}Pm mentioned above and in this respect the CVM model is better than the IMC-model.

There is in all odd-A Pm nuclei observed an isomeric $h_{11/2}$ level which in most cases decays via M2 and E3 transitions to the ground state and to the first excited state. In ^{149}Pm and ^{147}Pm no E3 transition is observed. Furthermore, in ^{145}Pm and ^{147}Pm the $11/2^-$ level decays to the $9/2^+$ level by a hindered E1 transition. The hindrance factors relative to the Weisskopf estimate are F_W(E1, 44.1 keV) = $(1.7 \pm 0.3) \times 10^4$ in ^{145}Pm and F_W(E1, 241.2 keV) = $(8.6 \pm 1.4) \times 10^5$ in ^{147}Pm. The experimental B(M2) and B(E3) transition rates measured in the present work are presented in table 23 for the Pm isotopes. The other available experimental data on B(E2) and B(E3) values in the region Z = 57 - 65 and N = 80 - 88 are collected in table B in Appendix 2. The B(M2) values seem in the Pm isotopes, as also in the other nuclei, to decrease very nicely when the neutron number is increasing or decreasing from the closed N = 82 shell. The situation is of the same kind for the B(E3) values. Also the B(M2) and B(E3) values seem to decrease when the proton number increases.

Theoretical predictions for the B(M2) and B(E3) transition rates for N = 82 nuclei are obtained on the basis of pure one-quasiparticle wave functions as well as by taking into account one- and three-quasiparticle components[78]. In the case of ^{143}Pm, the three-quasiparticle admixture lowers the reduced electromagnetic transition rate[78] by about 30 %, which gives the theoretical value B(M2) = 11.41 $\mu_N^2 fm^2$, when our experimental value is B(M2) = (11.4 ± 1.2) $\mu_N^2 fm^2$. The calculated value for B(E3) is 3.54×10^3 $e^2 fm^6$, which has to be compared with our experimental result $(12.3 \pm 2.0) \times 10^3$ $e^2 fm^6$. Ejiri et al.[22,25,30,79] have used the B(M2)/B(E3) branching ratio for ^{143}Pm and ^{145}Pm to determine effective coupling constants on the basis of pure one-quasiparticle excitations. They ascribed the reduction of the B(M2) transition probability to the isovector component of the spin-isospin core polarization. Electric octupole transitions between single-particle states may be enhanced due to the constructive effect of the octupole core polarization. This is because the attractive interaction pushes down the collective states adding some strength to the transitions between low-lying states.

Table 23. Experimental B(M2) and B(E3) transition rates, M2 hindrances and E3 enhancements for transitions from the $h_{11/2}$ level in odd-A Pm nuclei. The uncertainties of the last figures are in parentheses.

Nucleus	B(M2) ($\mu_N^2 fm^2$)	B(E3) ($\times 10^3\ e^2 fm^6$)	H(M2)	E(E3)
^{141}Pm	5.0(2)	2.8(3)	9.0(4)	2.4(3)
^{143}Pm	11.4(12)	12.3(20)	4.0(5)	10.2(15)
^{145}Pm	7.2(9)	8.8(36)	6.3(8)	7.1(29)
^{147}Pm	6.6(14)	-	6.9(14)	-
^{149}Pm	1.1(1)	-	42 (4)	-

5.4. General conclusions

In the present work we have investigated transitional odd-A Pm nuclei (A = 141 - 149) by using versatile methods of nuclear spectroscopy. We have obtained level schemes which contain dozens of new levels and make systematic comparisons possible. Also the half-lives of $h_{11/2}$ isomeric states have been measured and the missing $h_{11/2}$ state in ^{147}Pm has been observed. The level schemes exhibit only low- and medium-spin states; the high-spin states are still missing because of too low bombarding energies of proton and ^{3}He beams.

The level schemes of odd-proton Pm isotopes have been calculated using the intermediate-coupling model (IMC), the cluster-vibration model (CVM), the axial particle-rotor model (APR) and the triaxial particle-rotor model (TPR). The IMC model was modified to include the quasiparticle character of the active nucleons and it was programmed for the PDP-11/45 computer at JYFL. For the other models the computer codes were available. In general we can conclude that both vibration and rotation models are compatible in this transitional region. Both of the vibration models reproduce the experimentally observed level energies and also the branching ratios of some certain levels are compatible. The CVM model has some advantages when compared with the IMC model, especially for the branching ratios. Using the APR model we have identified rotational band structures in ^{149}Pm for the first time. Both the TPR model and the APR model are compatible for describing the negative-parity levels in the Pm isotopes. It is shown that the coupling of the $h_{11/2}$ proton to the quadrupole vibrations of the core nucleus is not adequate to describe the negative-parity level schemes in these nuclei.

Appendix 1.

Table A   Experimental data on B(M1) and B(E2) transition rates, M1 hindrances and E2 enhancements of $\pi g_{7/2} \leftrightarrows \pi d_{5/2}$ transitions in odd-A nuclei in the region Z = 57 - 63 N = 80 - 88. The uncertainties of the last figures are in parentheses.

Nucleus	B(M1) ($\times 10^{-3}\ \mu_N^2$)	B(E2) (e^2fm^4)	H(M1)	E(E2)	Ref. a)
N=80					
^{137}La	2.6(1)	-	676(30)	-	c) d)
^{139}Pr	5.3(3)	157(8)	338(17)	0.27(1)	c) e) f)
^{141}Pm	>4.2	-	<430	-	g) j)
N=82					
^{139}La	4.6(4)	4.8(5)	390(40)	0.11(1)	c) h) i)
^{141}Pr	4.7(5)	12.9(26)	379(38)	0.30(10)	f) j) c)
^{143}Pm	1.2(5)	105(42)	1560(600)	2.4 (8)	g) k)
N=84					
^{141}La	3.8(2)	-	464(30)	464 (30)	j)
^{143}Pr	6.7(5)	44(4)	267(22)	1.0 (1)	c) f) k)
^{145}Pm	8.7(25)	47(15)	204(70)	1.0 (3)	g) p)
^{147}Eu	15.2(15)	42(4)	118(12)	0.9 (1)	c) l)
N=86					
^{147}Pm	6.4(16)	182(45)	280(70)	3.9(10)	g) m)
^{149}Eu	24.5(25)	-	73(8)	-	c) n)
N=88					
^{149}Pm	4.8(14)	145(41)	373(90)	3.1 (9)	g) o) n)
^{151}Eu	15.5(15)	982(100)	115(12)	20.7 (21)	c) q)

The total conversion coefficients are obtained by using the approximation $\alpha_t = \alpha_K + \frac{4}{3}\alpha_L$. Experimental coefficients α_t are used whenever possible. Theoretical α_t are taken from ref. b below.

a) References for α_t, $T_{1/2}$, I_γ and δ^2.

b) R.S. Hager and E.C. Seltzer, Nucl. Data A4 (1968) 1.

c) J.S. Geiger, R.L. Graham, I. Bergström and F. Brown, Nucl. Phys. 68 (1965) 352.

d) A. Morinaga and K. Hisatake, J. Phys. Soc. Japan 38 (1975) 322.

e) V.S. Butsev, Ts. Vylov, V.G. Kalinnikov, N.A. Tikhonov and E. Herrmann, Bull. Acad. Sci. USSR, Phys. Ser. 35 (1971) 1474.

f) V.S. Buttsev, Ts. Vylov, K. Ya. Gromov, V.G. Kalinnikov, I.I. Gromova, V.A. Morozov, T.M. Muminov, Kh. Fuya and A.B. Khalikulov, Bull. Acad. Sci. USSR, Phys. Ser. 37 (1973) 39.

g) Present work.

h) L.R. Greenwood, Nucl. Data Sheets 12 (1974) 139.

i) H.H. Hansen and D. Mouchel, Z. Physik A276 (1976) 303.

j) J.K. Tuli, Nucl. Data Sheets 23 (1978) 529.

k) J.F.Flemming, Nucl. Data Sheets 13 (1974) 229.

l) Ya.Vavryshchuk, V. Zhuk, E. Krupta, V.I. Razov, Ya. Sazhinski, N.A. Tikhonov and Kh. Fuya, Bull. Acad. Sci. USSR, Phys. Ser. 35 (1971) 2115.

m) T. Al-Janabi, W.D. Hamilton and D.D. Warner, J. of Phys. G3 (1977) 1415.

n) G.E. Holland, Nucl. Data Sheets 19 (1976) 337.

o) A. Bäcklin, S.G. Malmskog and H. Solhed, Arkiv Fysik 34 (1966) 495.

p) T.W. Burrows, Nucl. Data Sheets 12 (1974) 203.

q) B. Harmatz, Nucl. Data Sheets 19 (1976) 33.

Appendix 2.

Table B Experimental B(M2) and B(E3) transition rates, M2 hindrances and E3 enhancements for transitions from the $h_{11/2}$ level in odd-A nuclei in the region Z = 57 - 65, N = 80 - 88. The uncertainties of the last figures are in parentheses.

Nucleus	B(M2) ($\mu_N^2 fm^2$)	B(E3) ($\times 10^3$ $e^2 fm^6$)	H(M2)	E(E3)	Ref. a)
N=80					
^{137}La	>4.8	>9.1	<9.1	>8.2	c)
^{139}Pr	6.8(4)	5.8(6)	6.5(4)	5.1(5)	d) e)
^{141}Pm	5.0(2)	2.8(3)	9.0(4)	2.4(3)	f)
^{143}Eu	4.2(2)	0.93(5)	10.6(5)	0.77(4)	g) h)
N=82					
^{139}La	>8.6	-	<5.2	-	i)
^{141}Pr	11.0(6)	11.6(22)	4.1(8)	9.9(19)	i) e)
^{143}Pm	11.4(12)	12.3(20)	4.0(5)	10.2(15)	f)
^{145}Eu	8.6(9)	4.1(8)	3.2(9)	3.3(9)	i)
N=84					
^{145}Pm	7.2(9)	8.8(36)	6.3(8)	7.1(29)	f)
^{147}Eu	5.3(4)	4.8(3)	8.7(7)	3.8(4)	j) k)
N=86					
^{147}Pm	6.6(14)	-	6.9(14)	-	f)
^{149}Eu	3.2(2)	4.3(3)	4.7(7)	3.3(3)	j) l) m)
^{151}Tb	-	0.063(7)		0.047(5)	n)
N=88					
^{149}Pm	1.1(1)	-	42 (4)	-	f) o)
^{151}Eu	1.4(2)	1.7(2)	33 (4)	1.3(2)	p)
^{153}Tb	1.6(2)	-	29 (3)	-	q)

The total conversion coefficients are obtained by using the approximation $\alpha_t = \alpha_K + \frac{4}{3}\alpha_L$. Experimental coefficients α_t are used whenever possible. Theoretical α_t are taken from ref. b below.

a) References for α_t, $T_{1/2}$, I_γ and δ^2.

b) R.S. Hager and E.C. Seltzer, Nucl. Data A4 (1968) 1.

c) J.R. Van Hise, G. Chilosi and N.J. Stone, Phys. Rev. 161 (1967) 1254.

d) G.G. Kennedy, J. Deslauriers, S.C. Gujrathi and S.K. Mark, Phys. Rev. C 15 (1977) 792.

e) H. Ejiri, T. Shibata and M. Fujiwara, Phys. Rev. C 8 (1973) 1892.

f) Present work.

g) R.B. Firestone, R.A. Warner, Wm.C. McHarris and W.H. Kelly, Phys. Rev. C 17 (1978) 718.

h) K. Wisshak, A. Hanser, H. Klewe-Nebenius, J. Buschmann, H. Rebel, H. Faust, H. Toki and A. Fässler, Z. Physik A277 (1976) 129.

i) W.D. Fromm, L. Funke and K.D. Schilling, Physica Scripta 12 (1975) 91.

j) T. Shibata, Y. Nagai, M. Fujiwara and H. Ejiri, Nucl. Phys. A257 (1976) 303.

k) T. Shibata, H. Ejiri and M. Sano, Nucl. Phys. A254 (1975) 7.

l) M.V. Klimentovskaya, N.A. Lebedev and A.A. Sorokin, Soviet J. Nucl. Phys. 12 (1971) 251.

m) H. Nakayama, J. Chiba, M. Sekimoto and K. Nakai, Nucl. Phys. A293 (1977) 137.

n) P. Kemnitz, L. Funke, F. Stary, E. Will, G. Winter, S. Elfström, S.A. Hjorth, A. Johnson and Th. Lindblad, Nucl. Phys. A311 (1978) 11.

o) A. Bäcklin, S.G. Malmskog and H. Solhed, Arkiv Fysik 34 (1966) 495.

p) B. Harmatz, Nucl. Data Sheets 19 (1976) 33.

q) G. Winter, J. Döring, L. Funke, P. Kemnitz, E. Will, S. Elfström, S.A. Hjorth, A. Johnson and Th. Lindblad, Nucl. Phys. A299 (1978) 285.

References

1) D.C. Choudhury and T.F. O'Dwyer, Nucl. Phys. A93 (1967) 300

2) K. Heyde and P.J. Brussaard, Nucl. Phys. A104 (1967) 81

3) G. Alaga, Bull. Am. Phys. Soc. 4 (1959) 359

4) V. Paar, Nucl. Phys. A211 (1973) 29; Z. Physik 271 (1974) 11; Phys. Rev. C 11 (1975) 1432

5) P. Kleinheinz, S. Lunardi, M. Ogawa and M.R. Maier, Z. Physik A284 (1978) 351

6) E. Osnes, J. Rekstad and O.K. Gjøtterud, Nucl. Phys. A253 (1975) 45 and references therein

7) J. Meyer-ter-Vehn, Nucl. Phys. A249 (1975) 111; 141

8) G. Ehrling and S. Wahlborn, Physica Scripta 6 (1972) 94; W. Ogle, S. Wahlborn, R. Piepenbring and S. Fredriksson, Rev. Mod. Phys. 43 (1971) 424

9) W.-D. Schmidt-Ott and R.W. Fink, Z. Physik 249 (1977) 286; R.J. Gehrke, R.G. Helmer and R.C. Greenwood, Nucl. Instr. and Meth. 147 (1977) 405; G.L. Borchert, KFA - Jülich, Annual Report 1975

10) T. Komppa, Dept. of Physics, Univ. of Jyväskylä, JYFL Annual Report 1976, p. 25

11) T. Yamazaki, Nucl Data A3 (1967) 1

12) H. Helppi, Dept. of Physics, Univ. of Jyväskylä, Laboratory Report 1/1976

13) M. Luontama, J. Kantele, R. Julin, A. Passoja, T. Poikolainen and M. Pylvänäinen, Nucl. Instr. and Meth. 159 (1979) 339

14) E. Liukkonen, M. Sakkinen, T. Komppa, M. Nieminen and R. Komu, Dept. of Physics, Univ. of Jyväskylä, JYFL Annual Report 1976, p. 19

15) J.K. Tuli, Nucl. Data Sheets 23 (1978) 529

16) C. Ekström, S. Ingelman, M. Olsmats and B. Wannberg, Physica Scripta 6 (1972) 181

17) R. Arlt, G. Beyer, Y. Vavryschuk, V.A. Morosov, T.M. Muminov, V.I. Rasov, J. Sazynski, H. Fuia, H. Strusny and E. Herrman, JINR report no. P6-5517 (1970) unpublished

18) L. Funke, W.D. Fromm, H.J. Keller, R. Arlt and P.M. Gopytsch, Nucl. Phys. A274 (1976) 61

19) G.G. Kennedy, J. Deslauries, S.C. Gujrathi and S.K. Mark, Phys. Rev. C 15 (1977) 792

20) R.E. Epply, R.R. Todd, R.A. Warner, Wm.C. McHarris and W.H. Kelly, Phys. Rev. C 5 (1972) 1084

21) J.F. Flemming, Nucl. Data Sheets 13 (1974) 229

22) T. Shibata, H. Ejiri, H. Kawakami, H. Kusakari, M. Sakai and N. Yoshikawa, J. Phys. Soc. Japan 35 (1973) 633

23) W.D. Fromm, L. Funke and K.D. Schilling, Physica Scripta 12 (1975) 91

24) B.H. Wildenthal, E. Newman and R.L. Auble, Phys. Rev. C 3 (1971) 1199

25) Y. Nagai, T. Shibata, S. Nakayama and H. Ejiri, Nucl. Phys. A282 (1977) 29

26) R.W. Grant and D.A. Shirley, Phys. Rev. 130 (1963) 1100

27) T.W. Burrows and R.L. Auble, Nucl. Data Sheets 16 (1975) 231

28) W. Andrejtscheff, U. Hagemann, L. Kaubler, H. Prade, K.D. Schilling, L. Schneider and F. Stary, Nukleonika 23 (1978) 159

29) T.W. Burrows, Nucl. Data Sheets 12 (1974) 203

30) Z. Roller-Ivanović, A. Ljubičić, V. Paar and B.A. Logan, Phys. Rev.C 16 (1977) 2376

31) T. Shibata, Y. Nagai, M. Fujiwara, H. Ejiri, N. Nakanishi and S. Takeda, Nucl. Phys. A257 (1976) 303

32) R.G. Summers-Gill, private communication, 1976

33) S.S. Bhati, N. Singh, P.C. Mangal and P.N. Trehan, J. Phys. Soc. Japan 36 (1974) 326 and references therein

34) N. Blaskovich, Jr. and A.P. Arya, Phys. Rev. C 2 (1970) 1881; B.K. Sinha, S. Sen and R. Bhattacharyya, J. of Phys. G1 (1975) 92

35) C. Rangcharyulu, G.K. Mehta, S.N. Chaturvedi and N. Nath, Austral. J. Phys. 27 (1974) 869

36) P.F.A. Klinkenberg and F.S. Tomkins, Physica 26 (1960) 103

37) H. Singh, B. Sethi and S.K. Mukherjee, Nucl. Phys. A174 (1971) 437

38) R.S. Hager and E.C. Seltzer, Nucl. Data A4 (1968) 1

39) G.A. Westenbarger and D.A. Shirley, Phys. Rev. 123 (1961) 1812

40) O. Straume, private communication, 1977 and O. Straume, G. Løvhøiden and D.G. Burke, Z. Physik 290 (1979) 67

41) T. Al-Janabi, W.D. Hamilton and D.D. Warner, J. of Phys. G3 (1977) 1415

42) G.E. Holland, Nucl. Data Sheets 19 (1976) 337

43) O. Straume, G. Løvhøiden and D.G. Burke, Nucl. Phys. A266 (1976) 390

44) A. Cabezas, I. Lindgren and R. Marrus, Phys.Rev. 122 (1961) 1796

45) W.B. Walters, private communication, 1978

46) G. Winter, J. Döring, L. Funke, P. Kemnitz, E. Will, S.E. Elfström, S.A. Hjorth, A. Johnson and Th. Lindblad, Nucl. Phys. A299 (1978) 285
M.D. Devous, Sr. and T.T. Sugihara, Phys. Rev. C 15 (1977) 740

47) H. Taketani, H.L. Sharma and Norton M. Hintz, Phys. Rev. C 12 (1975) 108

48) T. Seo, Nucl. Phys. A282 (1977) 302

49) A. Bäcklin, S.G. Malmskog and H. Solhed, Arkiv Fysik 34 (1966) 495

50) A. Bohr, Mat. Fys. Medd. Dan. Vid. Selsk. 26, No. 14 (1952)

51) A. Bohr and B.R. Mottelson. Mat. Fys. Medd. Dan. Vid. Selsk. 27, No. 16 (1953)

52) D.C. Choudhury, Mat. Fys. Medd. Dan. Vid. Selsk. 28, No. 4 (1954)

53) D.C. Choudhury and E. Kujawski, Phys. Rev. 144 (1966) 1013

54) N. Freed and W. Miles, Nuovo Cimento 60 (1969) 301

55) D.C. Choudhury and J.N. Friedman, Phys. Rev. C 3 (1971) 1619

56) B.K. Sinha, S. Sen and R. Bhattacharyya, J. Phys. G2 (1976) 159

57) B.J. Raz, Phys. Rev. 114 (1959) 1116

58) O. Straume, G. Løvhøiden and D.G. Burke, Z. Physik 290 (1979) 67

59) G. Vanden Berghe and K. Heyde, Nucl. Phys. A163 (1971) 478

60) L.S. Kisslinger and R.A. Sorensen, Rev. Mod. Phys. 35 (1963) 853

61) M. Kortelahti, M. Piiparinen, A. Pakkanen, T. Komppa, R. Komu, S. Brant, Lj. Udovičić and V. Paar, Dept. of Phys., Univ. of Jyväskylä, Res . Rep. No. 4/1979

62) R. Katajanheimo and E. Hammarén, Physica Scripta 19 (1979)

63) E. Hammarén, Dept. of Phys., Univ. of Jyväskylä, Res. Rep. No. 3/ 1978

64) B. Harmatz and W.B. Ewbank, Nucl. Data Sheets 25 (1978) 113

65) V. Paar, E. Coffon, U. Eberth and J. Eberth, J. Phys. G2 (1976) 917; V. Paar, Ch. Vieu and J.I. Dionisio, Nucl. Phys. A284 (1977) 199

66) R.A. Meyer, K.V. Marsh, D.I. Brenner and V. Paar, Phys. Rev. C 16 (1977) 417

67) H. Toki and A. Faessler, Nucl. Phys. A253 (1975) 231 and Z. Physik A276 (1976) 35

68) J. van Klinken and S.J. Feenstra, Phys. Rev. C 12 (1975) 2111

69) I. Stephens, Rev. Mod. Phys. 47 (1975) 43

70) H. Klewe-Nebenius, D. Habs, K. Wisshak, H. Faust, G. Nowicki, S. Göring, H. Rebel, G. Schatz and M. Schwall, Nucl. Phys. A240 (1975) 137

71) K. Wisshak, H. Klewe-Nebenius, D. Habs, H. Faust, G. Nowicki and H. Rebel, Nucl. Phys. A247 (1975) 59

72) J.G. Fleissner, E.G. Funk, F.P. Venezia and J.W. Mihelich, Phys. Rev. C 16 (1977) 227

73) H. Nakayama, J. Chiba, M. Sekimoto and K. Nagai, Nucl. Phys A293 (1977) 137

74) M. Piiparinen, M. Kortelahti, T. Komppa, R. Komu and A. Pakkanen, Proc. of Ann. Conf. of the Finnish Phys. Soc., Febr. 2-3, 1979, Jyväskylä, Finland, p. 2:6; Dept. of Phys., Univ. of Jyväskylä, Res. Rep. No. 2/1979

75) J. Meyer-ter-Vehn, J. de Physique C3 (1978) 154

76) A. Bohr and B.R. Mottelson, Nuclear Structure, Vol. II, Benjamin, 1975

77) V. Paar and S. Brant, Phys. Lett. 74B (1978) 297; Nucl. Phys. A303 (1978) 96

78) M. Waroquier and G. van den Berghe, Phys. Lett. 41B (1972) 267

79) H. Ejiri, T. Shibata and M. Fujiwara, Phys. Rev. C 5 (1973) 1892